Stochastic population oscillators in ecology and neuroscience

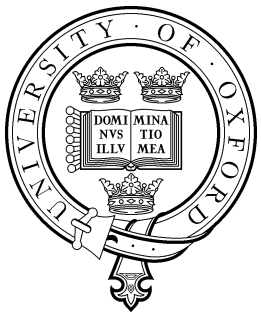

Yi Ming Lai

St Anne's College

University of Oxford

A thesis submitted for the degree of

Doctor of Philosophy

Michaelmas 2012

Abstract

In this thesis we discuss the synchronization of stochastic population oscillators in ecology and neuroscience. Traditionally, the synchronization of oscillators has been studied in deterministic systems with various modes of synchrony induced by coupling between the oscillators. However, recent developments have shown that an ensemble of uncoupled oscillators can be synchronized by a common noise source alone.

By considering the effects of noise-induced synchronization on biological oscillators, we are able to explain various biological phenomena in ecological and neurobiological contexts - most importantly, the long-observed Moran effect. Our formulation of the systems as limit cycle oscillators arising from populations of individuals, each with a random element to its behaviour, also allows us to examine the interaction between an external noise source and this intrinsic stochasticity. This provides possible explanations as to why in ecological systems large-amplitude cycles may not be observed in the wild. In neural population oscillators, we were able to observe not just synchronization, but also clustering in some parameter regimes.

Finally, we are also able to extend our methods to include coupling in our models. In particular, we examine the competing effects of dispersal and extrinsic noise on the synchronization of a pair of Rosenzweig-Macarthur predator-prey systems. We discover that common environmental noise will ultimately synchronize the oscillators, but that the approach to synchrony depends on whether or not dispersal in the absence of noise supports any stable asynchronous states. We also show how the combination of correlated (shared) and uncorrelated (unshared) noise with dispersal can lead to a multistable steady-state probability density. Similar analysis on a coupled system of neural oscillators would be an interesting project for future work, which, among other future directions of research, is discussed in the concluding section of this thesis.

Acknowledgements

Firstly, this work would not have been possible without the exceptional guidance and mentoring of my supervisor Paul Bressloff. I would also like to thank Jay Newby and other colleagues for useful discussions.

This degree was funded by a studentship from the Oxford Centre for Collaborative Applied Mathematics. This included several opportunities for travel, which were facilitated by the helpful administrative team.

Personally, I am extremely grateful for the support of my partner, Alexandra, my parents, and my friends.

Contents

Chapter 1

Introduction

Biological oscillations, the subject of this thesis, are one of the most striking and fundamental phenomena, observed across a variety of systems. In this thesis we consider two types of biological oscillators: ecological and neural. These have traditionally been studied using deterministic methods where synchronization was induced by coupling, for example, synaptic coupling between neurons and dispersal between adjacent populations in ecology.

However, recent work on the synchronization of oscillators in general [97] has led to the discovery of an alternative mechanism - it has been found that an ensemble of uncoupled oscillators can be somewhat counter-intuitively synchronized by a common noise source alone.

Our main goal in this thesis is to apply this theory of noise-induced synchronization to biological systems. This will allow us to obtain new insights into how ecological and neurobiological systems exhibit various forms of synchrony or asynchrony. At the same time, biological systems tend to be very intrinsically noisy. For example, in population ecology, the size of a population is the variable of interest but the behaviour of an individual organism is often unpredictable. Similarly, in neuroscience, it is known that the individual cortical neurons fire stochastically, with the distribution of inter-spike intervals close to a Poisson distribution [115], and spontaneous waves and oscillations have been observed in vivo and in vitro.

In order to deal with this intrinsic stochasticity, we formulate a master equation description for each of our ecological and neuronal populations, where each event (births, deaths, etc in the ecological case, and a neuron firing or ceasing to fire in the neuronal case) is a transition between states, and hence modelled as an exponential random variable. By choosing transition rates appropriately, we are able to show that in the thermodynamic limit (where an extensive parameter cor-

responding to the system size goes to infinity), that our averaged population variables can be described by ordinary differential equations (ODEs) corresponding to canonical models commonly used to study biological oscillations. Furthermore, we show how can capture the effects of intrinsic and extrinsic noise by adding noisy perturbations to said ODE models, and hence apply the theory of noise-induced synchronization to our biological systems.

As such, the structure of this thesis is as follows. In the next chapter, we describe the theoretical basis for noise-induced synchronization of general limit cycle oscillators. This will include a discussion of phase reduction and averaging in general, which is also used to study the effects of coupling on oscillators.

In chapter three, we look at an ensemble of uncoupled Holling-Tanner predator-prey populations. We start with a master equation formulation of an individual-based description of a predator-prey system. We then perform a Kramers-Moyal expansion and choose the transition rates so that we can simplify the master equation to a Langevin equation. The resultant stochastic differential equation (SDE) has a deterministic component corresponding to the deterministic Holling-Tanner system, and a stochastic component representing the effect of intrinsic noise. At the same time, we show how similar techniques can be used to introduce a common source of extrinsic noise into an ensemble of populations. By using the theory from chapter two to study the behaviour of this ensemble, we are able to obtain various levels of synchrony depending on the ratio of intrinsic and extrinsic noise in the system. This allows us to explain the long-observed Moran effect, as well as obtaining insights into when a system may not exhibit large-amplitude oscillations despite the theory predicting it.

In chapter four, we use a similar approach to examine an ensemble of oscillating neuronal populations with a common synaptic input. First, we do this for an ensemble of E-I oscillators, so named because each oscillator consists of an excitatory subpopulation coupled to an inhibitory subpopulation. This has been used as a basic unit in various studies of synchrony and other phenomena in the brain. We successfully induce synchrony using noise alone, and proceed to find that changing the way the different populations respond to noise causes alternative modes of synchrony such as clustering. This is important because various neuropathological disorders are theorized to correlate to small changes in properties of neurons, such as their excitability. Due to the complexity of the system, much more work would have to be done, such as applying the theoretical framework introduced here to more realistic models of specific parts of the brain; however, it is con-

ceivable that the changes in the modes of synchrony experienced correspond to anomalous large-scale waves, such as those observed in patients suffering epilepsy or migraines. Finally, we demonstrate that our methods are also applicable when one considers the effects of synaptic depression. We do this by considering another simple and much-studied population oscillator, a recurrent excitatory population with synaptic depression. Mathematically, this is interesting as it is an example of a stochastic hybrid system - the synaptic depression variable evolves deterministically between jumps of the stochastic activity variable.

Next, in chapter five, we provide an important contribution to the mathematical theory by studying a pair of coupled ecological populations with both extrinsic noise and dispersive coupling. In particular, we develop a complementary approach to that in [52] - there they start with predator-prey models coupled by dispersal and add correlated noise via spatially correlated Poisson inputs. Their results are mainly numerical, while we take a more analytical approach and examine the probability distribution function (PDF) of the phase difference between a pair of coupled populations with correlated and uncorrelated noise. This allows us to find many interesting types of behaviour, such as stochastic bistability between synchrony and asynchronous phase-locking. Asynchronous phase-locking may allow the persistence of endangered species where the metapopulation is in a spatially scattered habitat by ensuring that some populations are high when others are at their lowest (and hence at greatest danger of extinction). This would mean that should the species die out in one area, it could then be repopulated by dispersal from another, more fecund, area [58]. While the extinction or survival of a species ultimately rests on many factors that have to be studied carefully on a case-by-case basis, we hope that the work presented in this thesis will contribute to the mathematical toolbox used in such an analysis. Finally, in chapter six, we summarize our findings, as well as discuss the many fecund areas of future research that could spring from the work presented here.

Chapter 2

Noise-induced synchronization

2.1 Stochastic processes

In this chapter, we outline the concept of noise-induced synchronization as first described in [97]. However, we first need to introduce some of the tools we use to study noisy processes in general, and why we choose these specific methods to model the biological processes we study in this thesis.

Firstly, we introduce the notion of random processes and sample paths. A random process is a collection of random variables, for example a sequence of coin-flips. A sample path would refer to ever possible outcome of these coin-flips, and we are able to average over the different sample paths in order to obtain desired properties of the system, such as the mean and the variance in the number of heads obtained. That particular example is discrete in both time and the state space of outcomes; in the systems studied here, we have to deal with random processes in both continuous time and space.

In this thesis, we model most of our continuous random processes using the Wiener process or Brownian motion. In the original work on Brownian motion, particles suspended by a fluid moved randomly due to their many collisions with the smaller fast moving particles of the fluid. As such, these approaches are commonly used to model the impact of processes occuring on a much smaller timescale, such as the relationship between stock prices and the individual transactions. As these techniques were originally designed to deal with diffusion, it is unsurprising that the probability distribution function $p(w,t)$ of the Wiener pro-

cess satisfies the one-dimensional heat equation

$$\frac{\partial}{\partial t}p(w,t) = \frac{1}{2}\frac{\partial^2}{\partial w^2}p(w,t). \tag{2.1}$$

In general the equation describing the time-evolution of the probability distribution function of a random variable is called a Fokker-Planck equation. For the case of the standard Brownian motion above it can be solved for an initial condition (w_0, t_0) exactly to give

$$p(w,t|w_0,t_0) = \frac{1}{\sqrt{2\pi(t-t_0)}}\exp(-\frac{(w-w_0)^2}{2(t-t_0)}) \tag{2.2}$$

which is simply a Gaussian distribution with $\langle W(t)\rangle = w_0$ and $\langle [W(t)-w_0]^2\rangle = t-t_0$.

In our ecological systems, we assume that the impact of the individual behaviour of organisms can be captured using this approach, and derive a specific form for the noise starting from a master equation. Similarly as we deal with populations of neurons, we assume that the randomness in the synaptic input can be represented by using Wiener processes. This is analogous to the fact that the Wiener process can be said to be the limit of a one-dimensional random walk as the step-size in space and time goes to zero. (This would of course be different if one was studying individual neurons, where individual spikes would be important. In that case one would look for alternative approaches, for example, by using a Poisson process to model spikes from an adjacent neuron.) By combining these with existing ODE models for our systems, we arrive at Langevin equation descriptions for our systems which have long been used in physics.

One can also show that a Master Equation model can be approximated a Fokker-Planck equation, and hence that the evolution of the underlying system can be approximated by these Langevin equations. A Master Equation is a set of differential equations used to describe exactly the time-evolution of a system that switches between discrete states probabilistically. For example, consider a birth-death process in one variable $M \in \mathbb{Z}^*$. Say the probability of $M \to M+1$ is $T^+(M)$, and the probability of $M \to M-1$ is $T^-(M)$. Then, denoting the probability that the system is in state M at time t by $\mathbb{P}_M(t)$, we can describe this system entirely by the master equation

$$\frac{\partial \mathbb{P}_M}{\partial t} = T^+(M-1)\,\mathbb{P}_{M-1} + T^-(M+1)\,\mathbb{P}_{M+1} - [T^+(M)+T^-(M)]\,\mathbb{P}_M\,. \tag{2.3}$$

The first two terms on the right hand side represent the transitions into the state M, while the last term represents the transitions out of it. In general, we can write a Master Equation (in one dimension) as

$$\frac{\partial \mathbb{P}_M}{\partial t} = \sum_{\forall M'} T(M|M')\,\mathbb{P}_{M'} - \left[\sum_{\forall M'} T(M'|M)\right]\mathbb{P}_M \tag{2.4}$$

$$= \int \left(T(M|M')\,\mathbb{P}_{M'} - T(M'|M)\,\mathbb{P}_M\right) dM'. \tag{2.5}$$

The Master Equations considered in this thesis will essentially be multi-dimensional versions of the above equation, with additional transitions between the states other than just births and deaths. Exact solutions of Master Equations can rarely be found. As one might expect, solving them numerically is also impractical as the number of possible states increases. Hence, it is often necessary to consider some form of approximation. In the Kramers-Moyal approximation, we introduce a (large) extensive parameter N and a new variable $x = M/N$ (N in our systems is typically the maximum population size). We also introduce the variable $y = x' - x$, (where $x' = M'/N$), and define $T^*(y,x) = T(x+y|x)$. Then the above master equation becomes

$$\frac{\partial \mathbb{P}_x}{\partial t} = \int \left(T^*(y, x-y)\,\mathbb{P}_{x-y} - T^*(y,x)\,\mathbb{P}_x\right) dy. \tag{2.6}$$

As N increases, the size of the jumps of the birth process (here they are y) become infinitesimal compared to our population variable x, so we treat it as a continuous variable. We can then do a Taylor expansion of the terms on the right hand side to obtain

$$\frac{\partial \mathbb{P}_x}{\partial t} = \int \left(\sum_{i=1}^{\infty} \frac{(-y)^i}{i!} \frac{\partial^i}{\partial x^i} [T^*(y,x)\,\mathbb{P}_x] \right) dy \tag{2.7}$$

$$= \sum_{i=1}^{\infty} \frac{(-1)^i}{i!} \frac{\partial^i}{\partial x^i} [A_i(x)\,\mathbb{P}_x], \tag{2.8}$$

where $A_i(x) = \int y^n T^*(y,x) dy$. By truncating this after the second term, we obtain the Fokker-Planck equation. This Fokker-Planck equation then has a unique Langevin equation associated with it, as we shall see later.

Simply speaking, a Langevin equation can be described as an ODE in which a

random function of time appears. It is commonly written in the form:

$$\frac{dx}{dt} = a(x,t) + b(x,t)\xi(t) \tag{2.9}$$

where $\xi(t)$ is the random term. Furthermore we require $\langle \xi(t) \rangle = 0$ (that its expectation is zero) and $\langle \xi(t)\xi(t') = \delta(t-t')$ (that it has no correlation between different times). For this equation to make sense, the equation must be in some way integrable, leading us to the concept of a stochastic integral. By assuming that the integral of ξ is continuous and using the properties of ξ listed, we are able to show that its integral can be interpreted as the Wiener process. (Hence we use the formulation of the SDE as $dx = a(x,t)dt + b(x,t)dW(t)$ interchangeably.)

Next, we need to establish the properties of this integral. The most common form of stochastic integral is the Itō integral, which is a generalization of a Riemann-Stieltjes integral. That is, in order to compute the stochastic integral $\int_{t_0}^{t} G(t')dW(t')$, we first divide the interval $[t_0, t]$ into n subintervals. Say we choose partioning points $t_0, \ldots, t_n$ such that $t_0 \leq t_1 \leq \cdots \leq t_n \leq t$, then the Itō stochastic integral is defined as the limit of the partial sums:

$$\int_{t_0}^{t} G(t')dW(t') = \text{ms} - \lim_{n\to\infty} \left(\sum_{i=1}^{n} G(t_{i-1})[W(t_i) - W(t_{i-1})] \right), \tag{2.10}$$

where by ms-lim we mean the mean square limit. Using this definition of the integral, we are able to perform various computations. This Itō calculus obeys different rules from normal calculus; in particular, a key formula is the Itō-Döblin Theorem, also known as Ito's lemma. For a general one-dimensional Itō drift-diffusion process

$$dX_t = A(X)dt + B(X)dW \tag{2.11}$$

and for $f(t, X)$ a twice differentiable function of t and x,

$$df = [\partial_t f + A(X)\partial_X f + \frac{B}{2}\partial_X^2 f]dt + B\partial_X f\, dW\,. \tag{2.12}$$

It is possible to manipulate the above relationship and integrate by parts to show that the PDF of X must evolve according to

$$\partial_t \mathbb{P}(X,t) = -\partial_X A(X)\,\mathbb{P} + \frac{1}{2}\partial_X^2[B(X)^2\,\mathbb{P}], \tag{2.13}$$

which must therefore be the Fokker-Planck equation for the system.

However, there are other possible formulations of the stochastic integral. If for each subinterval in $[t_0, t]$ we choose an intermediate point $\tau_i = \alpha t_i + (1-\alpha)t_{i-1}$ for $\alpha \in [0,1)$, and take the integral to be given by

$$\int_{t_0}^{t} G(t')dW(t') = \text{ms} - \lim_{n\to\infty}\left(\sum_{i=1}^{n} G(\tau_i)[W(t_i) - W(t_{i-1})]\right), \tag{2.14}$$

then we have a family of integrals parametrized by α. (The Itō integral defined earlier sets $\alpha = 0$.) For example, a common alternative to the Itō integral is the Stratonovich integral which is given by $\alpha = 1/2$. It is possible to convert between the Itō and Stratonovich formuations - if some process $X(t)$ is a solution of the Itō SDE $dX = adt + bdW(t)$, then it is also a solution of the Stratonovich SDE $dX = (a = \frac{1}{2}b\partial_x b)dt + b \circ dW$. In fact it is often convenient to convert between the two formulations, as the rules for a change of variables in the Stratonovich calculus are the same as normal calculus. An important point to note is that in the definition above of the Stratonovich integral, the final term in the series has a dependence on t, and is therefore not non-anticipating; the non-anticipating property of the Itō integral is important not just from an intuitive standpoint but also because various theoretical properties of the Itō calculus derive from it. However, in the physical sciences, the Stratonovich formulation of the integral often arises naturally. In this thesis, we follow an approach taken in the physical sciences and treat extrinsic sources of noise in the sense of Stratonovich, rather than the sense of Itō. This is not because we consider our systems to be "anticipatory", but rather to reflect the fact that noise in real systems often has a small but nonzero correlation time τ_η. One can therefore envision that each realization of the noise is a solution of a zero-mean Ornstein-Uhlenbeck process with that correlation time:

$$\tau_\eta d\eta = -\eta dt + dW^*, \tag{2.15}$$

where dW^* is a Brownian motion. It is known that as $\tau_\eta \to 0$ the Ornstein-Uhlenbeck process η approaches white noise in the sense of Stratonovich [133, 5]. This is somewhat similar to the elimination of fast variables from a system - a relevant discussion in systems similar to those discussed here is in [123]. Another reason that we switch between different formulations of the stochastic integral in this thesis is that the Euler-Maruyama scheme for numerically simulating a SDE demands

that it be in Itō form. In this scheme, to simulate an SDE

$$dX = a(X)dt + b(X)dW \tag{2.16}$$

by a sequence y_n at points in time $\tau_n = n\tau$ (so τ is our mesh size in time), we set:

$$y_{n+1} = y_n + a(y_n)\tau + b(y_n)\delta W_n, \tag{2.17}$$

where we draw the δW_n from a normal distribution with mean 0 and variance τ since one of the properties of a Wiener process is that $\langle dW(t)^2 \rangle = dt$. It can be shown that this simple algorithm has an order of strong convergence $\tau^{1/2}$ and an order of weak convergence τ^1. The order of strong convergence tells us about how close our stochastic simulations are to the trajctories of the SDEs, while the order of weak convergence is a measure of how close the averages of functions of our stochastic simulations are to the averages of functions of the SDEs. In this thesis we mostly consider averages, and hence considering the order weak convergence is sufficient; in any case the precise trajectory of a given Wiener process used to generate a realisation is unknowable.

For example, another common algorithm used is the Milstein method, which improves the order of strong convergence but has the same order of weak convergence. Further higher-order methods have been developed, such as those listen in [93]. However, as shown in [23], it is non-trivial to create stochastic extensions of famous numerical algorithms for solving ODEs. In that paper, the authors carefully develop a stochastic equivalent to the Runge-Kutta method. However, as we are only interested in considering the averages of our quantities over long periods of time, we decline to use such high-order methods for simplicity. Besides the additional complexity and number of operations required to implement higher-order methods, some of them, such as stochastic Runge-Kutta methods, require the stochastic increment to be evaluated at half-steps - which would be equivalent (in terms of computational effort) to running the Euler algorithm on a mesh twice as fine. As such, we choose to use our computational power on running Euler algorithms on finer meshes, sampling the parameter space more, and running more realizations for our simulations.

2.2 Phase reduction method

In this thesis, we will consider population models which are described by a pair of ODEs. In order to understand their synchronization, and to consider large ensembles of populations, it is necessary to simplify our situation by representing each oscillator by a single phase variable. This will also enable one to extend the methods described here to more complicated systems with larger numbers of ODEs describing each population. For example, this would be necessary in order to consider ecological webs with large numbers of species, or perhaps even structured populations of a single species.

In the later chapters of this thesis, we will study the bifurcations of our models and find parameter regimes in which they exhibit large-amplitude limit cycle oscillations. For these limit cycle oscillators, we make the key assumption that the perturbations due to noise (or coupling) are weak enough for us to assume that the trajectories of the system remain close to the original limit cycle. This will allow us to use a phase reduction method, following the approach of [97, 84, 74, 36, 66]. In practice, the allowable size of perturbations to the limit cycle depends on how attracting the limit cycle is as well as the presence of other critical points. The models we will consider here have strongly attracting limit cycles which are the only stable solutions, so noise and/or coupling can be relatively large. This is further verified when we run stochastic simulations and observe that the trajectories always return to a vicinity of the limit cycle. (There has been work on certain systems where it is possible to extend the analysis to a regime where perturbations are strong enough to cause the system to move far away from the limit cycle - for example, in [13, 14], integrate-and-fire neurons were studied where the coupling changed the fundamental behaviour of the system. Introducing correlated noise in such a regime would be an interesting direction for future work but is nontrivial in general.)

Mathematically, we outline the phase reduction method as follows. Starting with a general dynamical system $\dot{\mathbf{X}} = \mathbf{F}(\mathbf{X}(t))$, we assume it has an underlying attracting limit cycle $\mathbf{X}_0$ such that $\mathbf{X}_0(t) = \mathbf{X}_0(t + nT)$ for all integers n, where T is the period of the limit cycle. Hence we can associate a phase $\theta(t) \in [-\pi, \pi)$ with the limit cycle, and arbitrarily set $\theta = 0$ somewhere on the limit cycle. (In oscillators modelling a single neuron, $\theta = 0$ is often set at the time of the spike, but there is no equivalent in population oscillators.) As such, the individual dynamics of an oscillator in the absence of external influences simply reduces to $\dot{\theta} = \omega$,

where $\omega = 2\pi/T$ is the natural frequency of the oscillator. Now the phase reduction method exploits the observation that the notion of phase can be extended into a neighbourhood $M \subset \mathbb{R}^2$ of a limit cycle - that is, there exists an isochronal mapping $\Theta : M \to [-\pi, \pi)$ with $\theta = \Theta(\mathbf{X})$.

In order to define the concept of an isochron, we start by considering a point $\mathbf{x}_0 \in M$ but not on the limit cycle $\mathbf{x}^*(t)$. Then there exists an asymptotic phase $\theta(\mathbf{x}_0)$ such that the trajectory $\mathbf{x}(t)$ starting from the point $\mathbf{x}_0$ satisfies

$$\lim_{t\to\infty} |\mathbf{x}(t) - \mathbf{x}^*(t + \theta(\mathbf{x}_0))| = 0$$

and we can loosely define an isochron as the collection of points in M with the same associated θ.

From this, we can see that weak perturbations change the phase of an oscillator by moving its trajectory from one isochron to another. This brings us to the crucial concept of a phase response (or resetting) curve (PRC). Consider a perturbation $\mathbf{x}$ with at least one non-zero component transverse to the limit cycle (perturbations parallel to the limit cycle result in a change of phase exactly equal to the size of the perturbation). This pushes the trajectory off the limit cycle, but if $\mathbf{x}$ is sufficiently small (in practice, depending on the stability of the system, $\mathbf{x}$ can be quite large), the trajectory is merely pushed onto a different isochron, and returns to the limit cycle with a change of phase. That is, $\theta(\mathbf{x}^* + \mathbf{x})$ is still defined, where the point $\mathbf{x}^*$ is on the limit cycle. Hence, we can associate with the perturbation $\mathbf{x}$ to the point $\mathbf{x}^*$ the change in phase $\Delta(\mathbf{x}, \mathbf{x}^*) = \Theta(\mathbf{x}^* + \mathbf{x}) - \Theta(\mathbf{x}^*)$, and we define the phase response curve $\mathbf{Z}$ such that:

$$Z_i(t) = \lim_{x_i \to 0} \frac{\Delta(x_i, \mathbf{x}^*(t))}{x_i}. \tag{2.18}$$

Hence, recalling the definition of the derivative:

$$\mathbf{Z} = \nabla_{\mathbf{x}} \Theta|_{\mathbf{x}=\mathbf{x}^*(\theta)}. \tag{2.19}$$

Given that the required function $\mathbf{Z}$ is the infinitesimal limit of how the phase of the oscillator changes with respect to perturbations, we are left with the problem of evaluating it. The original use of phase response curves was in the study of systems such as spiking neurons [36] and circadian rhythms [25], where there was often an event occuring (such as a neuron firing) that was of interest at a certain point along the limit cycle. Hence, experimentally, phase response curves were calculated by perturbing the system, then measuring the delay or the acceleration

to the event in question. However, there is a more elegant way of calculating $\mathbf{Z}$, attributed to Malkin in [66].

We start by defining the operator $\mathcal{L}$ such that

$$(\mathcal{L}\mathbf{x})(t) \equiv \frac{d\mathbf{x}}{dt} - D_{\mathbf{x}}\mathbf{F}(\mathbf{x})|_{\mathbf{x}^*(t)} \cdot \mathbf{x}, \tag{2.20}$$

that is, the linearization of the system around the limit cycle. Then the adjoint L^* (with respect to the standard inner product on T-periodic functions in $\mathbb{R}^n$) is given by

$$(\mathcal{L}^*\mathbf{y})(t) = -\frac{d\mathbf{y}}{dt} - [D_{\mathbf{x}}\mathbf{F}(\mathbf{x})|_{\mathbf{x}^*(t)}]^T \cdot \mathbf{y}. \tag{2.21}$$

It can then be shown that $\mathbf{Z}$ is the unique solution of

$$\mathcal{L}^*\mathbf{Z} = 0 \tag{2.22}$$

$$\mathbf{Z} \cdot \frac{d\mathbf{x}^*}{dt} = \omega, \tag{2.23}$$

where ω is the frequency and is defined as $2\pi/T$ where T is the period of the limit cycle.

In most cases Z has to be evaluated numerically. As the dynamical system has a stable limit cycle, all of its Floquet exponents are negative except one which is zero (corresponding variations along the limit cycle itself). As such the Floquet exponents of the adjoint equation (2.22) are all positive except one which is zero. Integrating backwards in time dampens out the positive multipliers and gives us the periodic solution we require corresponding to the zero multiplier.

Using the phase response curve Z to quantify how the phase of an oscillator responds to a perturbation now allows us to consider phase synchronization. This approach does have its limitations - for example, we are unable to look at perturbations large enough to move the system far from the limit cycle. As such, in this thesis, we are unable to examine stochastic extinctions, or systems in which there are multiple stable states. These may be studied with other methods, or complex refinements of those presented here. For instance, one could potentially extend the methods here to dynamical systems with two stable limit cycles separated by an unstable limit cycle. However, in this thesis, we focus our attention on applying our techniques to the study of noise-induced phase synchronization to strongly attracting oscillators.

2.3 Noise-induced phase synchronization

The idea of noise-induced phase synchronization is relatively new [97] and counter-intuitive; it tells us that a group of oscillators can be synchronized merely by the effect of a common stochastic signal, without any need for coupling or peridiocitiy in the signal. In this section we outline the general theory for an ensemble of oscillators with correlated and uncorrelated noise; in the next chapters we shall proceed to illustrate its novel applications in terms of our ecological and neurobiological models.

Consider a group of M identical limit cycle oscillators in $\mathbb{R}^N$. In the absence of noise, their behaviour can be described by M N-dimensional ODEs of the form:

$$\frac{d\,\mathbf{x}^{(i)}}{dt} = \mathbf{F}(\mathbf{x}^{(i)}), \tag{2.24}$$

where we have labeled the oscillators by $i = 1,\ldots,M$. In order to illustrate the general idea we add correlated Stratonovich noise of strength σ and uncorrelated Stratonovich noise of strength ϵ to the first variable of each oscillator, so that

$$\frac{d\,\mathbf{x}^{(i)}}{dt} = \mathbf{F}(\mathbf{x}^{(i)}) + \sigma\,\mathbf{e}_1\,\xi(t) + \epsilon\,\mathbf{e}_1\,\xi^{(i)}(t), \tag{2.25}$$

where $\mathbf{e}_1$ is the vector $(1,0,\ldots,0)^T$, ξ is a Stratonovich noise of unit intensity added to each oscillator, and $\xi^{(i)}$ also a Stratonovich noise of unit intensity but unique to the ith oscillator. Assuming we have used the techniques from the previous section to evaluate a phase response curve $\mathbf{Z}$, we can perform a phase reduction to obtain SDEs describing the time-evolution of the phases of the oscillators:

$$d\Theta_i = \omega dt + \epsilon Z_1(\Theta_i) \circ dW_i + \sigma Z_1(\Theta_i) \circ dW, \tag{2.26}$$

where Z_1 is the 1st component of the PRC, dW is the common noise signal added to all the oscillators, dW_i is the uncorrelated independent noise added to each one, and θ is taken to be 2π-periodic. As we expect, in the absence of noise, each oscillator simply oscillates at its natural frequency ω.

There have been various studies of the precise form of noise to be used in various systems [123, 73]. For example, in [123], the authors consider a general dynamical system similar to ours driven by an Ornstein-Uhlenbeck process with a finite correlation time. They explicitly introduce another time constant, $\tau_\wp$, representing the amplitude-relaxation time of the limit cycle (corresponding to how

attracting the limit cycle is). By performing a careful change of variables to a phase-amplitude system, they show that the precise form of a phase reduction depends on the ratio of the time constants $\tau_\jmath$ and $\tau_\wp$. In our case, as our limit cycles are very stable to perturbations away from the limit cycle, we are able to assume that $\tau_\jmath \gg \tau_\wp$, for which their results indicate that the correct phase reduction is the one we have carried out above.

Moreover, here we are interested in the synchronization of oscillators, which we shall study through the phase difference between them. In the analysis presented here, we shall see that the difference in choices of how to interpret the forms of noise merely lead to correction terms on the order of the square of the noise strength and do not affect our final results qualitatively. This is further verified by recent research on colored noise [75] as well as our work in [16]. There we consider a pair of coupled Rosenzweig-Macarthur systems, and carry out analysis as described in chapter five; however, in that publication we follow the approach of [38] and drive our system with partially correlated Itō noise instead. The fact that our results are qualitatively identical show that the principles discussed in this thesis are independent of the form of noise present in the system, and hence are applicable to a wide variety of biological systems.

Returning to our system, the above set of SDEs (2.26) are being treated in the sense of Stratonovich. In order to apply the Itō-Döblin lemma to look for a PDF of our ensemble, we must first convert them into Itō SDEs:

$$d\Theta_i = [\omega - \frac{\epsilon^2+\sigma^2}{2} Z_1(\Theta_i)Z_1'(\Theta_i)]dt + \epsilon Z_1(\Theta_i)dW_i + \sigma Z_1(\Theta_i)dW. \tag{2.27}$$

In order to look for the corresponding FPE describing the PDF of the ensemble, we write the SDEs in a more compact form:

$$d\Theta_i = \mathcal{A}(\Theta_i)dt + d\zeta_i(\mathbf{\Theta}, t), \tag{2.28}$$

where now $\mathbf{\Theta} = (\Theta_1, \ldots, \Theta_M)$, $\mathcal{A}(\Theta_i) = \omega - \frac{1}{2}Z_1(\Theta_i)Z_1'(\Theta_i)$ and $d\zeta_i(\mathbf{\Theta}, t) = \epsilon Z_1(\Theta_i)dW_i + \sigma Z_1(\Theta_i)dW$, so that $(\zeta_1, \ldots, \zeta_M)$ are a set of correlated Wiener processes with

$$\begin{aligned} \langle d\zeta_i \rangle &= 0 \\ \langle d\zeta_i d\zeta_j \rangle &= [\epsilon^2 Z_1(\Theta_i)Z_1(\Theta_j)\delta_{i,j} + \sigma^2 Z_1(\Theta_i)Z_1(\Theta_j)]dt. \end{aligned}$$

(The fact that for a Gaussian distribution, all higher order moments are expressible in terms of those of order 1 and 2 allows us to fully characterise our Wiener

processes with just the above information.)

Here we note that the multi-dimensional form of the Itō-Döblin Theorem states that for a general Itō drift-diffusion process

$$d\mathbf{X}_t = \mathbf{A}(\mathbf{X})dt + \mathcal{B}(\mathbf{X})d\mathbf{W}, \tag{2.29}$$

where $\mathcal{B}$ denotes a square matrix, $d\mathbf{W}$ is a vector of Wiener processes, and for $f(t,\mathbf{X})$ a twice differentiable function of t and $\mathbf{X}$,

$$df(\mathbf{X}) = \left[\sum_i A_i(\mathbf{X})\partial_{\mathbf{X}_i} f + \frac{1}{2}\sum_{i,j}[\mathcal{B}\mathcal{B}^T]_{ij}\partial_{\mathbf{X}_i}\partial_{\mathbf{X}_j} f\right]dt + \sum_{i,j}\mathcal{B}_{ij}\partial_{\mathbf{X}_i} f\, d\mathbf{W}_j\,. \tag{2.30}$$

Hence we can obtain the Fokker-Planck equation for the probability distribution of the oscillators:

$$\frac{\partial \mathbb{P}(\boldsymbol{\theta},t)}{\partial t} = -\sum_{i=1}^{M}\frac{\partial}{\partial\theta_i}[\mathcal{A}(\boldsymbol{\theta})\mathbb{P}(\boldsymbol{\theta})] + \frac{1}{2}\sum_{i=1}^{M}\sum_{j=1}^{M}\frac{\partial^2}{\partial\theta_i\partial\theta_j}[C(\boldsymbol{\theta})\mathbb{P}(\boldsymbol{\theta},t)], \tag{2.31}$$

where $C(\boldsymbol{\theta})$ is the equal-time correlation matrix given by $C_{i,j}(\boldsymbol{\theta})dt = \langle d\zeta_i d\zeta_j\rangle$. Having obtained this FPE, we carry out the averaging procedure as described in [97]: we note the effect of noise on the phase is small compared to the natural frequency ω for small ϵ and σ. As such, we convert our phase variables to slow time variables $\phi_i = \theta_i - \omega t$ - here ϕ_i now represents the deviation of the phase from the default ωt due to the weak noise, and hence we expect them to change much more slowly than the variables θ.These new variables have a corresponding PDF $Q(\boldsymbol{\phi},t) = \mathbb{P}(\omega t + \theta_i, t)$ with a corresponding FPE:

$$\frac{\partial Q(\boldsymbol{\phi},t)}{\partial t} = -\sum_{i=1}^{M}\frac{\partial}{\partial\phi_i}[(\mathcal{A}(\boldsymbol{\phi}+\omega t)-\omega)Q(\boldsymbol{\phi})] + \frac{1}{2}\sum_{i=1}^{M}\sum_{j=1}^{M}\frac{\partial^2}{\partial\phi_i\partial\phi_j}[C(\boldsymbol{\phi}+\omega t)Q(\boldsymbol{\phi},t)]. \tag{2.32}$$

Q is slowly varying so we can average the effect of the noise over a whole limit cycle of length $2\pi/\omega$. Thus we make the assumption that we can approximate the terms $(\mathcal{A}(\boldsymbol{\phi}+\omega t)-\omega t)$ and $C(\boldsymbol{\phi}+\omega t)$ by their time-averaged counterparts $\bar{\mathcal{A}}(\boldsymbol{\phi})$ and

$\bar{C}(\boldsymbol{\phi})$. These are defined as:

$$\begin{aligned}\bar{\mathcal{A}}(\phi_i) &= \frac{1}{T}\int_t^{t+T} \mathcal{A}(\phi_i+\omega s)-\omega ds \\ &= \frac{1}{T}\int_t^{t+T} \frac{1}{2}Z_1(\phi_i+\omega s)Z_1'(\phi_i+\omega s)ds \\ &= \frac{1}{T}[Z_1(\phi_i+\omega s)^2]_{s=t}^{s=t+T} = 0 \end{aligned} \tag{2.33}$$

by the periodicity of our phase response curve Z; and

$$\bar{C}_{ij}(\boldsymbol{\phi},t) = \frac{1}{T}\int_t^{t+T} \epsilon^2 Z_1(\phi_i+\omega s)Z_1(\phi_j+\omega s)\delta_{i,j}+\sigma^2 Z_1(\phi_i+\omega s)Z_1(\phi_j+\omega s)ds. \tag{2.34}$$

Noting that the period $T = 2\pi/\omega$:

$$\begin{aligned}\bar{C}_{ij}(\boldsymbol{\phi},t) &= \frac{1}{2\pi}\int_0^{2\pi} \epsilon^2 Z_1(s')Z_1(s'+(\phi_j-\phi_i))\delta_{i,j}+\sigma^2 Z_1(s')Z_1(s'+(\phi_j-\phi_i))ds' \\ &= \sigma^2 g(\phi_i-\phi_j)+\epsilon^2 g(0)\delta_{i,j}, \end{aligned} \tag{2.35}$$

where we have defined the function g as:

$$g(\phi) := \frac{1}{2\pi}\int_{-\pi}^{\pi} Z_1(s)Z_1(\phi+s)ds. \tag{2.36}$$

This gives us an averaged FPE for $Q(\boldsymbol{\phi},t)$:

$$\frac{\partial Q(\boldsymbol{\phi},t)}{\partial t} = \frac{1}{2}\sum_{i=1}^{M}\sum_{j=1}^{M}\frac{\partial^2}{\partial\phi_i\phi_j}C(\bar{\boldsymbol{\phi}},t)Q(\boldsymbol{\phi},t). \tag{2.37}$$

Unlike in the Kuramoto model of synchronized oscillators, there is no easy way here to decouple an individual oscillator from the ensemble by defining a suitable order parameter. Hence, analysis of a full M-oscillator system is non-trivial and a potential area of future work - we discuss this in the concluding section of the thesis. For tractability, we now focus on a pair of oscillators, as in [97, 84]. This means we set $M = 2$ in Equation 2.37 to obtain:

$$\frac{\partial Q(\phi_1,\phi_2,t)}{\partial t} = \frac{(\epsilon^2+\sigma^2)g(0)}{2}\left[\left(\frac{\partial^2}{\partial\phi_1^2}\right)+\left(\frac{\partial^2}{\partial\phi_2^2}\right)\right]Q+\sigma^2\frac{\partial^2}{\partial\phi_1\partial\phi_2}[g(\phi_1-\phi_2)Q]. \tag{2.38}$$

The quantity of interest here is the phase difference between two oscillators, as its

behaviour is an indication of whether synchronization occurs. As such, we change variables to the mean and difference of the two phases - $\lambda = (\phi_1+\phi_2)/2$, $\phi = \phi_2-\phi_1$. This gives us expressions for the derivatives of the form

$$\begin{aligned}\frac{\partial^2}{\partial\phi_1^2} &= \frac{1}{4}\frac{\partial^2}{\partial\lambda^2} - \frac{\partial^2}{\partial\lambda\partial\phi} + \frac{\partial^2}{\partial\phi^2}\\ \frac{\partial^2}{\partial\phi_2^2} &= \frac{1}{4}\frac{\partial^2}{\partial\lambda^2} + \frac{\partial^2}{\partial\lambda\partial\phi} + \frac{\partial^2}{\partial\phi^2}\\ \frac{\partial^2}{\partial\phi_1\partial\phi_2} &= \frac{1}{4}\frac{\partial^2}{\partial\lambda^2} - \frac{\partial^2}{\partial\phi^2}.\end{aligned}$$

Substituting these into Equation (2.38) yields:

$$\begin{aligned}\frac{\partial Q(\lambda,\phi,t)}{\partial t} &= \frac{(\epsilon^2+\sigma^2)g(0)}{4}\left[(\frac{\partial^2}{\partial\lambda^2}) + 4(\frac{\partial^2}{\partial\phi^2})\right]Q\\ &\quad + \frac{\sigma^2}{4}\left[(\frac{\partial^2}{\partial\lambda^2}) - 4(\frac{\partial^2}{\partial\phi^2})\right][g(\phi)Q].\end{aligned} \tag{2.39}$$

Looking for separable solutions of the form

$$Q(\phi_1,\phi_2,t) = \Lambda(\lambda,t)\Phi(\phi,t) \tag{2.40}$$

gives us:

$$\begin{aligned}\Phi\frac{\partial\Lambda}{\partial t} + \Lambda\frac{\partial\phi}{\partial t} &= \frac{(\epsilon^2+\sigma^2)g(0)}{4}\left[\Phi\frac{\partial^2\Lambda}{\partial\lambda^2} + 4\Lambda\frac{\partial^2\Phi}{\partial\phi^2}\right] + \frac{1}{4}\sigma^2 g(\phi)\Phi\frac{\partial^2\Lambda}{\partial\lambda^2}\\ &\quad -\sigma^2\Lambda\frac{\partial^2}{\partial\phi^2}[g(\phi)\Phi],\end{aligned} \tag{2.41}$$

since Λ is independent of ϕ and Φ is independent of λ. Holding λ constant while varying ϕ, and *vice versa*, gives us a pair of PDEs:

$$\frac{\partial\Lambda}{\partial t} = \frac{1}{4}[(\epsilon^2+\sigma^2)g(0) + \sigma^2 g(\phi)]\frac{\partial^2\Lambda}{\partial\lambda^2} \tag{2.42}$$

$$\frac{\partial\Phi}{\partial t} = \frac{\partial^2}{\partial\phi^2}[(\sigma^2+\epsilon^2)g(0) - \sigma^2 g(\phi)]\Phi. \tag{2.43}$$

But, looking at Equation (2.42), Λ is independent of ϕ as we are looking for separable solutions. Thus we must have $\frac{\partial^2\Lambda}{\partial\lambda^2} = 0$. Since we are interested in looking for a synchronized steady-state, we set $\partial\Lambda/\partial t = \partial\Phi/\partial t = 0$ and look for time-

independent solutions Λ_0 and Φ_0, which gives us a pair of ODEs. For Λ_0:

$$\frac{d^2\Lambda_0}{d\lambda^2} = 0. \tag{2.44}$$

This means that our solution for Λ_0 must be linear or uniform. As we are looking for 2π-periodic solutions, we can exclude the linear solution. Hence we have

$$\Lambda_0(\lambda) = \frac{1}{2\pi} \tag{2.45}$$

after normalizing. For Φ_0:

$$\begin{aligned} \frac{d^2}{d\phi^2}[\sigma^2(g(0) - g(\phi)) + \epsilon^2 g(0)]\Phi_0 = 0 \\ \frac{d}{d\phi}[\sigma^2(g(0) - g(\phi)) + \epsilon^2 g(0)]\Phi_0 = \Gamma_1, \end{aligned} \tag{2.46}$$

where Γ_1 is a constant of integration. Integrating up again:

$$\Phi_0 = \frac{\Gamma_0 + \Gamma_1\phi}{\sigma^2(g(0) - g(\phi)) + \epsilon^2 g(0)}, \tag{2.47}$$

where Γ_0 is a constant of integration. Since g is periodic (from its definition), and Φ_0 must be periodic, enforcing the condition $\Phi_0(-\pi) = \Phi_0(\pi)$ gives us $\Gamma_1 = 0$. This means that:

$$\Phi_0(\phi) = \frac{\Gamma_0}{\sigma^2(g(0) - g(\phi)) + \epsilon^2 g(0)}, \tag{2.48}$$

where we can evaluate our normalization constant as

$$\Gamma_0 = [\int_{-\pi}^{\pi} \frac{ds}{\sigma^2(g(0) - g(s)) + \epsilon^2 g(0)}]^{-1}$$

since Φ_0 is a probability distribution function.

A number of general results immediately follow from the form of the steady-state distribution $\Phi_0(\phi)$ for the phase difference ϕ of two oscillators. First, in the absence of a common extrinsic noise source ($\sigma = 0$) and $\epsilon > 0$, $\Phi_0(\phi)$ is a uniform distribution, which means that the oscillators are completely desynchronized. This agrees with our intuition regarding uncoupled oscillators given uncorrelated noise, since there is no source of synchrony in the system in this case.

On the other hand, when $\epsilon \to 0$ the independent noise source vanishes. The distribution $\Phi_0(\phi)$ then diverges at $\phi = 0$ while keeping positive since it can be

shown that $g(0) \geq g(\phi)$ from the periodicity of Z_1. Hence, the phase difference between any pair of oscillators accumulates at zero, resulting in complete noise-induced synchronization (at least as time $\to \infty$ - time taken to synchronization is explored briefly in later sections).

One way to estimate the degree of synchrony is to Taylor expand $g(\phi)$ to second order in ϕ. We see that, in a neighbourhood of the maximum at $\phi = 0$, we can approximate $\Phi_0(\phi)$ by the Cauchy distribution

$$\Phi_0(\phi) \approx \frac{\Gamma_2}{\phi^2\sigma^2|g''(0)|/2 + \epsilon^2 g(0)}$$

for an appropriate normalization constant Γ_2. Thus the degree of broadening depends on the ratio

$$\Delta = \frac{\epsilon^2 g(0)}{\sigma^2|g''(0)|}.$$

As such, uncorrelated noise broadens the distribution of phase differences. By carefully considering individual-level models, we will be able to show in later chapters that in our population oscillators, the system size is related to the strength of uncorrelated noise by $N = \epsilon^{-1/2}$. This tells us that for large numbers of organisms or neurons in each of our oscillators, we should be able to see clear noise-induced synchronization occurring, while at lower values of the population, the fundamentally noisy nature of our oscillators obscures this effect, decreasing the overall synchrony. This leads us to suggest that experimental verification of our theories could be accomplished by obtaining data from predator-prey populations of different sizes, for instance, zooplankton-phytoplankton ecosystems grown in stock tanks of different sizes. However, keeping all other parameters the same while varying the sizes of such populations could be a challenge.

Having established the mathematical toolbox necessary, in the subsequent chapters, we show how applying this theory of noise-induced synchronization to our biological models provides novel ways of explaining long-studied synchronization phenomena. We also look at the effect of intrinsic noise on this synchrony. In the following sections, we will start with individual-level models in order to calculate how exactly this intrinsic noise can be captured when one moves to population-level modelling. This will also give us clues as to how exactly extrinsic sources of noise may affect the system, for example, by altering transition rates in a probabilistic individual-level model.

Chapter 3

Uncoupled ecological populations

3.1 Ecological oscillators, metapopulations and the Moran effect

In ecology, the cause of the rise and fall of population levels over time has been one of the most basic questions - especially in exploiter-victim or predator-prey ecosystems, which are one of the most fundamental and striking situations in which such oscillations appear. In the early part of the 20th century, the Lotka-Volterra equations were formulated:

$$\begin{aligned} \frac{dx}{dt} &= x(\alpha - \beta y) \\ \frac{dy}{dt} &= -y(\gamma - \delta x) \end{aligned} \tag{3.1}$$

where x and y represent the prey and predator populations respectively. Essentially the prey reproduce exponentially with rate α and are consumed by the predators with a rate proportional to the size of their populations and a coefficient β. Meanwhile, the predators reproduce with a rate proportional to the amount of food (prey) available and with coefficient δ; they also die of natural causes with rate γ. This simple model exhibits oscillatory solutions and is still taught in most mathematical ecology courses. However, it has a number of flaws and oversimplifications which make it necessary to improve it.

For example, in the absence of predators, the prey grow exponentially to infinity. Moreover, the oscillatory solutions obtained are a family of periodic orbits as opposed to a true limit cycle, meaning that small perturbations cause the system to move from one orbit to another. This is very unrealistic, especially consider-

ing that biological systems are often very noisy. In addition, the orbits often go through periods of extremely low population before recovering, whereas in reality such low population levels would lead to extinction. This has led to several refinements, and (among others), the Rosenzweig-Macarthur and Holling-Tanner models we deal with in this thesis.

Besides these modifications to a predator-prey model, one may also have to take into account spatial factors. For example, there may be situations where it is no longer realistic to model an area as a single population. This may occur when the habitat is broken, for example by impassable terrain, or, more increasingly, by human encroachment into the environment. It may also be that the size of the area is too large for one to assume that the population density is approximately homogeneous. As such, it is often instructive to consider a metapopulation, or ensemble of populations, and attempt to understand the mechanisms underlying its synchronization or desynchronization. This is a crucial factor in conservation because synchrony is strongly correlated with the chances of global extinction [58]. Conversely, synchrony can help to eliminate an outbreak in pest or pathogen control. For example, work on measles has shown that although vaccination reduces the size of an epidemic, it can also desynchronize populations thus promoting persistence [32, 107].

In addition, ecologists have observed a "paradox of enrichment" in some systems. This is where one enriches a system with nutrients, thus moving it into a parameter regime where one would expect large-amplitude oscillations, but these fail to occur. One instance of this was studied in [96] in a Daphnia-algae system (Daphnia being plankton which feed on algae). In this thesis we suggest that such instances may be caused by the population behaving as an ensemble of subpopulations, each of which exhibits limit cycle oscillations, but that are insufficiently synchronized for these oscillations to be observed for the whole system. This could motivate more studies, perhaps involving sampling across multiple locations in a habitat simultaneously - one key problem in ecological research is lack of detailed data.

There are two main mechanisms causing synchrony [82] - dispersal between populations in a constant environment [102, 67, 26], which has been long-studied, as well as isolated patches being driven by common environmental noise, known as the Moran effect [94]. More specifically, the effect refers to the case where correlations between populations are driven by correlations in external environmental variations [63]. Our work on the noise-induced synchronization of a metapopula-

tion of oscillating predator-prey systems is particularly interesting as it allows us to provide a rigorous mathematical explanation behind this effect, which was observed as early as 1953 in Canadian lynx populations. Since then, these have been observed in several species, for example in the context of feral sheep on adjacent Hebridean islands subject to similar climactic conditions but without any migration between them [56, 8]. Similar effects were also found in a study of mink and muskrats in Canada, where the synchronization of populations over large areas was found to be correlated to the climactic data [37].

However, a detailed mechanism behind it is not known - most theoretical studies have been done using statistical tools on linear models. Another hindrance to our understanding of population synchrony is the complex ecological food webs that occur and multiple factor affecting any data collected from the wild. Often only data from one season - corresponding to one point of a population cycle - is available per year, which has biased the literature towards year-on-year autocorrelation models. It was only as recently as 2009 [128] that one was able to obtain experimental evidence of phase-locking in predator-prey cycles caused by dispersal and the Moran effect. In this paper the authors conducted a study of Euplotes-Tetrahymena systems. In order to simulate environmental noise, they randomly varied the temperature of culture jars daily - in tandem for pairs of jars simulating correlated noise and independently for those without. In agreement with our model, the authors find that the Moran effect only causes synchrony when predator-prey oscillations are present, lending weight to our argument that the Moran effect is caused by noise-induced phase synchronization of oscillators. The work presented in this chapter is the first detailed mathematical model to explain this long-observed effect, and provides a theoretical basis for more mathematical approaches to studying ecological systems. Finally, in a later chapter, we will also extend our model to include dispersal, in order to study the competing effects of correlated noise and dispersal between populations.

3.2 Holling-Tanner model

First, let us introduce the predator-prey model used in this chapter. One key assumption in many models is that in the absence of predators, the prey multiply up to a finite maximum determined by resources available, i.e. the "carrying capacity" of the system. This is going to be especially necessary if one envisions that each of the populations we work with here is only one of many in a metapopula-

tion. Hence we require a modification to our Lotka-Volterra equations. The one we consider here was first proposed by Pierre Verhulst in the 19th century as the logistic function:

$$\frac{dx}{dt} = \alpha x(1 - \frac{x}{K}), \tag{3.2}$$

where K here is the carrying capacity of the system. This models sigmoidal growth up to a population K and has been widely used, not just in population biology.

In addition, we introduce the concept of a functional response, or the intake rate of a consumer with respect to food density (here it refers to the rate at which predators consume prey). The Canadian ecologist C.S. Holling classified these into three types. The first type is a linear response which we have already seen in the Lotka-Volterra model. Holling's type II functional response, which we will be using in this thesis, is hyperbolic:

$$p(x) = \frac{mx}{A + x}, \tag{3.3}$$

where m is the maximum rate of predation and A is a constant related to the time required for the predator to locate prey. This was proposed by Holling in 1959 based on field data and the assumption that predators searching for prey and then processing the prey are two different behaviours. Interestingly, this corresponds to Michaelis-Menten enzyme kinetics.

Combining these ideas gives us the Holling-Tanner model:

$$\begin{aligned} \frac{dx}{dt} &= rx(1 - \frac{x}{K}) - \frac{mxy}{A_0 + x} \\ \frac{dy}{dt} &= sy(1 - \frac{hy}{x}), \end{aligned} \tag{3.4}$$

where x and y are the prey and predators as before. In this model, the prey grow logistically with rate r up to a carrying capacity K and are predated upon with a Holling type II functional response, while the predators grow logistically with rate s up to a prey-dependent carrying capacity x/h. (Here h is a constant that tells us how many prey are required to support 1 predator.) In order to consider the effects of noise-induced synchronization, we look for parameter regimes where this system exhibits limit cycle oscillations by examining the stability of its critical points. (There are other methods of looking for limit cycles, for example, using the Poincare-Bendixson theorem.)

3.2.1 Critical points and stability analysis

In analysing this system we follow the approach of [43]. We start by rescaling the equations by $\bar{t} = rt$, $\bar{x} = x/K$, $\bar{y} = my/rK$ and drop the overbars to obtain:

$$\begin{aligned} \frac{dx}{dt} &= x(1-x) - \frac{xy}{a+x} \\ \frac{dy}{dt} &= y(\delta - \frac{\beta y}{x}), \end{aligned} \tag{3.5}$$

with $a = A_0/K$, $\beta = sh/m$, $\delta = s/r$. Note that $a, \beta, \delta > 0$, $x, y \in [0,1]$.

In order to look for the critical points, we set $dy/dt = dx/dt = 0$. Setting $dy/dt = 0$ implies $y = 0$ or $\beta y = \delta x$. Substituting $y = 0$ into $dx/dt = 0$ in turn gives us $x = 0$, $x = 1$, while substituting $y = (\delta/\beta)x$ in gives us a unique solution (x^*, y^*) where x^* is the positive root $\frac{1}{2}(1-a-\frac{\delta}{\beta}+\sqrt{4a+(\frac{\delta}{\beta}+a-1)^2})$ of the quadratic $x^2+(\frac{\delta}{\beta}+a-1)x-a=0$. (The negative root is unphysical, as we require $x, y > 0$ to have positive population sizes.)

Next, we can calculate the Jacobian of the system as

$$J = \begin{pmatrix} 1 - 2x + \frac{ay}{(a+x)^2} & \frac{x}{a+x} \\ \frac{\beta y}{x^2} & \delta - \frac{2\beta y}{x} \end{pmatrix} \tag{3.6}$$

which will allow us to classify the critical points. From this we can see immediately that $(1,0)$ is a saddle point. The treatment of the origin requires more care - in [43] it is shown that it is a saddle by introducing another rescaling $dt/d\tau = x$. At (x^*, y^*), we can simplify to obtain:

$$J|_{(x^*,y^*)} = \begin{pmatrix} 1 - a + (a-2)x^* & \frac{\beta}{\delta}(1-x^*) \\ \frac{\delta}{x^*} & -2\delta \end{pmatrix} \tag{3.7}$$

The dynamics of this system is extremely rich and interesting - for example, there is a range of parameter values for which an unstable limit cycle separates a stable equilibrium and a stable limit cycle. However, we are interested in the parameter regime for which there exists a stable limit cycle around an unstable equilibrium. From [43] we know that as x^* is increased from $\alpha_1 = \frac{1}{4}(1 - a - \delta - \sqrt{a^2 - 6a\delta - 2a + (\delta-1)^2})$ it passes through a Hopf bifurcation, and the stable equilibrium at (x^*, y^*) becomes unstable with a limit cycle around it. Similarly there is another Hopf bifurcation as x^* is decreased from $\alpha_2 = \frac{1}{4}(1 - a - \delta + \sqrt{a^2 - 6a\delta - 2a + (\delta-1)^2})$, giving us a parameter regime with which to work with:

$\alpha_1 < x^* < \alpha_2$.

In the cases in this thesis we will work with $r = 1$, $A_0 = 0.1$, $s = 0.1$, $h = 2$, $m = 3$ and $K = 0.5$ so that $a = 0.2$, $\beta = 1/15$, $\delta = 0.1$, which gives us $\alpha_1, \alpha_2 = \frac{1}{40}(7 \mp \sqrt{33})$, $x^* = \frac{1}{20}(\sqrt{129} - 7)$. However, the results we obtain in later sections are similar for any set of parameters that yield limit cycles. See Figure 3.1 for a bifurcation diagram.

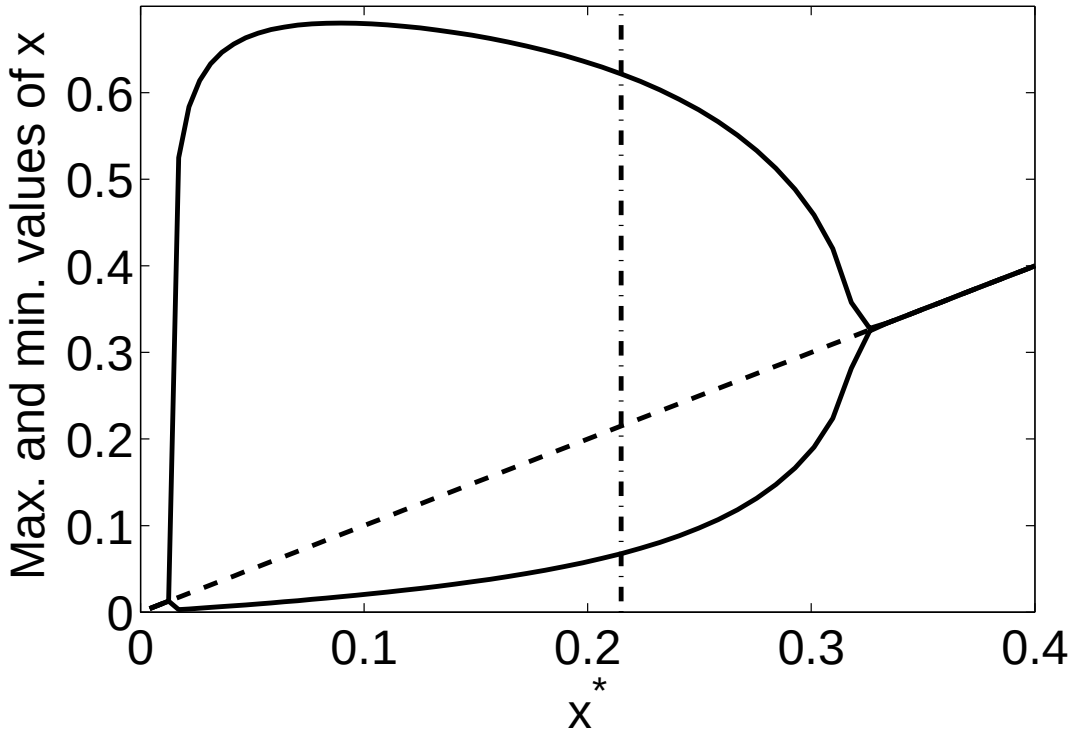

Figure 3.1: Bifurcation diagram for the Holling-Tanner model. Here we kept a and δ constant while varying β. The x-axis is the equilibrium x^* while the y-axis shows the maximum and minimum values of x in the limit cycles where they exist, or x^* when it is the stable equilibrium (it is represented as a dotted line when unstable). The vertical dotted line corresponds to the parameter value $\beta = 1/15$ which is used in later chapters.

3.3 Stochastic urn model of ecological oscillators

Besides the stochasticity induced by environmental fluctuations, we have also mentioned that we would also like to study the effects of intrinsic noise in our model. In this section, we show that by starting with an individual-based model, we are able to characterise this intrinsic noise in terms of noisy perturbations to the ODEs we have just obtained. We proceed along the lines of [91, 92], based on a stochastic urn model. In this type of model a single patch is divided into M plots of equal area, with the plot size chosen to be small enough so that each one contains one prey (species C_1) or one predator (species C_2) or neither (an empty plot denoted by E). This is similar to drawing coloured balls from an urn in textbook examples of probability theory. One then imagines taking all the C_1, C_2 and E from their particular sites and mixing them together into a single patch in which spatial location is ignored. The time evolution of the model is then specified as follows: at each time step randomly select either a single individual or a pair of individuals from the population and implement a set of rules associated with the given model. These rules take the form of state transitions with model-dependent transition rates - and model the interaction of the two individuals. Here, we consider a predator-prey system and follow the approach of [91]. This general stochastic urn model consists of the following processes: birth processes $C_jE \xrightarrow{b_j} C_jC_j$, death processes $C_j \xrightarrow{d_j} E$, intraspecies competition $C_jC_j \xrightarrow{c_j} C_jE$, and predator-prey interactions $C_1C_2 \xrightarrow{p_1} C_2E, C_1C_2 \xrightarrow{p_2} C_2C_2$. Here b_j, d_j, c_j are the birth, death and competition rates, p_1 is the rate of prey consumption due to predation, and p_2 is the growth rate of predators at the expense of prey. Suppose that a pair of constituents is drawn with probability μ and a single constituent is drawn with probability $1-\mu$. We can then write down the following transition rates $T_{r,s}(m,n)$ from state (m,n) to $(m+r, n+s)$:

$$
\begin{aligned}
T_{-1,0}(m,n) &= (1-\mu)d_1 m/N + 2\mu c_1 \eta_{m,m-1} + 2\mu p_1 \eta_{m,n} \\
T_{0,-1}(m,n) &= (1-\mu)d_2 n/N + 2\mu c_2 \eta_{n,n-1} \\
T_{1,0}(m,n) &= 2\mu b_1 \eta_{m,N-m-n} \\
T_{0,1}(m,n) &= 2\mu b_2 \eta_{n,N-m-n} \\
T_{-1,1}(m,n) &= 2\mu p_2 \eta_{m,n},
\end{aligned}
$$

where we have simplified the expressions by introducing $\eta_{n,m} = nm/(N(N-1))$. The master equation for the probability $\mathbb{P}_{m,n}(t)$ that the system consists of m prey and n predators at time t then takes the form

$$\frac{d\,\mathbb{P}_{m,n}}{dt} = \sum_{r,s}\left[T_{r,s}(m',n')\,\mathbb{P}_{m',n'} - T_{r,s}(m,n)\,\mathbb{P}_{m,n}\right] \tag{3.8}$$

with $m' = m-r, n' = n-s$. The first term on the right hand side represents all possible transitions into the state (m,n), while the second term represents all possible transitions out of the state.

Here, we would like to carry out a Kramers-Moyal expansion of the master equation (3.8) [42] as mentioned before. Introduce new variables $x_1 = m/N, x_2 = n/N$ and set $\mathbb{P}_{m,n}(t) = \mathbb{P}(x_1,x_2,t)$. Since as N becomes large, the size of the jumps becomes infinitesimal compared to x_1 and x_2, we can treat them as continuous variables. This allows us to return to our original premise and think about the population sizes in terms of densities within each population.

Taylor expanding each term on the right–hand side of equation (3.8) gives us:

$$\frac{\partial\,\mathbb{P}}{\partial t} = \sum_{i=0}^{\infty}\sum_{j=0}^{\infty}\frac{(-1)^{i+j}}{i!j!}\frac{\partial^{i+j}}{\partial x_1^i\,\partial x_2^j}[\aleph_{i,j}\,\mathbb{P}] - \aleph_{0,0}\,\mathbb{P}, \tag{3.9}$$

where the $\aleph_{i,j}$s are functions of $\mathbf{x}$ that can be determined from the transition rates $T_{r,s}$. Truncating the series after the $1/N$ term yields the Fokker-Planck equation (FPE):

$$\frac{\partial\,\mathbb{P}}{\partial t} = -\sum_{i=1,2}\frac{\partial\,(A_i(\mathbf{x})\,\mathbb{P})}{\partial x_i} + \frac{1}{2N}\sum_{i,j=1,2}\frac{\partial^2\left(G_{ij}(\mathbf{x})\,\mathbb{P}\right)}{\partial x_i\,\partial x_j} \tag{3.10}$$

where $\mathbf{x} = (x_1,x_2)$, $\epsilon = 1/\sqrt{N} \ll 1$,

$$\begin{aligned}
A_1(\mathbf{x}) &= 2b_1x_1(1-x_1-x_2) - 2c_1x_1^2 - d_1x_1 \\
&\quad -2(p_1+p_2)x_1x_2 \\
A_2(\mathbf{x}) &= 2b_2x_2(1-x_1-x_2) - 2c_2x_2^2 - d_2x_2 + 2p_2x_1x_2 \\
G_{11}(\mathbf{x}) &= 2b_1x_1(1-x_1-x_2) + 2c_1x_1^2 + d_1x_1 \\
&\quad +2(p_1+p_2)x_1x_2 \\
G_{22}(\mathbf{x}) &= 2b_2x_2(1-x_1-x_2) + 2c_2x_2^2 + d_2x_2 + 2p_2x_1x_2 \\
G_{12}(\mathbf{x}) &= G_{21}(\mathbf{x}) = -2p_2x_1x_2
\end{aligned} \tag{3.11}$$

We have rescaled the various rates according to $d_k \to (1-\mu)d_k/N$, $b_k \to \mu b_k/(N-1)$, $c_k \to \mu c_k/(N-1)$, $p_k \to \mu p_k/(N-1)$.

3.3.1 Reduction to a Langevin equation

The Fokker-Planck equation describes the evolution of the PDF of the system. However, we would like to compare our system to the mean-field ODEs to ensure agreement in the limit $N \to \infty$, which will allow us to choose parameters for our transition rates. Furthermore, once we obtain the Langevin equation associated with our system, we can proceed to apply the phase reduction method previously discussed, where the noise can now be treated as additional perturbative terms to our differential equation for the phase of the system.

In order to consider the Langevin equation associated with this system, we recall that in section two we had used the Itō-Döblin Theorem to give us the FPE for the evolution of a probability distribution function. Conversely, this theorem also allows us to obtain the unique SDE associated with a given FPE. Here, we first introduce the three stoichiometric vectors $\mathbf{v}_1 = (1,0)^T, \mathbf{v}_2 = (0,1)^T, \mathbf{v}_3 = (-1,1)^T$, which (up to a sign) represent all possible increments in the number of predator and prey induced by single interactions. For example, predation $C_1C_2 \to C_2C_2$ is represented by the stoichiometric vector $(-1,1)^T$. It can then be shown that the solution to the FPE (3.10) determines the probability density function for a corresponding stochastic process $\mathbf{X} = (X_1, X_2)$ that evolves according to an Itō type Langevin equation

$$d\mathbf{X} = \mathbf{A}(\mathbf{X})dt + \frac{1}{\sqrt{N}} \sum_{i=1}^{3} \mathbf{B}^{(i)}(\mathbf{X}) dW_i \tag{3.12}$$

where $\mathbf{A} = (A_1, A_2)^T$. Upon substituting this into the Itō-Döblin Theorem, we find that we require

$$\begin{aligned} \mathbf{B}^{(1)} &= \sqrt{G_{11}(\mathbf{x}) - 2p_2x_1x_2}\,\mathbf{v}_1 \\ \mathbf{B}^{(2)} &= \sqrt{G_{22}(\mathbf{x}) - 2p_2x_1x_2}\,\mathbf{v}_2 \\ \mathbf{B}^{(3)} &= \sqrt{2p_2x_1x_2}\,\mathbf{v}_3 \end{aligned}$$

and here W_i denotes an independent Wiener process such that

$$\begin{aligned} \langle dW_i(t) \rangle &= 0 \\ \langle dW_i(t) dW_j(t) \rangle &= \delta_{i,j} dt \end{aligned}$$

This Langevin equation approximates the effects of demographic noise arising from the finite size N of the local predator–prey population. We can immediately see that this demographic noise takes the form of order $1/\sqrt{N}$ fluctuations about a solution to the ODE $d\mathbf{X}/dt = \mathbf{A}(\mathbf{X})$, which agrees with the literature from chemical master equations. Also note that here we have taken the square roots of terms which are not obviously non-negative; we are able to do so as the procedures we have carried so far guarantee that the matrix G is positive semidefinite.

In order to consider the effects of extrinsic noise on an ensemble of populations, we note that this representation of our system gives us a natural way to include a common extrinsic noise source due to environmental fluctuations as an additional noisy term in our Langevin equations. While our results are not sensitive to the particular form of noise added, for concreteness, suppose that we add a stochastic term to the birth rates b_k. Hence we change it according to $b_k \to b_k + \sigma\xi(t)/2$, where $\xi(t)$ is a white noise term and σ is the strength of environmental noise. (To ensure that the enviromental noise and demographic noise are of similar order, we specify $\frac{1}{N} \ll \sigma \ll 1$.) We can then substitute for b_k in equations (3.10) and (3.11) and expand as before - truncating after $\mathcal{O}(\sigma)$ leads to an additional multiplicative term in the Langevin equation of the form $\sigma\,\hat{\mathbf{B}}(\mathbf{X})dW$, where

$$\hat{\mathbf{B}} = \begin{pmatrix} H_1 \\ H_2 \end{pmatrix} = \begin{pmatrix} b_1 x_1(1 - x_1 - x_2) \\ b_2 x_2(1 - x_1 - x_2) \end{pmatrix}$$

and $dW(t) = \xi(t)dt$ is an additional independent Wiener process, treated in the sense of Stratonovich.

Returning to our system, we can simplify notation by introducing $\epsilon = \frac{1}{\sqrt{N}}$ as mentioned earlier - the Langevin equation then becomes

$$d\mathbf{X} = \mathbf{A}(\mathbf{X})dt + \epsilon \sum_{i=1}^{3} \mathbf{B}^{(i)}(\mathbf{X})dW_i + \sigma\,\hat{\mathbf{B}}(\mathbf{X}) \circ dW. \tag{3.13}$$

From this we can see that we have encapsulated the complex noisy behaviour of the system in the form of noisy perturbations to a limit cycle solution of an ODE - independent noises proportional to the births, deaths and predations occuring in the system, as well as an extrinsic noise term corresponding in changes in fecundity due to environmental fluctuations. Of course, the extrinsic source of noise can be introduced in any of the other variables - in [128], the authors suggest the environmental fluctuations may affect the mortality rate as poor weather kills off

vulnerable sheep. On the other hand, in other cases where the noise is modelled more phenomenologically, it may be more straightforward to introduce extrinsic noise additively, as in chapter five of this thesis.

Next, for the Holling-Tanner model we study here, we choose the rate constants appropriately. This will reduce our Langevin equation to the known deterministic models in the limit $\epsilon \to 0$, $\sigma \to 0$ - a key assumption of our modelling. We recall that the deterministic equations were given by:

$$\begin{aligned} \dot{x}_1 &= A_1(\mathbf{x}) = rx_1(1-\frac{x_1}{K}) - \frac{mx_1x_2}{A_0+x_1} \\ \dot{x}_2 &= A_2(\mathbf{x}) = sx_2(1-\frac{hx_2}{x_1}). \end{aligned} \tag{3.14}$$

By comparing this with the coefficients from the stochastic urn model, we get that:

$$\begin{aligned} 2b_1x_1(1-x_1-x_2) - 2c_1x_1^2 - d_1x_1 &= rx_1(1-\frac{x_1}{K}) - \frac{mx_1x_2}{A_0+x_1} \\ 2b_2x_2(1-x_1-x_2) - 2c_2x_2^2 - d_2x_2 + 2p_2x_1x_2 &= sx_2(1-\frac{hx_2}{x_1}). \end{aligned}$$

Comparing the coefficients of $x_1, x_2, x_1^2, x_2^2, x_1x_2$ gives us:

$$\begin{aligned} b_1 &= \frac{r}{2K} \\ b_2 &= \frac{s+d_2}{2} \\ d_1 &= r(\frac{1}{K}-1) \\ c_1 &= 0 \\ c_2 &= \frac{sh}{2x_1} - \frac{s+d_2}{2} \\ p_1 &= \frac{m}{2(A_0+x_1)} - \frac{s+d_2}{2} - \frac{r}{2K} \\ p_2 &= \frac{s+d_2}{2} \end{aligned}$$

where d_2 is a free parameter; we set $d_2 = s$ for concreteness as it simplifies some expressions.

This means that we have:

$$\begin{aligned}
\mathbf{B}^{(1)} &= \sqrt{rx_1(\frac{1}{K}(2-x_1-2x_2)-1)+(\frac{m}{A_0+x_1}-2s)x_1x_2}\,\mathbf{v}_1 \\
\mathbf{B}^{(2)} &= \sqrt{sx_2(3-x_1-4x_2+\frac{hx_2}{x_1})}\,\mathbf{v}_2 \\
\mathbf{B}^{(3)} &= \sqrt{2sx_1x_2}\,\mathbf{v}_3 \\
\hat{\mathbf{B}} &= \begin{pmatrix} \frac{rx_1}{2K}(1-x_1-x_2) \\ sx_2(1-x_1-x_2) \end{pmatrix}
\end{aligned}$$

In order to demonstrate that the principles illustrated in this thesis are independent of the form of noise present in the system, we do not use the stochastic urn method for the Rosenzweig-Macarthur system, but instead add correlated and uncorrelated noise additively. As we will see in later sections, our results are qualitatively unchanged. This indicates that the phenomenon of noise-induced synchronization is ubiquitous and deserves more study in the context of ecology.

3.4 Noise-induced synchronization of uncoupled ecological populations

Having established the model we work with, our primary result is that we can explain the Moran effect in ecology by applying the theory of noise-induced synchronization to population oscillators - that is, the many observations of statistical correlations between populations linked to correlations in environmental fluctuations can be explained in many cases by the phase-synchronization of said populations. In some cases, especially in data from the wild, a clear limit cycle has not been observed; we hypothesize that the underlying population dynamics are complex, noisy, and multi-dimensional, and as such, the data obtained is too sparse to fully obseve the rich behaviour of the system. However, as mentioned before, recent experimental findings have been made [128] where environmental fluctuations were unable to synchronize a population of protozoa; only when predators were introduced to cause predator-prey cycles could the Moran effect be observed, strongly reinforcing the findings of this thesis. Hence, while the theory of noise-induced synchronization in itself is not new, its application to oscillating populations of organisms is a novel and potentially important breakthrough in mathematical ecology.

We first illustrate this by considering the effects of correlated noise on an ensemble of uncoupled Holling-Tanner predator-prey populations. Recall that in we have just derived, from an individual-level stochastic urn model, that each population in the ensemble can be described approximately by a SDE of the form:

$$d\mathbf{X} = \mathbf{A}(\mathbf{X})dt + \epsilon \sum_{i=1}^{3} \mathbf{B}^{(i)}(\mathbf{X}) dW_i + \sigma \hat{\mathbf{B}}(\mathbf{X}) \circ dW \tag{3.15}$$

where $d\mathbf{x} = \mathbf{A}(\mathbf{x})dt$ describes the behaviour of the Holling-Tanner model in the absence of noise (as mentioned earlier), and we have derived functions $\mathbf{B}^{(i)}$ and $\hat{\mathbf{B}}$ from our stochastic urn model and the way we introduce environmental stochasticity as fluctuations in the birth rates.

We choose the parameters of our model so that in the absence of noise, we obtain stable limit cycles, as discussed in section 3.2.1 - we plot this in Figure 3.2. We can obtain the limit cycles by simply taking the equations governing a single population in the absence of noise:

$$\begin{aligned} \dot{x}_1 &= A_1(\mathbf{x}) = r x_1 (1 - \frac{x_1}{K}) - \frac{m x_1 x_2}{A_0 + x_1} \\ \dot{x}_2 &= A_2(\mathbf{x}) = s x_2 (1 - \frac{h x_2}{x_1}), \end{aligned} \tag{3.16}$$

and running them forward in time using a simple forward Euler method:

$$\mathbf{x}(t + \delta t) = \mathbf{x}(t) + \delta t \, \mathbf{A}(\mathbf{x}(t)), \tag{3.17}$$

where $\mathbf{A} = (A_1, A_2)^T$ and $\delta t \ll 1$ is our time-step, until a limit cycle was observed. While it would have been possible to use a better numerical scheme, we were able to reach the desired accuracy with our scheme. More importantly, it is a direct analogue of the Euler-Maruyama scheme we have used to simulate the behaviour of our systems in the presence of noise, so we are able to compare our results directly without worrying about the differences in precision due to different numerical schemes.

Note that our dW_is are treated in the sense of Itō as they arise from the stochastic model, while we treat dW in the sense of Stratonovich as it is an extrinsic source of noise. In order to apply the conventional rules of calculus we convert

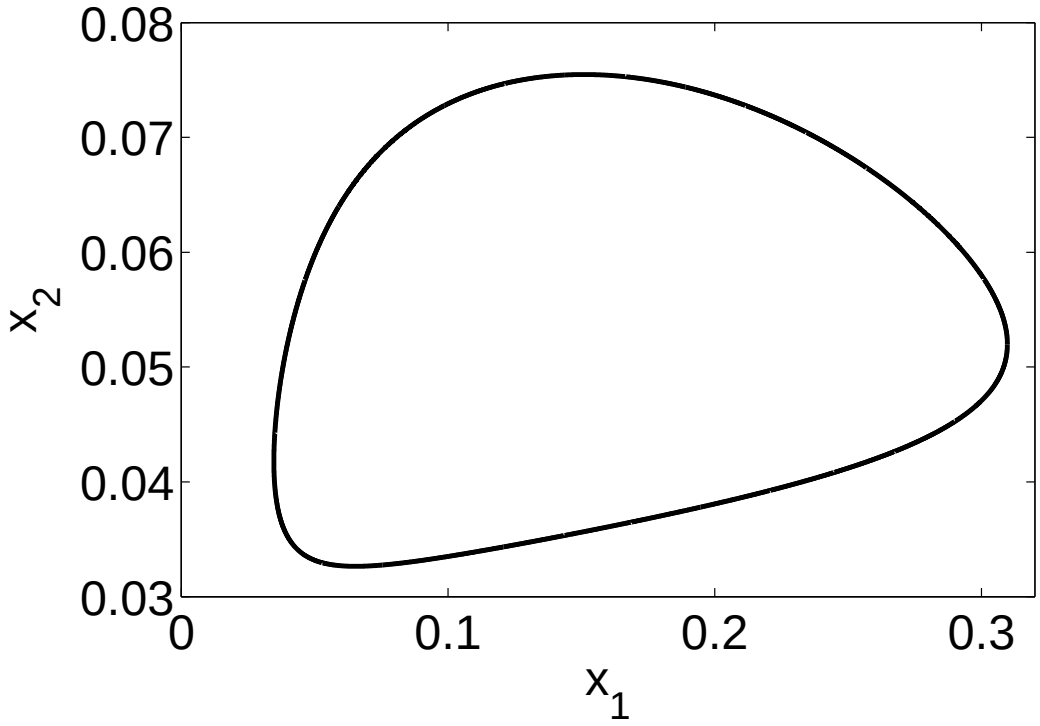

Figure 3.2: Plot of a limit cycle solution for the Holling-Tanner equations. As in the earlier section, the parameters are $r = 1$, $A_0 = 0.1$, $s = 0.1$, $h = 2$, $m = 3$ and $K = 0.5$, so we are in the regime exhibiting robust limit cycles.

our Langevin equation into a Stratonovich SDE:

$$d\mathbf{X} = [\mathbf{A}(\mathbf{X}) - \frac{\epsilon^2}{2}\sum_{i=1}^{3}\mathbf{B}^{(i)}(\mathbf{X}) \times D\,\mathbf{B}^{(i)}(\mathbf{X})]dt + \epsilon\sum_{i=1}^{3}\mathbf{B}^{(i)}(\mathbf{X}) \circ dW_i + \sigma\,\hat{\mathbf{B}}(\mathbf{X}) \circ dW \quad (3.18)$$

where $\times$ denotes componentwise multiplication, and $\mathcal{D}$ is shorthand for the componentwise partial derivative $(\frac{\partial}{\partial x_1}, \frac{\partial}{\partial x_2})^T$ (so $\mathcal{D}\,\mathbf{B}^{(i)}(\mathbf{X}) = (\frac{\partial B_1^{(i)}(\mathbf{X})}{\partial x_1}, \frac{\partial B_2^{(i)}(\mathbf{X})}{\partial x_2})^T$). In order to use the theory of noise-induced synchronzation discussed in the previous section, we would like to represent each of the populations by a phase variable θ. Then the phase θ of each oscillator evolves according to

$$d\theta = d\,\mathbf{X} \cdot \nabla_{\mathbf{X}}\Theta(\mathbf{X}).$$

Next we apply the techniques discussed in section 2.1 on phase reduction. We assume that the limit cycle is robust, so that when perturbations occur, the system moves back to the limit cycle with a small change of phase. Hence we can

approximate these changes by evaluating the gradient function on the limit cycle:

$$\mathbf{Z}(\theta) = \nabla_{\mathbf{X}}\Theta(\mathbf{X})|_{\mathbf{X}=\mathbf{X}_0(\theta)} \approx \nabla_{\mathbf{X}}\Theta(\mathbf{X})$$

and as before calculate the corresponding phase response curve $\mathbf{Z}(\theta)$ using the adjoint method. We plot this in Figure 3.3.

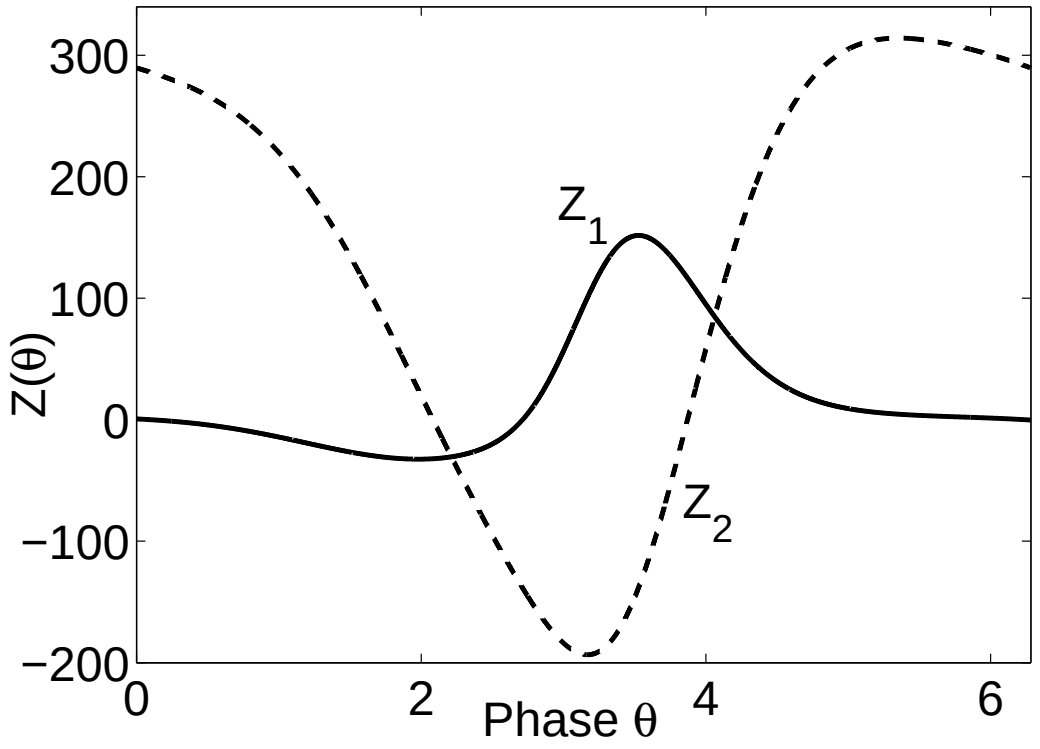

Figure 3.3: Plot of the PRC $\mathbf{Z}$ for the Holling-Tanner equations corresponding to the limit cycle in Fig 3.2.Parameters as before. The solid line is the component corresponding to x_1 and the dashed line is the component corresponding to x_2 .

(Note that from the calculation of the PRC, $\mathbf{Z}(\Theta(\mathbf{X})\cdot\mathbf{A}(\mathbf{X}) = \omega$.) Hence we obtain a single Stratonovich SDE for the phase of each oscillator:

$$\begin{aligned} d\Theta &\approx [\omega - \frac{\epsilon^2}{2}\sum_{i=1}^{3}\mathbf{Z}(\Theta)\cdot\left(\mathbf{B}^{(i)}(\mathbf{x}(\Theta))\cdot\mathcal{D}\mathbf{B}^{(i)}(\mathbf{x}(\Theta))\right)]dt \\ &\quad +\epsilon\sum_{i=1}^{3}\mathbf{Z}(\Theta)\cdot\mathbf{B}^{(i)}(\mathbf{x}(\Theta))\circ dW_i + \sigma\,\mathbf{Z}(\Theta)\cdot\hat{\mathbf{B}}(\mathbf{x}(\Theta))\circ dW. \end{aligned} \tag{3.19}$$

To apply our analysis as in the previous chapter (section 2.2), we would like to

convert this into an Itō SDE:

$$d\Theta = \mathcal{A}(\Theta)dt + \epsilon \sum_{i=1}^{3} \beta_i(\Theta) dW_i + \sigma\alpha(\Theta)dW, \tag{3.20}$$

where we have defined $\mathcal{A}$, β_i and α as:

$$\begin{aligned}
\beta_i(\theta) &= \mathbf{Z}(\theta) \cdot \mathbf{B}^{(i)}(\mathbf{x}(\theta)) \\
\alpha(\theta) &= \mathbf{Z}(\theta) \cdot \hat{\mathbf{B}}(\mathbf{x}(\theta)) \\
\mathcal{A}(\theta) &= \omega - \frac{\epsilon^2}{2} \sum_{i=1}^{3} \mathbf{Z}(\theta) \cdot \left(\mathbf{B}^{(i)}(\mathbf{x}(\theta)) \cdot \mathcal{D}\mathbf{B}^{(i)}(\mathbf{x}(\theta)) \right) \\
&\quad + \frac{\epsilon^2}{2} \sum_{i=1}^{3} \left(\beta_i(\theta) \frac{\partial}{\partial\theta} \beta_i(\theta) \right) + \frac{\sigma^2}{2} \alpha(\theta) \frac{\partial \alpha(\theta)}{\partial\theta}
\end{aligned}$$

in order to simplify notation. As in the previous section, we can label the phases of the oscillators in the ensemble by $(\Theta^{(1)}, \ldots, \Theta^{(\mu)}, \ldots, \Theta^{(M)})$, and hence write down a compact Itō SDE for the evolution of the phases of the ensemble:

$$d\Theta^{(\mu)} = \mathcal{A}(\Theta^{(\mu)})dt + d\zeta^{(\mu)}, \tag{3.21}$$

where $(\zeta^{(1)}, \ldots, \zeta^{(M)})$ are now correlated Wiener processes such that

$$\begin{aligned}
\langle d\zeta^{(\mu)} \rangle &= 0 \\
\langle d\zeta^{(\mu)} d\zeta^{(\nu)} \rangle &= \epsilon^2 \sum_{i=1}^{3} \beta_i(\Theta^{(\mu)}) \beta_i(\Theta^{(\nu)}) \delta_{\mu,\nu} + \sigma^2 \alpha(\Theta^{(\mu)}) \alpha(\Theta^{(\nu)}).
\end{aligned}$$

As before, if we denote the equal-time correlation matrix as $C(\theta)$ where $C_{\mu,\nu}(\boldsymbol{\theta})dt = \langle d\zeta^{(\mu)} d\zeta^{(\nu)} \rangle$, we can write down a FPE, similar to Eq. 2.31:

$$\frac{\partial \mathbb{P}(\boldsymbol{\theta}, t)}{\partial t} = -\sum_{\mu=1}^{M} \frac{\partial}{\partial \theta^{(\mu)}} \mathcal{A}(\boldsymbol{\theta}) \mathbb{P}(\boldsymbol{\theta}) + \frac{1}{2} \sum_{\mu=1}^{M} \sum_{\nu=1}^{M} \frac{\partial^2}{\partial \theta^{(\mu)} \partial \theta^{(\nu)}} [C(\boldsymbol{\theta}) \mathbb{P}(\boldsymbol{\theta}, t)]. \tag{3.22}$$

Next, we use the same averaging procedure as described in section 2.2 to obtain slow time variables $\boldsymbol{\phi}$ and an FPE for the averaged PDF $Q(\boldsymbol{\phi}, t)$:

$$\frac{\partial Q(\boldsymbol{\phi}, t)}{\partial t} = -\bar{\Omega} \sum_{\mu=1}^{M} \frac{\partial Q}{\partial \phi^{(\mu)}} + \frac{1}{2} \sum_{\mu=1}^{M} \sum_{\nu=1}^{M} \frac{\partial^2}{\partial \phi^{(\mu)} \phi^{(\nu)}} \bar{C}(\boldsymbol{\phi}, t) Q(\boldsymbol{\phi}, t), \tag{3.23}$$

where, as before, the overbar denotes averaging over a limit cycle, and $\Omega = \mathcal{A} - \omega$ is the higher-order correction to the drift term:

$$\begin{aligned}\bar{\Omega} = \frac{1}{2\pi}\int_{-\pi}^{\pi}\Omega d\theta &= \frac{1}{2\pi}\int_{-\pi}^{\pi}\frac{\epsilon^2}{2}\sum_{i=1}^{3}\left(\beta_i(\theta)\frac{\partial}{\partial\theta}\beta_i(\theta)\right)+\frac{\sigma^2}{2}\alpha(\theta)\frac{\partial\alpha(\theta)}{\partial\theta} \\ &\quad -\frac{\epsilon^2}{2}\sum_{i=1}^{3}\mathbf{Z}(\theta)\cdot\left(\mathbf{B}^{(i)}(\mathbf{x}(\theta))\cdot\mathcal{D}\mathbf{B}^{(i)}(\mathbf{x}(\theta))\right)d\theta.\end{aligned}$$

In this case the averaged correlation matrix $\bar{C}$ is given by:

$$\bar{C}_{\mu\nu}(\boldsymbol{\phi}, t) = \sigma^2 g(\phi^{(\mu)} - \phi^{(\nu)}) + \epsilon^2 h(0)\delta_{i,j}, \tag{3.24}$$

where the functions g and h are defined as:

$$\begin{aligned}g(\phi) &:= \frac{1}{2\pi}\int_{-\pi}^{\pi}\alpha(s)\alpha(\phi+s)ds \\ h(\phi) &:= \frac{1}{2\pi}\int_{-\pi}^{\pi}\sum_{i=1}^{3}\beta_i(s)\beta_i(\phi+s)ds.\end{aligned}$$

This allows us to see how the correlation structure of the system depends on the pairwise phase differences of the oscillators. From the numerically evaluated limit cycle and PRC, we can also calculate for our choice of parameters the functions g and h - Figure 3.4.

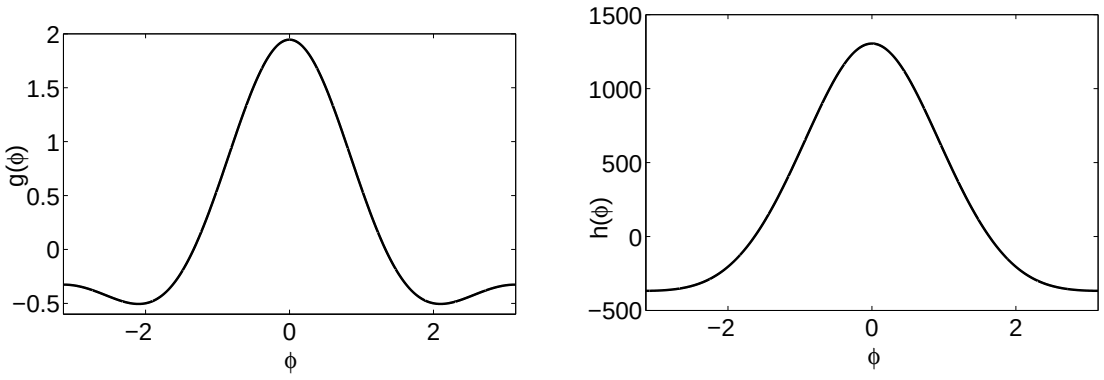

Figure 3.4: Plot of the g- and h-functions for this system, parameters as before. Left: g. Right: h.

In order to make our calculations tractable, we set $M = 2$. While this may not seem realistic in the case where one is dealing with many populations over

large habitats, due to the fact that our oscillators are identical, the PDF of the phase-difference between any two populations is representative of the behaviour of the ensemble. In addition, it corresponds to experimental cases where only 2 populations were considered, such as [56]. In this case our averaged FPE becomes:

$$\begin{aligned}\frac{\partial Q(\phi^{(1)},\phi^{(2)},t)}{\partial t} &= -\bar{\Omega}[\frac{\partial Q}{\partial \phi^{(1)}}+\frac{\partial Q}{\partial \phi^{(2)}}]+\sigma^2\frac{\partial^2}{\partial\phi^{(1)}\partial\phi^{(2)}}\Big[g(\phi^{(1)}-\phi^{(2)})Q\Big]\\ &\quad+\frac{1}{2}(\epsilon^2 h(0)+\sigma^2 g(0))\left[(\frac{\partial^2}{\partial {\phi^{(1)}}^2})+(\frac{\partial^2}{\partial {\phi^{(2)}}^2})\right]Q. \end{aligned} \tag{3.25}$$

As before we change variables to look at the mean and difference of the two phases - $\lambda = (\phi^{(1)}+\phi^{(2)})/2$, $\phi = \phi^{(2)}-\phi^{(1)}$. Noting that

$$\begin{aligned}\frac{\partial Q}{\partial \phi^{(1)}} &= \frac{1}{2}\frac{\partial Q}{\partial \lambda}-\frac{\partial Q}{\partial \phi}\\ \frac{\partial Q}{\partial \phi^{(2)}} &= \frac{1}{2}\frac{\partial Q}{\partial \lambda}+\frac{\partial Q}{\partial \phi}\end{aligned}$$

gives us

$$\begin{aligned}\frac{\partial Q(\lambda,\psi,t)}{\partial t} &= -\bar{\Omega}\frac{\partial Q}{\partial\lambda}+\frac{\epsilon^2 h(0)+\sigma^2 g(0)}{4}\left[(\frac{\partial^2}{\partial\lambda^2})+4(\frac{\partial^2}{\partial\psi^2})\right]Q\\ &\quad+\frac{\sigma^2}{4}\left[(\frac{\partial^2}{\partial\lambda^2})-4(\frac{\partial^2}{\partial\psi^2})\right][g(\psi)Q].\end{aligned} \tag{3.26}$$

Looking for separable solutions $Q(\phi^{(1)},\phi^{(2)},t)=\Lambda(\lambda,t)\Phi(\phi,t)$:

$$\frac{\partial\Lambda}{\partial t} = -\bar{\Omega}\frac{\partial\Lambda}{\partial\lambda}+\frac{1}{4}\Big(\epsilon^2 h(0)+\sigma^2[g(0)+g(\phi)]\Big)\frac{\partial^2\Lambda}{\partial\lambda^2} \tag{3.27}$$

$$\frac{\partial\Phi}{\partial t} = \frac{\partial^2}{\partial\phi^2}\Big(\sigma^2[g(0)-g(\phi)]+\epsilon^2 h(0)\Big)\Phi. \tag{3.28}$$

This is extremely similar to the form of the equations obtained in section 2.2., with an extra $\bar{\Omega}$ term in this case. This extra term corresponds to small correlations (of the order of ϵ^2 and σ^2) to the mean frequency of the ensemble, and are present due to correction terms obtained when switching between the Itō and Stratonovich calculi. (Hence, it is evident that the Itō and Stratonovich noise have the same effects on the synchronization of the system, while possibly having slightly different effects on the mean frequency of it.) However, when looking for steady-state solu-

tions $\Lambda_0(\lambda)$, $\Phi_0(\phi)$, we still obtain solutions similar to before:

$$\Lambda_0(\lambda) = \frac{1}{2\pi} \tag{3.29}$$

$$\Phi_0(\phi) = \frac{\Gamma_0}{\sigma^2[g(0)-g(\phi)]+\epsilon^2 h(0)} \tag{3.30}$$

where Γ_0 in this case is $[\int_{-\pi}^{\pi} ds/(\sigma^2[g(0)-g(s)]+\epsilon^2 h(0))]^{-1}$. This shows that the while the correction terms may have to be dealt with carefully in general [123], they do not affect our results here regarding the synchrony of the system - further implying that whether our noise is introduced in the sense of Itō or Stratonovich is not of much import in this particular application.

Next, we look at the implications of this analysis. As in the previous section the shape of the PDF is dependent on the g- and h-functions - as the g-function is peaked at $\phi = 0$ (with a much smaller peak at $\phi = \pi$) we expect to see mainly synchronization at $\phi = 0$ depending on the ratio of extrinsic to intrinsic noise.

From these we can calculate the steady-state distributions for the phase differences, $\Phi_0(\phi)$, for different values of the noise strengths ϵ and σ. Our results agree with the general form obtained in section 2.2 - increasing the ratio of extrinsic noise to intrinsic noise tends to synchronize the metapopulation, as shown in Figures 3.5, 3.6, and 3.7.

We also verify our results by comparing them with direct numerical simulations of the Langevin equation for our system. We have carried these out with an Euler-Maruyama scheme - denoting the realization of $\mathbf{X}$ at time-step N by $\mathbf{X}^N$:

$$\mathbf{X}^{N+1} = \mathbf{X}^N + \delta\mathbf{X}^N \tag{3.31}$$

$$\delta\mathbf{X}^N = \mathbf{A}(\mathbf{X}^N)\delta t + \sigma\hat{\mathbf{B}}(\mathbf{X}^N)\delta W^N + \epsilon\sum_{i=1}^{3}\mathbf{B}^{(i)}(\mathbf{X}^N)\delta W_i^N$$

where $\delta t = t^{N+1} - t^N$ the size of the time-step, each of the δW_i^N are drawn from a zero-mean normal distribution with variance δt, and the Stratonovich noise δW^N is treated as the solution of a zero-mean Ornstein-Uhlenbeck process with a small but finite correlation time, following the approach of [123]. We use this to an simulate an ensemble of $M = 200$ oscillators, and introduce ensemble averaged concentrations of prey and predator according to $\bar{X}_j(t) = M^{-1}\sum_{\mu=1}^{M} X_j^{(\mu)}(t), j = 1, 2$. This was motivated by the fact that in ecological systems one is much more likely to be able to make observations of mean population levels rather than the phase

of a population in a limit cycle - often the limit cycle itself is obscured by the noisiness of biological data.

Furthermore, stochastic simulations of the full system allow us to look at the accuracy of the various assumptions and approximations made in the analysis used. For example, the assumption that noise-induced synchronization is slow compared to the frequency of the oscillators was observed to be very accurate. Our oscillators also remained very close to the limit cycle in most cases. While some oscillators deviated from the limit cycle in Figure 3.7, due to the dynamics of the system, they returned to the limit cycle rapidly, and did not affect our results qualitatively. Future work includes studying systems where rare deviations could be large enough to push the system into another metastable state, using techniques such as those in [12]. This could correspond in the ecological case to phenomena such as rare stochastic extinctions.

Using techniques such as the Gillespie algorithm, one could also simulate the stochastic urn model of our populations. However, the highest level of intrinsic noise we consider here ($\epsilon = 10^{-3}$) corresponds to 10^6 individuals in each subpopulation, which is far too computationally expensive. Moreover, it is well known that the approximation of such systems by a Langevin equation is sufficiently accurate even for numbers of individuals much smaller than those we consider here.

Finally, we present plots of our results. For a high ratio of extrinsic to extrinisic noise (Figure 3.5), there is significant synchronization of the metapopulation, as indicated by the sharp peak of the steady-state distribution $\Phi(\phi)$ at $\phi = 0$ and the corresponding clustering of the individual oscillators on the deterministic limit cycle (bottom, inset). It can also be seen that $\mathbf{X}_j(t)$ traces out a trajectory in the phase plane that remains close to the deterministic limit cycle. This would be representative of a metapopulation strongly synchronized by environmental fluctuations - giving us a clear theoretical mechanism for the origin of the Moran effect.

This theoretical work could help us obtain a greater understanding of the synchrony of populations. For example, it explains neatly why in [128] it was observed that the Moran effect only came into play when predator-prey cycles were present. It could also help in cases where the underlying cyclical behaviour is poorly understood. For example, in [56], sheep populations were only counted annually, and as such the data was fitted using a nonlinear self-exciting autoregressive model. Cyclical crashes were observed - possible causes cited were food shortages and parasitism. If the populations instead were modelled as limit cycles, one may be able to obtain additional insights into the behaviour of the system, such as other

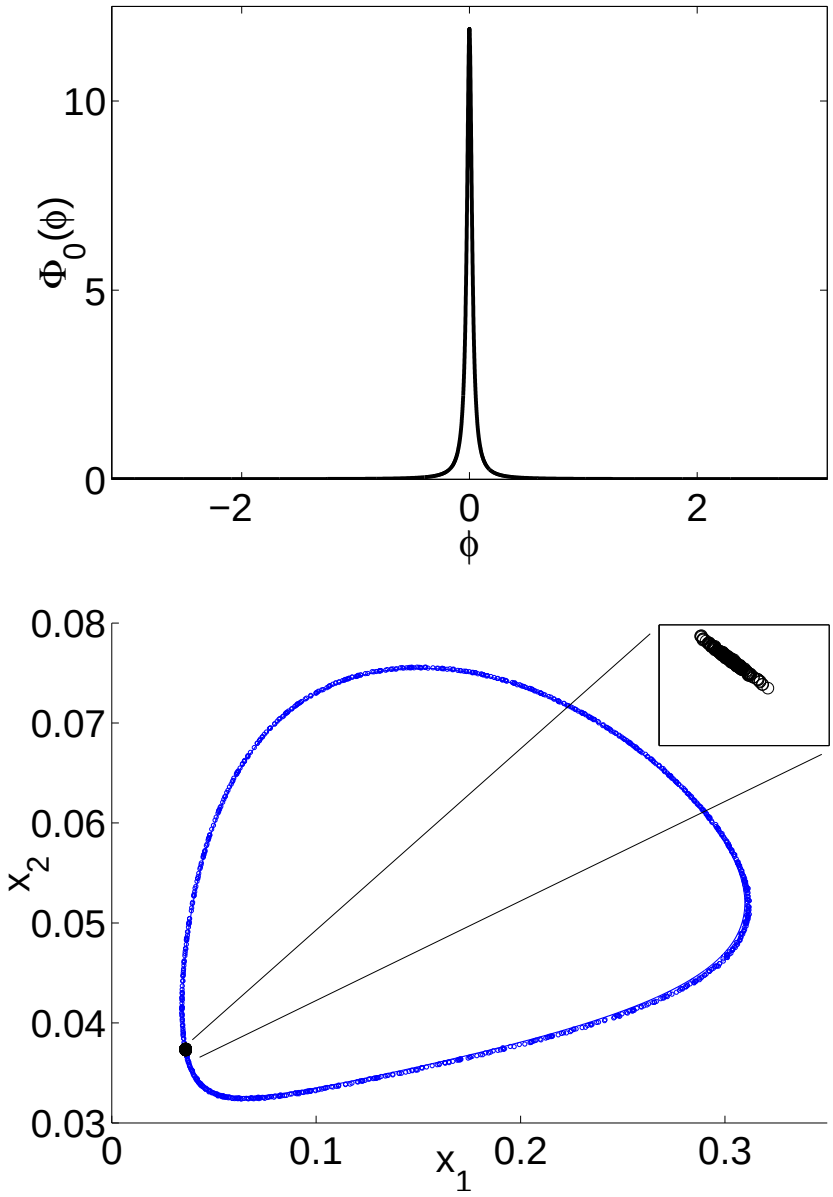

Figure 3.5: Comparison of numerical simulations and analytical results for $M = 200$ Holling-Tanner oscillators, using the same parameters as before. In this figure there is a high ratio of extrinsic to intrinsic noise: $\sigma = 10^{-3}$, $\epsilon = 10^{-6}$. Top: Steady-state PDF from our analytical calculations. Bottom: Corresponding ensemble dynamics in state space showing a snapshot of all the oscillators (black dots) and a scatterplot of the averaged trajectory $\bar{\mathbf{X}}_j(t)$ of the metapopulation over multiple realizations (blue/gray dots). The inset shows the oscillators remaining tightly packed.

trophic interactions. This would also provide motivation for experimental studies involving more frequent observations of populations. Furthermore, the intrinsic

noise caused by the behaviour of individual sheep was not taken into account - this would be significant as in this particular paper the sizes of the populations were $O(10^4)$. As such, we believe there is a rich area of future work involving re-interpretation of data using models similar to ours, as opposed to more traditional methods.

Next, we consider a situation where there is only a moderate ratio of extrinsic to intrinsic noise. Figure 3.6 shows our analytical results and numerical simulations. The metapopulation is only partially synchronized and the distribution Φ_0 is much broader (Fig. 3.6(top)). Although the oscillators tend to remain close to the deterministic limit cycle, they are no longer tightly clustered. Thus, $\bar{X}_j(t)$ still exhibits some oscillatory behavior but the amplitude of oscillations is reduced (Fig. 3.6(bottom)).

Finally, for a low ratio of extrinsic to intrinsic noise, the metapopulation is completely desynchronized. The density Φ is almost flat (Fig. 3.7(top)), and individual oscillators are much more scattered in the phase-plane so that $\bar{X}_j(t)$ exhibits small fluctuations about the mean of the limit cycle (Fig. 3.7(bottom)). One major implication of this is that the stabilizing effects of demographic noise could provide an explanation for why oscillations are often not observed in real ecological systems, contrary to predictions from deterministic models [90, 96]. Specifically, in [96], a Daphnia-algae system was studied, where increasing the nutrient levels should theoretically cause the system to move into a parameter regime with limit cycles, but this was not observed. We advance the theory that this phenomenon is due to the system behaving as a metapopulation of multiple populations, with asynchrony between the populations leading to the lack of large cycles being observed.

In [90], the authors tested the hypothesis that inedible algae in natural lakes was suppressing the formation of limit cycles. They did this by running experiments in a laboratory environment without the inedible algae, and successfully observed the expected limit cycles. However, as these experiments were conducted in much smaller tanks, these results also lend weight to our hypothesis that limit cycles may occur in smaller environments, but that the organisms are insufficiently motile for a large natural habitat to be considered a single population. This would lead one to suggest future experiments to confirm or disprove this assertion. In this system in particular one could look at smaller stock tanks with inedible algae, or obtain more detailed spatio-temporal data from larger habitats. In tandem, one could extend the methods presented here from a simple predator-prey model to a higher-dimensional model taking into account the age-structuring of the popula-

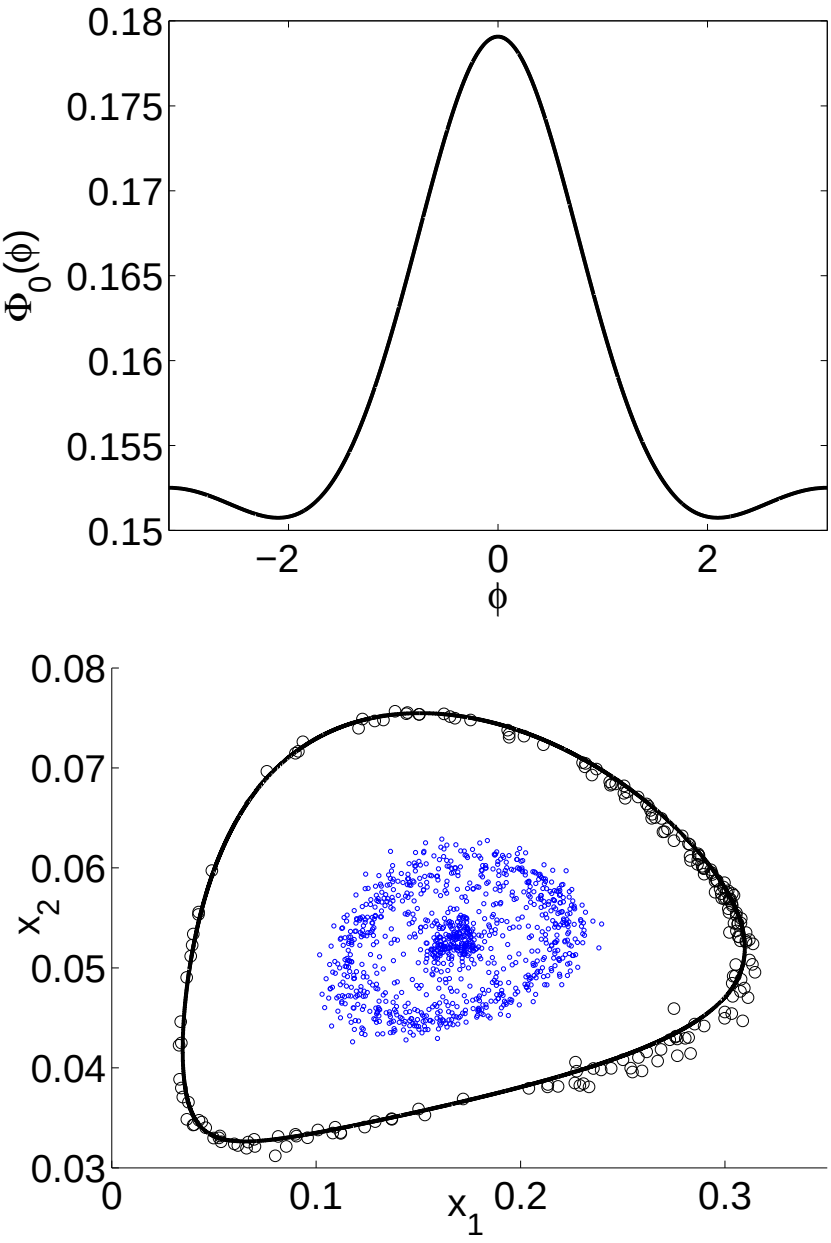

Figure 3.6: Comparison of numerical simulations and analytical results for $M = 200$ Holling-Tanner oscillators, using the same parameters as before. In this figure there is a moderate ratio of extrinsic to intrinsic noise: $\sigma = 10^{-2}$, $\epsilon = 10^{-3}$. Top: Steady-state PDF from our analytical calculations. Bottom: Corresponding ensemble dynamics in state space showing a snapshot of all the oscillators (black dots) and a scatterplot of the averaged trajectory $\bar{\mathbf{X}}_j(t)$ of the metapopulation over multiple realizations (blue/gray dots).

tions.

In systems of oscillators, one often wants to identify appropriate macroscopic

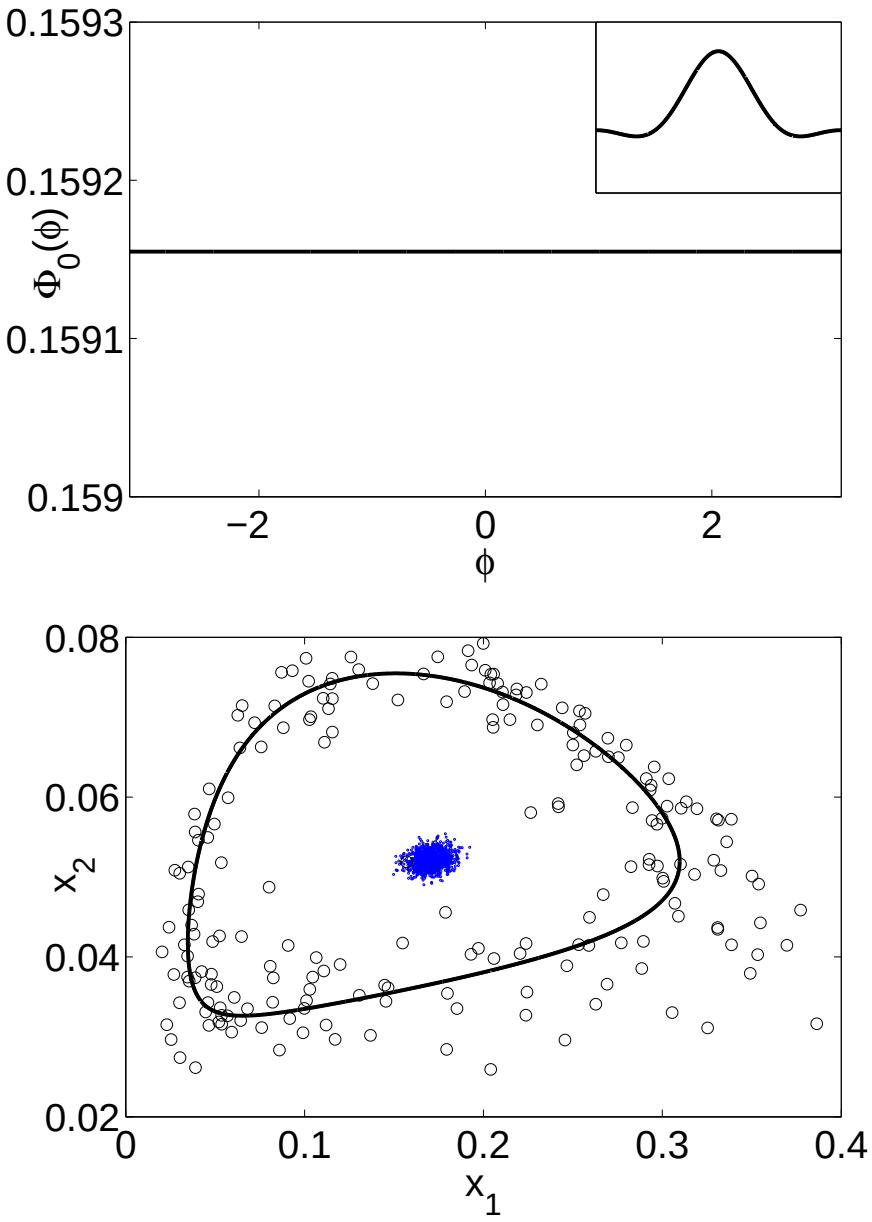

Figure 3.7: Comparison of numerical simulations and analytical results for $M = 200$ Holling-Tanner oscillators, using the same parameters as before. In this figure there is a low ratio of extrinsic to intrinsic noise: $\sigma = 10^{-6}$, $\epsilon = 10^{-3}$. Top: Steady-state PDF from our analytical calculations. The inset shows the PDF when zoomed in around $\Phi_0(\phi) \approx 1/2\pi$. Bottom: Corresponding ensemble dynamics in state space showing a snapshot of all the oscillators (black dots) and a scatterplot of the averaged trajectory $\bar{\mathbf{X}}_j(t)$ of the metapopulation over multiple realizations (blue/gray dots).

variables that characterize the degree of synchrony for the system. Following pre-

vious studies of the Kuramoto model [74, 117], a common choice is the complex amplitude defined according to

$$R\exp(i\urcorner) = \frac{1}{M}\sum_{i=1}^{M}\exp(i\theta_i). \tag{3.32}$$

where there are M oscillators with phases labelled by θ_i, and the amplitude $R \in [0,1]$ with $R = 1$ denoting complete synchrony and $R = 0$ denoting complete asynchrony. Often in Kuramoto-type systems one is able to make the approximation as the number of oscillators $M \to \infty$ that

$$R\exp(i\urcorner) \approx \int_0^{2\pi}\exp(i\theta)\rho(\theta)d\theta, \tag{3.33}$$

where $\rho(\theta)$ is a variable representing the density of oscillators. Since the oscillators are identical, one then makes the ansatz that the density of oscillators is accurately captured by the steady-state probability density for a single oscillator, which allows one to calculate an analytical estimate for R. However, in our case, as synchrony is generated by a common noise source, one cannot decouple the probability density of one oscillator from the joint PDF of the ensemble, which makes any analytical progress very difficult.

In addition, for $M = 2$, R is not a good representation of synchrony. For instance, consider the case where the oscillators are desynchronized (and hence one would expect $R = 0$), with their phase difference $\phi = \theta_2 - \theta_1$ being distributed uniformly:

$$\begin{aligned} R\exp(i\urcorner) &= \frac{1}{2}\sum_{i=1}^{2}\exp(i\theta_i) \\ &= \frac{1}{2}\exp(i\theta_1)(1+\exp(i\theta_2-\theta_1)). \end{aligned} \tag{3.34}$$

Taking the absolute value of both sides gives us:

$$|R| = \frac{1}{2}|1+\exp(i\phi)|. \tag{3.35}$$

Since $R \in \mathbb{R}_r^+$ the left-hand side is just R. Now we can take the expectation of both

sides:

$$\mathbb{E}(R) = \frac{1}{2}\int_0^{2\pi} |1 + \exp(i\phi)|\Phi(\phi)d\phi, \tag{3.36}$$

where the probability distribution of the phase difference $\Phi(\phi) = 1/2\pi$. The above integral can be evaluated exactly giving us $\mathbb{E}(R) = 2/\pi >> 0$.

However, while it is nontrivial to extend our analysis to $M > 2$, we find that our calculated quantity, the PDF of the pairwise phase difference $\Phi(\phi)$, can be an excellent estimator of the synchrony of a large ensemble. For different values of the system size parameter $N = \epsilon^{-1/2}$, we calculate the half-width Δ of the peak of our PDF, defined such that

$$\int_{-\Delta/2}^{\Delta/2} \Phi(\phi)d\phi = \frac{1}{2}. \tag{3.37}$$

At the same time, we can obtain an estimate of synchrony from our stochastic simulations of an ensemble of 200 oscillators. We define

$$R(t) = \frac{1}{M}|\sum_{i=1}^{M} \exp(i\Theta_i)|, \tag{3.38}$$

where $M = 200$ in this case, and take the time-average over a long period of time $\bar{R}$. In Figure 3.8 we show how $\bar{R}$ is strongly correlated with how narrow the peak of our PDF is, defined as $1 - \Delta/2\pi$. This further verifies that the analysis carried out here accurately captures the behaviour of systems of large numbers of oscillators.

It must be noted that this method of estimating synchrony is only valid when increasing synchrony causes the oscillators to form one cluster, as indicated by the PDF having one peak. One can see that if the PDF has multiple peaks, then increasing synchrony could cause oscillators to form multiple clusters, leading to low values of R. We will see modes of behaviour with clustering in the next section, as well as in other cases not covered in this thesis.

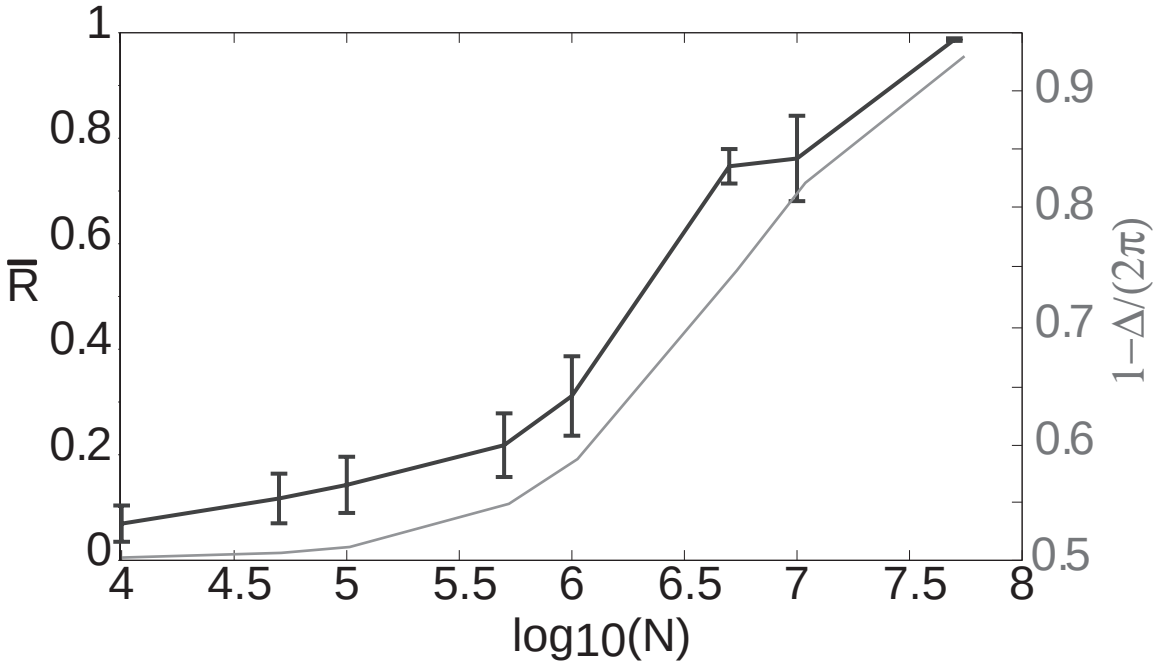

Figure 3.8: Plots of time-averaged order parameter $\overline{R}$ (black curve) and half-width $1-\Delta/(2\pi)$ (gray curve) as a function of system size N. Variance of $R(t)$ with respect to time is shown by error bars. Parameters as before with $\sigma = 0.01$.

Chapter 4

Uncoupled neuronal populations

4.1 Neural population oscillations and synchronization

Next, we would like to explore how the theory of noise-induced synchronization works in the context of neuronal populations, where the subject of synchronized oscillations is also very important. In the brain, synchronous oscillations are prevalent in many areas, including the sensory cortices, hippocampus, and thalamus [24]. These neuronal oscillations can arise due to the intrinsic properties of single cells or may be due to excitatory and inhibitory synaptic interactions within a local population of cells. The activity of a single neuron has been a long-studied area, with the celebrated Hogkin-Huxley model [60] endlessly researched and refined since 1952. However, studying the behaviour of large numbers of neurons by modelling each one with a Hogkin-Huxley-type model rapidly becomes intractable. Hence, large-scale neural behaviour has been traditionally treated with continuum models of neural tissue [27]. In these models, the variable of interest is the population-averaged firing rate of the neurons, and the spatial distribution of synaptic connections between neurons can be modelled by integral kernels. Seminal work was carried out by Wilson, Cowan and Amari in the 1970s [131, 132, 3, 4]. Following that, there have been a plethora of analytical and numerical results demonstrating the existence and stability of spatially structured solutions. These have included EEG rhythms [99, 68, 106], geometric visual hallucinations [34, 35, 121, 17] stationary pulses [79, 80] and spiral waves [62, 69, 78, 125], many of which correspond to experimentally observed modes of neural activity.

One of the subjects of this thesis is an aspect of the dichotomy between single-cell and population models, in particular, how noise at the single-cell level can affect large-scale behaviour. This is especially relevant with the recent surge of interest in stochastic phenomena in the neural context [40, 84, 81]. As mentioned previously, individual cortical neurons fire stochastically, and various forms of spontaneous neuronal activity has been observed in vivo and in vitro. While there has been work done on how noise affects neurons on a cellular level, it is not straightforward to determine how such noise affects the system at a population level. Here we will attempt to study it by using a neural master equation. This master equation approach allows one to deal with the stochastic firing of individual neurons by tracking a population variable which counts the number of active neurons at any given time. The stochasticity is then captured by the transition rates between states of the population variable, which are modelled as exponential random variables. By considering the particular version of the neural master equation introduced by Bressloff [11], we obtain agreement with the deterministic Wilson-Cowan equations in the thermodynamic limit $N \to \infty$; the "intrinsic" noise from the stochastic firing rates then can be treated as fluctuations about a well-known deterministic ODE. Using this method we will examine two of the simplest neural networks known to generate limit cycle oscillations at the population level: firstly, a pair of mutually coupled excitatory (E) and inhibitory (I) populations; and secondly, a recurrent excitatory population with synaptic depression.

The rationale behind this is that a number of modeling studies of stimulus-induced oscillations and synchrony in primary visual cortex have taken the basic oscillatory unit to be an E-I network operating in a limit cycle regime [112, 54], while the recurrent excitatory network with synaptic depression has been used as the basis of various studies of spontaneous synchronous oscillations in the cortex. For example, in [118, 119], the authors considered Wilson-Cowan mean-field equations representing a recurrent excitatory network with both slow and fast forms of synaptic depression. This was used this to model the dynamics of synchronized population bursts in developing chick spinal cord. An excitatory network with synaptic depression and extrinsic noise has also been used to model transitions between cortical Up and Down states [61, 69, 70]. In addition to the relevance of synaptic depression in the generation of neural oscillations, it is interesting from a mathematical perspective since the resulting master equation provides a novel example of a so-called stochastic hybrid system [20, 101].

By then introducing a common stochastic input to our oscillating neuronal

populations, we can apply the theory of noise-induced synchronization to examine the resulting behaviour, and the interplay between this noise-induced synchronization and the decorrelating effects of intrinsic noise. This is motivated by experimental studies - evidence of neuronal synchronization through correlated noise has been found in, for instance, the olfactory bulb [40]. There the authors were able to synchronize oscillatory firing in olfactory mitral cells with shared fast fluctuations in stochastic inputs across neurons. It is also suggested by the related phenomenon of spike-time reliability, in which the reproducibility of a single neuron's output spike train across trials is greatly enhanced by a fluctuating input when compared to a constant input [41, 85].

Our results confirm our initial hypothesis that a common noisy input is indeed a possible mechanism for the synchronization of neuronal populations, as we observe synchrony in both of the neural population models we consider in this thesis. Furthermore, by varying the way the noise is introduced in the system, we were also able to find parameter regimes where the oscillators form clusters, and switch between the clusters intermittently, which may have implications in future experimental work.

4.2 Excitatory-inhibitory network

As in the ecological case, we start by analysing the behaviour of an individual population in the absence of noise. Let us consider two coupled subpopulations of neurons, where one subpopulation is excitatory (E) and the other inhibitory (I) (see Figure 4.1), which is one of the simplest and best-studied network models that supports limit cycle oscillations at the population level. We assume that all the neurons of each population are equivalent in that the synaptic interaction between a neuron in population i and a neuron in population j depends only on i and j, and can write the mean-field equations explicitly:

$$\begin{aligned} \alpha_E \frac{d\nu_E}{dt} &= -\nu_E + F(w_{EE}\nu_E + w_{EI}\nu_I + h_E) \\ \alpha_I \frac{d\nu_I}{dt} &= -\nu_I + F(w_{IE}\nu_E + w_{II}\nu_I + h_I), \end{aligned} \tag{4.1}$$

where ν_k is the mean activity in each subpopulation, α_ks are rate constants, w_{kl} is the effective synaptic weight from the lth to the kth population, and h_ks are

external inputs. The function F is defined as

$$F(x) = \frac{F_0}{1 + \exp(-\gamma(x - \kappa))}, \tag{4.2}$$

the sigmoid function with gain γ, threshold κ and maximum F_0. The $-v_i$ term in each of the equations corresponds to the fact that a neuron firing at a time t is no longer firing at time $t + \delta t$, while the second term corresponds to the neuronal activity being excited depending on the synaptic input given to it, modelled phenomenologically by a sigmoid function. The fact that one population is excitatory and the other inhibitory is represented by the fact that $w_E E, w_I E > 0$ and $w_E I, w_I I < 0$. We also set $\alpha_E, \alpha_I = 1$ for simplicity. (The membrane time constant $\alpha^{-1} \approx 10$ msec in physical units).

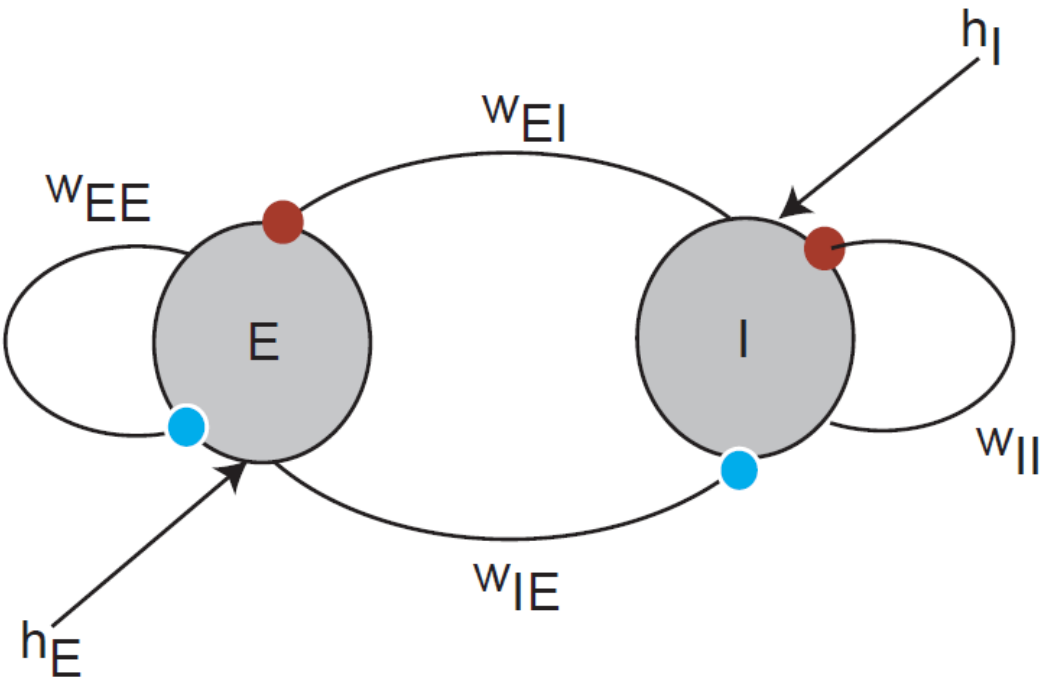

Figure 4.1: Schematic diagram of the E-I network architecture. The synaptic weights w_{ij} and external inputs h_i determine the total synaptic input $X_i = \sum_{j=E,I} w_{ij} v_j + h_i$.

4.2.1 Bifurcation structure

The bifurcation structure of this model has been analysed in detail in [9]. Here we give an outline of the analysis. We assume the synaptic weights w_{ij} are constant and vary the h_is to get a two-dimensional parameter space. An equilibrium point $\boldsymbol{\nu}^*$ is obtained a solution of:

$$\begin{aligned} \nu_E^* &= F(w_{EE}\nu_E^* + w_{EI}\nu_I^* + h_E) \\ \nu_I^* &= F(w_{IE}\nu_E^* + w_{II}\nu_I^* + h_I). \end{aligned} \tag{4.3}$$

We invert this to get expressions for the h_is:

$$\begin{aligned} h_E &= F^{-1}(\nu_E^*) + w_{EE}\nu_E^* + w_{EI}\nu_I^* \\ h_I &= F^{-1}(\nu_I^*) + w_{IE}\nu_E^* + w_{II}\nu_I^*. \end{aligned} \tag{4.4}$$

The Jacobian evaluated at these equilibrium points is:

$$\mathbf{J} = \begin{pmatrix} -1 + w_{EE}F'(w_{EE}\nu_E^* + w_{EI}\nu_I^* + h_E) & w_{EI}F'(w_{EE}\nu_E^* + w_{EI}\nu_I^* + h_E) \\ w_{IE}F'(w_{IE}\nu_E^* + w_{II}\nu_I^* + h_I) & -1 + w_{II}F'(w_{IE}\nu_E^* + w_{II}\nu_I^* + h_I). \end{pmatrix} \tag{4.5}$$

To simplify this further, we assume that the sigmoidal function F has gain 1, threshold 0, and maximum 1, that is, $F(x) = \frac{1}{1+\exp(-x)}$, so it satisfies $F' = F(1-F)$, (If this assumption is not made, $F' = \gamma F(1 - F/F_0)$.) Using this fact, and substituting in Equation (4.4), we get:

$$\mathbf{J} = \begin{pmatrix} -1 + w_{EE}\nu_E^*(1-\nu_E^*) & w_{EI}\nu_E^*(1-\nu_E^*) \\ w_{IE}\nu_I^*(1-\nu_I^*) & -1 + w_{II}\nu_I^*(1-\nu_I^*) \end{pmatrix}. \tag{4.6}$$

To get the eigenvalues $\lambda_\pm$ of $\mathbf{J}$, we need to solve $\mathrm{Det}(\lambda \boldsymbol{I} - \mathbf{J}) = 0$, which gives us:

$$(\lambda - \mathbf{J}_{11})(\lambda - \mathbf{J}_{22}) - \mathbf{J}_{12}\mathbf{J}_{21} = 0. \tag{4.7}$$

a quadratic equation which yields

$$\lambda_\pm = \frac{1}{2}(\mathrm{Tr}\,\mathbf{J} \pm \sqrt{(\mathrm{Tr}\,\mathbf{J})^2 - 4\,\mathrm{Det}\,\mathbf{J}}). \tag{4.8}$$

For stability, the real parts of both eigenvalues must be negative, which gives us the conditions $\mathrm{Tr}\,\mathbf{J} < 0$ and $\mathrm{Det}\,\mathbf{J} > 0$. For Hopf bifurcations, we require a pair of complex conjugate eigenvalues to cross the imaginary axis, that is, $\mathrm{Det}\,\mathbf{J} > 0$ and

$\mathrm{Tr}\,\mathbf{J} = 0$. So we have the quadratic equation:

$$\mathrm{Tr}\,\mathbf{J} \equiv -2 + w_{EE}\nu_E^*(1-\nu_E^*) + w_{II}\nu_I^*(1-\nu_I^*) = 0. \tag{4.9}$$

Using this constraint we can express ν_I^* as a function of ν_E^* (or *vice versa*) and substitute this into Equation (4.9). This then gives curves of bifurcations in the (h_E, h_I) plane parametrised by ν_E^* (ν_I^*). In particular for Hopf bifurcations the quadratic constraint gives two branches of bifurcations. For saddle-node or fold bifurcations, a single real eigenvalue has to cross zero, so we get the constraints $\mathrm{Tr}\,\mathbf{J} < 0$ and $\mathrm{Det}\,\mathbf{J} = 0$. This gives us a quartic constraint which we then use to determine the bifurcation curves numerically. The full bifurcation diagram for a sample set of parameters is shown in Figure 4.2. (The precise parameters used are not important as long as the qualitative behaviour of the system remains the same.) The region we are interested in is the one that gives us limit cycles, lying between the two curves of Hopf bifurcations. In this thesis we choose parameters approximately in the centre of the region.

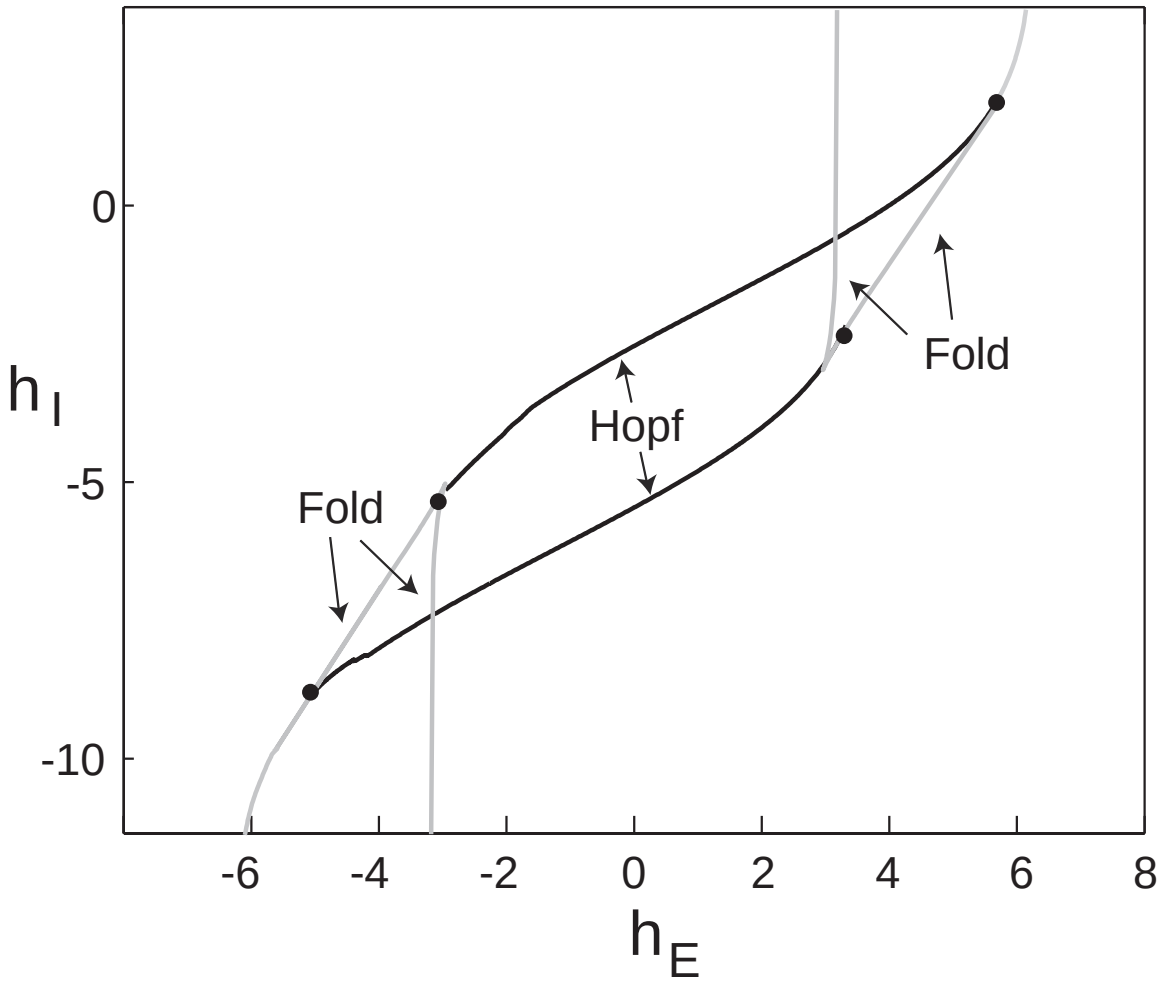

Figure 4.2: Bifurcation diagram of the two-population Wilson-Cowan model in (h_E, h_I) parameter space for a fixed set of synaptic weights $w_{EE} = w_{IE} = 10$, $w_{EI} = -10$, $w_{II} = -4$. The dots correspond to Takens-Bogdanov bifurcation points.

4.3 Recurrent excitatory network with synaptic depression

So far we have considered the E-I network. However, an even simpler population model known to exhibit limit cycle oscillations is a recurrent excitatory network with synaptic depression. The mean-field equations for a homogeneous network with synaptic depression are taken to be of the following form, based on previous studies [2, 126, 119, 70]

$$\begin{aligned} \frac{dx}{dt} &= -x + F(qx + h) \\ \frac{dq}{dt} &= k_+(1-q) - k_- xq, \end{aligned} \tag{4.10}$$

where we have again set the membrane rate constant $\alpha = 1$. The depression variable $q(t)$ can be interpreted as a measure of available presynaptic resources at the population level, which are depleted at a rate $k_-x(t)$, which is proportional to the mean population activity $x(t)$, and are recovered at a rate k_+.

In the E-I populations, for the parameter values we work with in this thesis, the population activity is relatively low. Hence, the inihibition due to the depletion of presynaptic resources is not of huge import, especially compared to the inhibition from the inhibitory population. However, in the case of a recurrent excitatory population, we can see that without synaptic depression, the population activity variable x saturates at a high value due to the recurrent excitation. This is an unrealistic mode of behaviour which does not occur in experimental data from such populations.

4.3.1 Bifurcation structure

In order to find a parameter regime which gives us limit cycles, we need to examine the bifurcations of the system as before. Solving for a fixed point (x^*, q^*) of the equations satisfies gives us

$$\begin{aligned} x^* &= F\left(\frac{k_+ x^*}{k_+ + k_- x^*} + h\right) \\ q^* &= k_+/(k_+ + k_- x^*). \end{aligned}$$

Now suppose that the network operates in a parameter regime where there exists a unique fixed point. By linearizing about the fixed point and calculating the eigenvalues of the Jacobian, we can find regimes where the fixed point destabilizes via a Hopf bifurcation leading to the formation of a limit cycle. We know that the Jacobian is given by

$$\mathbf{J} = \begin{pmatrix} -1 + qF'(qx+h) & xF'(qx+h) \\ -k_- q & -k_+ - k_- x \end{pmatrix}. \tag{4.11}$$

Here we assume that $F_0 = 1$, so we can make use of the fact that $F' = \gamma F(1-F)$, as well as that $x^* = F(q^* x^* + h)$:

$$\mathbf{J} = \begin{pmatrix} -1 + \gamma q^* x^*(1-x^*) & \gamma x^{*2}(1-x^*) \\ -k_- q^* & -k_+ - k_- x^* \end{pmatrix}. \tag{4.12}$$

As before we can look for Hopf bifurcations by setting $\mathrm{Tr}\,\mathbf{J} = 0$:

$$-1 + \frac{\gamma k_+ x^*(1-x^*)}{k_+ + k_- x^*} - k_+ - k_- x^* = 0,$$

together with the constraint that $x^* = F\left(\frac{k_+ x^*}{k_+ + k_- x^*} + h\right)$ which we solve numerically. An example bifurcation diagram is shown in Figure 4.3 with the depletion rate k_- treated as the bifurcation parameter. Using this, we choose $k_- = 0.1$ for our further analysis in later sections.

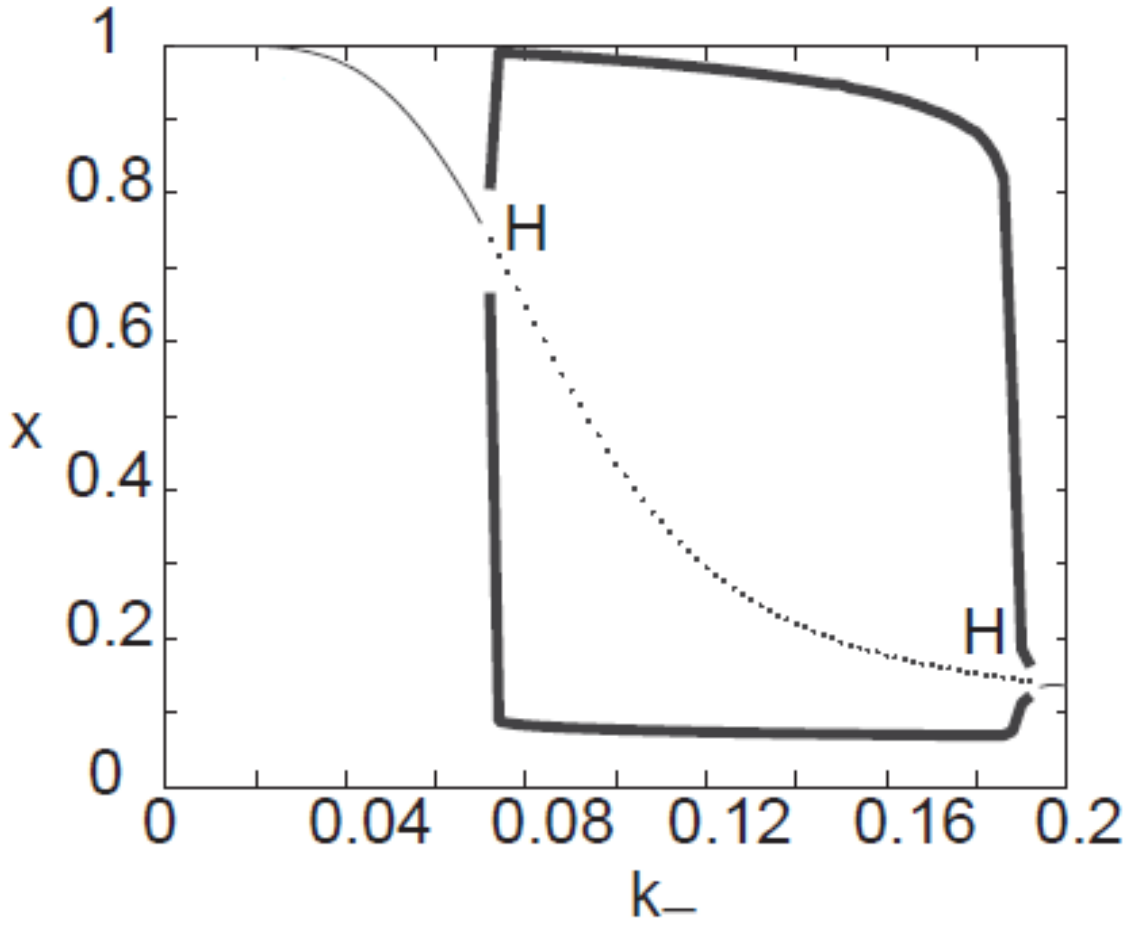

Figure 4.3: Deterministic excitatory network with synaptic depression. Bifurcation diagram for the excitatory network with synaptic depression, showing solutions as a function of the depletion rate k_-. Stable fixed point (thin solid curve) undergoes a Hopf bifurcation at the points H, resulting in an unstable fixed point (dotted curve) and a stable limit cycle (thick solid curve). Parameter values are $k_+ = 0.02, \gamma = 20, F_0 = 1$ and $h = -0.15$.

4.4 Neural master equation and reduction to a Langevin equation

In this chapter, we have considered either a pair of coupled excitatory-inhibitory subpopulations, or a recurrent excitatory population of neurons. Now we would like to study the effects of the finite sizes of these subpopulations, by saying that each of them is composed of N neurons. (It is an easy generalization to consider models with $\mathcal{M}$ homogeneous populations of interacting neurons. They can even be of different sizes as long as they scale with a common system-size parameter.) From before, we have assumed that all the neurons of each population are equivalent in that the synaptic interaction between a neuron in population i and a neuron in population j depends only on i and j. In order to move from a N-neuron model to a population-averaged model, we let $N_i(t)$ denote the number of spikes fired by the ith network in some time bin of width Δt centred around t.

Due to the stochastic nature of the individual neurons, we can treat each $N_i(t)$ as a discrete stochastic variable evolving according to a continuous Markov process. Then the state of the whole network can be described by the vector $\mathbf{N}(t) = (N_1(t),\dots,N_{\mathcal{M}}(t))$, where $\mathcal{M} = 2$ for the E-I network and $\mathcal{M} = 1$ for the recurrent excitatory network. Let $\mathbb{P}(\mathbf{n},t) = Prob[\mathbf{N}(t) = \mathbf{n}]$ denote the probability that the network is in state $\mathbf{n} = (n_1,\dots,n_{\mathcal{M}})$ at time t, given some initial distribution $\mathbb{P}(\mathbf{n},0)$. Then, our system is similar to the ecological case but has only births and deaths corresponding to a neuron firing or ceasing to fire respectively. As such we can describe the evolution of the probability distribution of the whole network with a Master Equation:

$$\frac{dP(\mathbf{n},t)}{dt} = \sum_{k=1}^{\mathcal{M}} \sum_{r=\pm 1} [T_{k,r}(\mathbf{n} - r\,\mathbf{e}_k)P(\mathbf{n} - r\,\mathbf{e}_k,t) - T_{k,r}(\mathbf{n})P(\mathbf{n},t)], \tag{4.13}$$

where $T_{k,r}$ is a transition rate corresponding the the kth population changing by r, and we have boundary conditions $P(\mathbf{n},t) \equiv 0$ if $n_i = -1$ or $N+1$ for some i. Also here we can set the stoichiometric vectors $(\mathbf{e}_1,\dots,\mathbf{e}_{\mathcal{M}})$ to be the canonical basis for $\mathbb{R}^{\mathcal{M}}$, as here the only transitions are neurons firing or ceasing to fire. This will make our analysis slightly simpler than in the ecological case.

As before, we can obtain a FPE by performing a Kramers-Moyal expansion of the Master equation and truncating appropriately. While in the ecological case we omitted lengthy calculations, due to the simpler forms of the stoichiometric

vectors, here we simply obtain

$$\frac{\partial \mathbb{P}}{\partial t} = -\sum_{i=1}^{\mathcal{M}} \frac{\partial (A_i(\mathbf{x})\mathbb{P})}{\partial x_i} + \frac{1}{2N}\sum_{i=1}^{\mathcal{M}} \frac{\partial^2 (G_i(\mathbf{x})\mathbb{P})}{\partial x_i^2}, \tag{4.14}$$

where there are no mixed derivatives due to the form of stoichiometric vectors, and A and G can be simply written in terms of transition rates:

$$\begin{aligned} A_i(\mathbf{x}) &= T_{k,+1} - T_{k,-1} \\ G_i(\mathbf{x}) &= T_{k,+1} + T_{k,-1}. \end{aligned}$$

This means that we can write the Langevin equation for the system in this form:

$$d\mathbf{X} = \mathbf{A}(\mathbf{X})dt + \epsilon \sum_{i=1}^{\mathcal{M}} \mathbf{B}^{(i)}(\mathbf{X})dW_i, \tag{4.15}$$

where $\mathbf{B}^{(i)} = \sqrt{G_i(\mathbf{x})}\,\mathbf{e}_i$. Since the stoichiometric vectors $\mathbf{e}_i$s are simply $(\delta_{1,i},\ldots,\delta_{\mathcal{M},i})^T$, we can conveniently rewrite our Langevin equation as:

$$d\mathbf{X} = \mathbf{A}(\mathbf{X})dt + \epsilon\, \mathbf{B}(\mathbf{X}) \times d\mathbf{W}, \tag{4.16}$$

where $\times$ represents componentwise multiplication, $d\mathbf{W} = (dW_1,\ldots,dW_{\mathcal{M}})^T$ independent Wiener processes, and $\mathbf{B} = (\mathbf{B}_1,\ldots,\mathbf{B}_{\mathcal{M}})^T = (\sqrt{G_1(\mathbf{x})},\ldots,\sqrt{G_{\mathcal{M}}(\mathbf{x})})^T$. In this thesis, we look at two examples of neuronal networks - a coupled E-I network ($\mathcal{M} = 2$) and a recurrent excitatory network ($\mathcal{M} = 1$), so we can write our transition rates explicitly. As we want the mean-field approximation to our stochastic description of the system to agree with the deterministic Wilson-Cowan equations for each model - equations 4.1 and 4.10 respectively, we set our transition rates to be

$$\begin{aligned} T_{k,+1}(\mathbf{x}) &= F(\sum_l w_{kl}x_l + h_k) \\ T_{k,-1}(\mathbf{x}) &= x_k \end{aligned}$$

for the E-I network, and correspondingly for the recurrent excitatory population

$$\begin{aligned} T_{+1}(x) &= F(qx + h) \\ T_{-1}(x) &= x. \end{aligned}$$

As in the ecological case, we would like to introduce an external source of noise in order to study the effects of noise-induced synchronization. In the neuronal context, a natural source of external noise is the background synaptic input received by a neuronal population. As the neuronal populations we examine here have been used as basic units in various studies of synchrony in the parts of the brain that deal with perception, noise-induced synchronization of our populations could be linked to various aspects of cognition. While somewhat tenuous, some have theorized that it could be linked to the binding problem. This area of study aims to understand the mechanism by which the brain assembles signals from different parts of the visual cortex into a coherent image. The results presented in this thesis show that noise-induced synchronization could synchronize networks of neurons in the cortex, it could potentially play a role in such visual processing.

Mathematically, we model a noisy input by replacing the constant terms h, h_k in the above transition rates by stochastic inputs I, I_k which can be decomposed into a deterministic part and a stochastic part according to

$$\begin{aligned} I_k &= h_k + \frac{2\sigma\chi_k}{\sqrt{F_0}}\xi(t) \\ I &= h + \frac{\sigma}{\sqrt{F_0}}\xi(t) \end{aligned}$$

where $\xi(t)$ is white noise, treated in the sense of Stratonovich as in the ecological case. For the E-I oscillators, the χ_ks are constants which allow us to study cases where the noise affects the excitatory and inhibitory subpopulations differently. (In the ecological case, introducing similar coefficients would correspond to the situation where the prey and predator populations are affected to different degrees, which is biologically plausible. Such refinements could be added in future work on specific biological cases, perhaps in tandem with experiments.)

Since we assume that the noise strength σ is small, we can substitute these expressions for the stochastic input into the expressions we have for the transition rates, and Taylor expand them to first order in σ:

$$\begin{aligned} T_{k,+1}(\mathbf{x}) &\approx F(\sum_l w_{kl}x_l + h_k) + \frac{2\sigma\chi_k}{\sqrt{F_0}}F'(\sum_l w_{kl}x_l + h_k)\xi(t) \\ T_{+1}(\mathbf{x}) &\approx F(qx+h) + \frac{\sigma}{\sqrt{F_0}}F'(qx+h)\xi(t), \end{aligned}$$

for the E-I oscillators and recurrent excitatory populations respecitvely.

Therefore for each of the models we work with, we are ultimately able to obtain a SDE of the form:

$$d\mathbf{X} = \mathbf{A}(\mathbf{X})dt + \epsilon\,\mathbf{B}(\mathbf{X}) \times d\mathbf{W} + \sigma\,\hat{\mathbf{B}}(\mathbf{X}) \circ d\hat{W}, \tag{4.17}$$

where the function $\hat{\mathbf{B}}$ is given by

$$\hat{\mathbf{B}}(\mathbf{X}) = \frac{2}{\sqrt{F_0}} \begin{pmatrix} \chi_1 F'(w_{11}x_1 + w_{12}x_2 + h_1) \\ \chi_2 F'(w_{21}x_1 + w_{22}x_2 + h_2) \end{pmatrix} \tag{4.18}$$

in the case of an E-I oscillator, and

$$\hat{\mathbf{B}}(\mathbf{X}) = \frac{1}{\sqrt{F_0}} F'(qx + h) \tag{4.19}$$

for a recurrent excitatory network.

To summarize, we are able to obtain for each oscillator, a SDE of the form:

$$d\mathbf{X} = \mathbf{A}(\mathbf{X})dt + \epsilon\,\mathbf{B}(\mathbf{X}) \times d\mathbf{W} + \sigma\,\hat{\mathbf{B}}(\mathbf{X}) \circ d\hat{W}, \tag{4.20}$$

where $d\mathbf{W} = (dW_E, dW_I)^T$ independent Wiener processes, and $d\hat{W}$ a different Wiener process, common to all the oscillators in the ensemble (and treated in the sense of Stratonovich). We have chosen the transition rates of a neural master equation in such a way that $d\mathbf{X} = \mathbf{A}(\mathbf{X})dt$ corresponds to the well-known deterministic Wilson-Cowan model of population activity. As such, we have captured both extrinsic and intrinsic noise as perturbations around a deterministic trajectory.

4.5 Noise-induced synchronization of E-I oscillators

We would like to proceed, as in the ecological case, to study the effects of noise-induced phase synchronization. First, we choose our parameters so that our system gives us stable limit cycles in the absence of noise - plotted in Figure 4.4.

This will allow us to perform a phase reduction as in section 2.1, in order to see how the phase of our limit cycle oscillators is perturbed by the intrinsic noise as well as the noisy input. We will then be able to apply the theoretical methods introduced in section 2.2 to look at the overall synchrony of the system. Our first step is to convert the above Langevin equations to the Stratonovich form in order

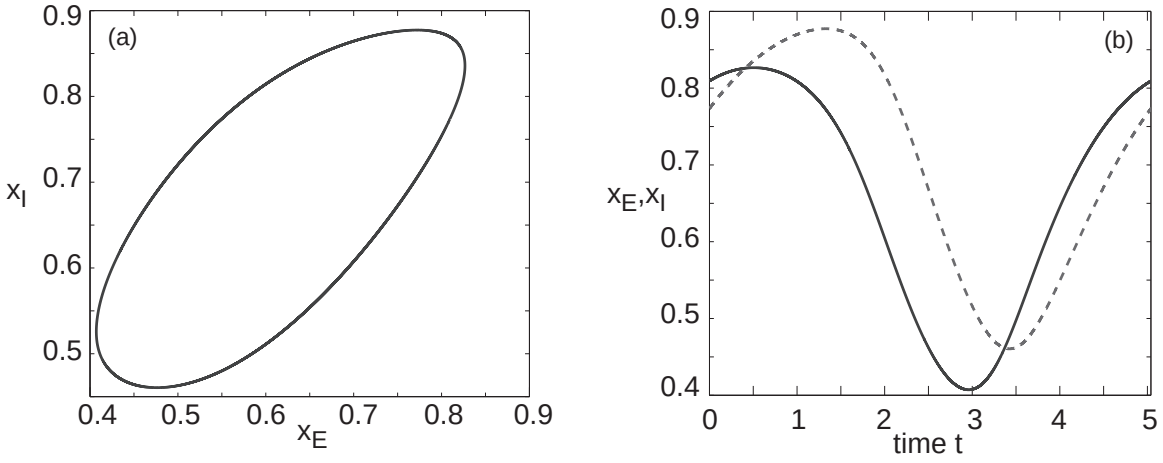

Figure 4.4: Limit cycle for the deterministic E-I network with parameters $w_{EE} = 11.5, w_{IE} = -w_{EI} = 10$, $w_{II} = -2$, $h_E = 0$ and $h_I = -4$. Also $\gamma = 1, F_0 = 1$ so that $F(u) = 1/(1 + \mathbf{e}^{-u})$. (a) Limit cycle in the (x_E, x_I)–plane. (b) Trajectories along the limit cycle for $x_E(t)$ (solid curve) and $x_I(t)$ (dashed curve).

to perform the phase reduction - we obtain:

$$d\,\mathbf{X} = [\mathbf{A}(\mathbf{X}) - \frac{\epsilon^2}{2}\,\mathbf{B}(\mathbf{x}) \circ \mathcal{D}\,\mathbf{B}(\mathbf{x})]dt + \epsilon\,\mathbf{B}(\mathbf{X}) \circ d\,\mathbf{W} + \sigma\,\hat{\mathbf{B}}(\mathbf{X}) \circ d\hat{W}. \tag{4.21}$$

As before, we would like to represent each oscillator by a phase variable. Again, we do this by calculating a phase response curve $\mathbf{Z}$ - plotted in figure 4.5 - allowing us to represent the effects of noise as a shift in phase. Hence the phase of each oscillator evolves approximately according to the following (Stratonovich) SDE:

$$\begin{aligned} d\Theta &= [\omega - \frac{\epsilon^2}{2}\,\mathbf{Z}(\Theta) \cdot [\mathbf{B}(\mathbf{x}(\Theta)) \circ \mathcal{D}\,\mathbf{B}(\mathbf{x}(\Theta))]]dt \\ &\quad + \epsilon\,\mathbf{Z}(\Theta) \cdot (\mathbf{B}(\mathbf{x}(\Theta)) \circ d\,\mathbf{W}) + \sigma\,\mathbf{Z}(\Theta) \cdot \hat{\mathbf{B}}(\mathbf{x}(\Theta))d\hat{W} \end{aligned} \tag{4.22}$$

where all the functions are evaluated on the limit cycle, as indicated by the notation $\mathbf{B}(\mathbf{x}(\Theta))$. This is important as it allows us to work entirely in terms of the phase variable.

Now we have obtained (Stratonovich) SDEs describing the phase of each of each oscillator, we would like to convert these into Itō SDEs in order to look at the corresponding Fokker-Planck equation describing the evolution of the PDF of the

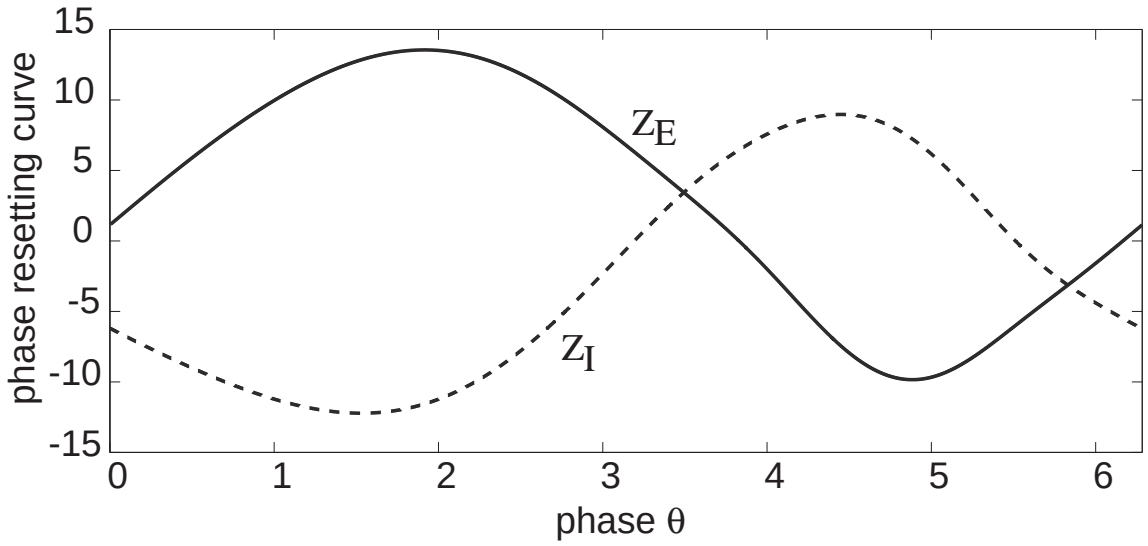

Figure 4.5: Components Z_E and Z_I of phase resetting curve for the E-I network. Same network parameter values as Fig. 4.4.

ensemble. As such it is convenient to simplify our notation by defining functions:

$$\begin{aligned}
\alpha(\theta) &= \mathbf{Z}(\theta)\cdot\hat{\mathbf{B}}(\mathbf{x}(\theta)) \\
\beta(\theta) &= \mathbf{Z}(\theta)\circ\mathbf{B}(\mathbf{x}(\theta)) \\
\mathcal{A}(\theta) &= \omega - \frac{\epsilon^2}{2}\mathbf{Z}(\Theta)\cdot[\mathbf{B}(\mathbf{x}(\Theta))\circ\mathcal{D}\mathbf{B}(\mathbf{x}(\Theta))] \\
&\quad + \frac{\epsilon^2}{2}\beta(\theta)\cdot\mathcal{D}\beta(\theta) + \frac{\sigma^2}{2}\alpha(\theta)\frac{\partial}{\partial\theta}\alpha(\theta).
\end{aligned}$$

With this notation, the phase of each of our oscillators can be said to evolve according to (in the Itō calculus)

$$d\Theta = \mathcal{A}(\Theta)dt + \epsilon\,\mathbf{Z}(\Theta)\cdot(\mathbf{B}(\mathbf{x}(\Theta))\circ d\,\mathbf{W}) + \sigma\alpha(\Theta)d\hat{W}. \tag{4.23}$$

Next, we label the oscillators by μ so that our ensemble is $\mathbf{\Theta} = (\Theta^{(1)},\ldots,\Theta^{(\mu)},\ldots,\Theta^{(M)})$, where M is the total number of E-I pairs. If we now introduce the correlated Wiener processes $(\zeta^{(1)},\ldots,\zeta^{(M)})$ such that

$$d\zeta^{(\mu)} = \epsilon\,\mathbf{Z}(\Theta^{(\mu)})\cdot(\mathbf{B}(\mathbf{x}(\Theta^{(\mu)}))\circ d\,\mathbf{W}^{(\mu)}) + \sigma\alpha(\Theta^{(\mu)})d\hat{W}, \tag{4.24}$$

then we know that

$$\langle d\zeta^{(\mu)}\rangle = 0;$$

and that the ζs have a correlation matrix $C(\boldsymbol{\theta})$ given by:

$$C_{\mu,\nu}(\boldsymbol{\Theta})dt = \langle d\zeta^{(\mu)} d\zeta^{(\nu)} \rangle = [\epsilon^2 \boldsymbol{\beta}(\Theta^{(\mu)}) \cdot \boldsymbol{\beta}(\Theta^{(\nu)}) \delta_{\mu,\nu} + \sigma^2 \alpha(\Theta^{(\mu)}) \alpha(\Theta^{(\nu)})]dt,$$

where we have made extensive use of the fact that the variance of the sum of independent normal random variables is the sum of the variances of the individual variables.

As before this allows us to write down a compact Itō SDE for the whole ensemble:

$$d\Theta^{(\mu)} = \mathcal{A}(\Theta^{(\mu)})dt + d\zeta^{(\mu)}. \tag{4.25}$$

This means that the PDF of our ensemble evolves according to a FPE of the form of Equation (3.22):

$$\frac{\partial \mathbb{P}(\boldsymbol{\theta}, t)}{\partial t} = -\sum_{\mu=1}^{M} \frac{\partial}{\partial \theta^{(\mu)}} \mathcal{A}(\boldsymbol{\theta}) \mathbb{P}(\boldsymbol{\theta}) + \frac{1}{2} \sum_{\mu=1}^{M} \sum_{\nu=1}^{M} \frac{\partial^2}{\partial \theta^{(\mu)} \partial \theta^{(\nu)}} [C(\boldsymbol{\theta}) \mathbb{P}(\boldsymbol{\theta}, t)], \tag{4.26}$$

where $\mathbb{P}(\boldsymbol{\theta}, t)$ is the multivariate PDF of the whole ensemble. This means we can can carry out an averaging procedure as before to obtain the PDF $Q(\boldsymbol{\phi}, t)$ of our slow variables $\phi^{(\mu)} = \theta^{(\mu)} - \omega t$:

$$\frac{\partial Q(\boldsymbol{\phi}, t)}{\partial t} = -\bar{\Omega} \sum_{\mu=1}^{M} \frac{\partial Q}{\partial \phi^{(\mu)}} + \frac{1}{2} \sum_{\mu=1}^{M} \sum_{\nu=1}^{M} \frac{\partial^2}{\partial \phi^{(\mu)} \phi^{(\nu)}} \bar{C}(\boldsymbol{\phi}, t) Q(\boldsymbol{\phi}, t), \tag{4.27}$$

where in this case the correction term to the drift is given by:

$$\Omega(\theta) = \frac{\epsilon^2}{2} \boldsymbol{\beta}(\theta) \cdot D\boldsymbol{\beta}(\theta) + \frac{\sigma^2}{2} \alpha(\theta) \frac{\partial}{\partial \theta} \alpha(\theta) - \frac{\epsilon^2}{2} \mathbf{Z}(\Theta) \cdot [\mathbf{B}(\mathbf{x}(\Theta)) \circ \mathcal{D}\mathbf{B}(\mathbf{x}(\Theta))].$$

As in the previous cases, it is useful to define functions g and h to look at the effect of noise averaged over a whole limit cycle:

$$\begin{aligned} g(\phi) &:= \frac{1}{2\pi} \int_{-\pi}^{\pi} \alpha(s)\alpha(\phi + s) ds \\ h(\phi) &:= \frac{1}{2\pi} \int_{-\pi}^{\pi} \boldsymbol{\beta}(s) \cdot \boldsymbol{\beta}(\phi + s) ds. \end{aligned}$$

This means that the averaged correlation matrix of the FPE for Q is $\bar{C} =_{\mu\nu} (\boldsymbol{\phi}, t) = \sigma^2 g(\phi^{(\mu)} - \phi^{(\nu)}) + \epsilon^2 h(0) \delta_{i,j}$. Having evaluated the limit cycle and PRC $\mathbf{Z}$ for our choice of parameters, we can also evaluate the g- and h-functions. However, we

have not yet chosen values for χ_k. First, we consider the case where noise affects both the excitatory and inhibitory population symmetrically, that is, $\chi_E = \chi_I = 1/2$. We plot the corresponding g- and h-functions in figure 4.6.

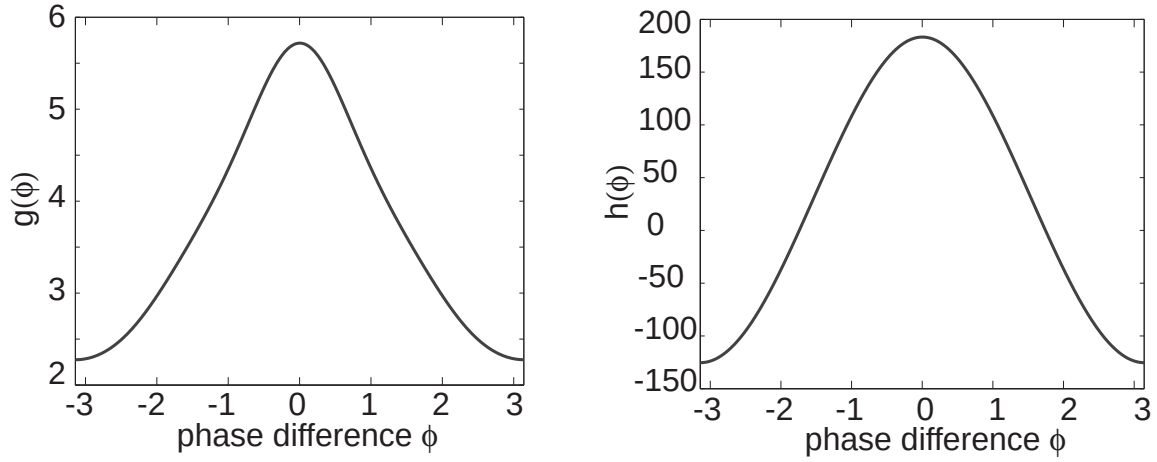

Figure 4.6: Plot of periodic functions g and h for an E-I limit cycle oscillator. Network parameters are the same as in the previous figures (4.4 and 4.5), and the stochastic drive is the same to the excitatory and inhibitory populations ($\chi_E = \chi_I = 1/2$).

As before, we now set the number of E-I pairs $M = 2$ for tractability. We note that this allows us to write down an explicit FPE for the PDF Q of our slow variables $\phi^{(1)}, \phi^{(2)}$, exactly of the form of equation 3.9 but with differently defined functions g, h and $\bar{\Omega}$:

$$\begin{aligned}\frac{\partial Q(\phi^{(1)},\phi^{(2)},t)}{\partial t} &= -\bar{\Omega}[\frac{\partial Q}{\partial \phi^{(1)}} + \frac{\partial Q}{\partial \phi^{(2)}}] + \sigma^2 \frac{\partial^2}{\partial \phi^{(1)} \partial \phi^{(2)}}\left[g(\phi^{(1)} - \phi^{(2)})Q\right] \\ &\quad + \frac{1}{2}(\epsilon^2 h(0) + \sigma^2 g(0))\left[(\frac{\partial^2}{\partial {\phi^{(1)}}^2}) + (\frac{\partial^2}{\partial {\phi^{(2)}}^2})\right] Q. \end{aligned} \tag{4.28}$$

Once again, we are interested in the phase difference, so we change variables to the mean phase $\lambda = (\phi^{(1)} + \phi^{(2)})/2$ and phase difference $\phi = \phi^{(2)} - \phi^{(1)}$. As our equations are of the same form as before, we can look for separable solutions $\Lambda(\lambda, t)$ and $\Phi(\phi, t)$ - then, the only steady-state solutions corresponding to 2π-periodic PDFs

are given by

$$\begin{aligned}\Lambda_0(\lambda) &= \frac{1}{2\pi} \\ \Phi_0(\phi) &= \frac{\Gamma_0}{\sigma^2[g(0)-g(\phi)]+\epsilon^2 h(0)}\end{aligned}$$

with the normalization constant $\Gamma_0 = [\int_{-\pi}^{\pi} ds/(\sigma^2[g(0)-g(\phi)]+\epsilon^2 h(0))]^{-1}$ as before.

From the shape of our g-function, we expect to be able to observe noise-induced synchronization of our neuronal populations. First, we calculate our steady-state distribuion Φ_0 for high, medium and low ratios of intrinsic to extrinsic noise. In this case we do it by keeping $\sigma = 0.08$ constant and varying $N = \epsilon^{-1/2}$ the number of neurons in each subpopulation (Figure 4.7). As expected, we see that for a low ratio of extrinsic to intrinsic noise ($N = 1000$), the PDF is almost flat indicating desynchronization, whereas for higher ratios of extrinsic to intrinsic noise ($N = 10000$), we observe much more synchronization as indicated by the sharper peak (see also [86]). This agrees with our hypothesis that noise-induced synchronization is a viable mechanism for explaining various synchronization phenomena in the brain; besides that, it also tells us, somewhat counterintuitively, that a stronger noisy input is required to synchronize smaller populations of neurons, due to the higher intrinsic noise, whereas a weaker noisy input may be sufficient to induce synchrony in larger populations of neurons.

Next, we confirm that our results hold when we keep the number of neurons in a population (and hence the intrinsic noise level) constant while varying the strength of the common noise (Figure 4.8). As we expect, the higher level of common noise induces a greater degree of synchrony. In this figure, we also verify our results by comparing our analytical curves to those obtained from stochastic simulations. The good agreement obtained is vindication of the approximations made in our analysis. These simulations were done by using a Euler-Maruyama scheme as before. The black dots were from stochastic simulations of an ensemble of a hundred oscillators, each described by a phase-reduced Langevin equation:

$$d\Theta = \mathcal{A}(\Theta)dt + \epsilon\,\mathbf{Z}(\Theta)\cdot(\mathbf{B}(\mathbf{x}(\Theta))\times d\,\mathbf{W}) + \sigma\,\mathbf{Z}(\Theta)\cdot\hat{\mathbf{B}}(\mathbf{x}(\Theta))\circ d\hat{W} \tag{4.29}$$

The ensemble was simulated for a sufficiently long time for it to reach synchrony. Then, the data points were obtained by putting the pairwise phase differences into 50 bins. This was repeated many times in order to obtain the average over multiple simulations (in total the number of data points used was on the order of 10^6).

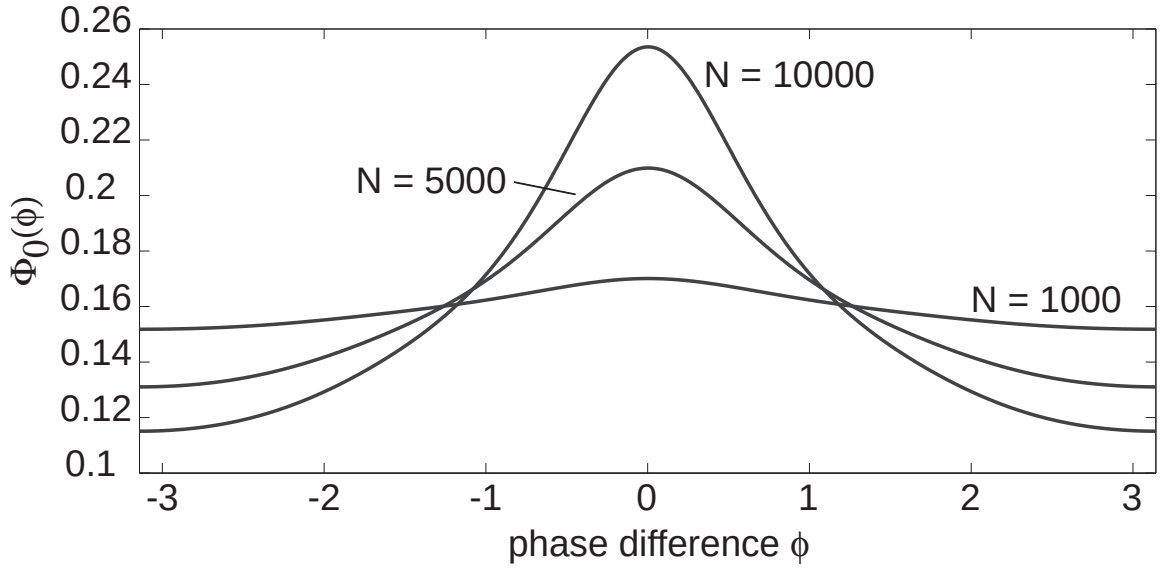

Figure 4.7: Steady-state PDF of the phase difference between two E-I oscillators for a fixed extrinsic noise strength $\sigma = 0.08$, and varying N the system size. Parameters as before.

For additional verification of our methods, we also conducted some simulations of the full system in the x_E, x_I plane (Equation 4.20). Once the ensemble was run to synchrony, the phase of the oscillators was obtained by using the least-squared method to map the oscillators onto the closest point on the limit cycle. When the isochrons are highly curved and/or the limit cycle has an irregular shape, this method can be inaccurate; however, we obtain good results here. (Computing isochrons accurately can be extremely difficult and computationally expensive [30, 57].) This was also indicative that we were working in an appropriate parameter regime such that the noise did not cause the trajectories to move too far away from the limit cycle.

Using this approximated phase, the pairwise phase differences were then placed into 25 bins (and repeated many times as in the phase-reduced case). The lower number of bins was due to the higher dimensionality of the system causing this method to be significantly more computationally expensive than the simulations of the phase-reduced equation. This is also the reason why, once we had verified that there was a reasonable fit, we did not carry out full simulations of all the cases presented here.

With both forms of our stochastic simulations, the fit with our analytical distribution not only verifies the various approximations made in the mathematical

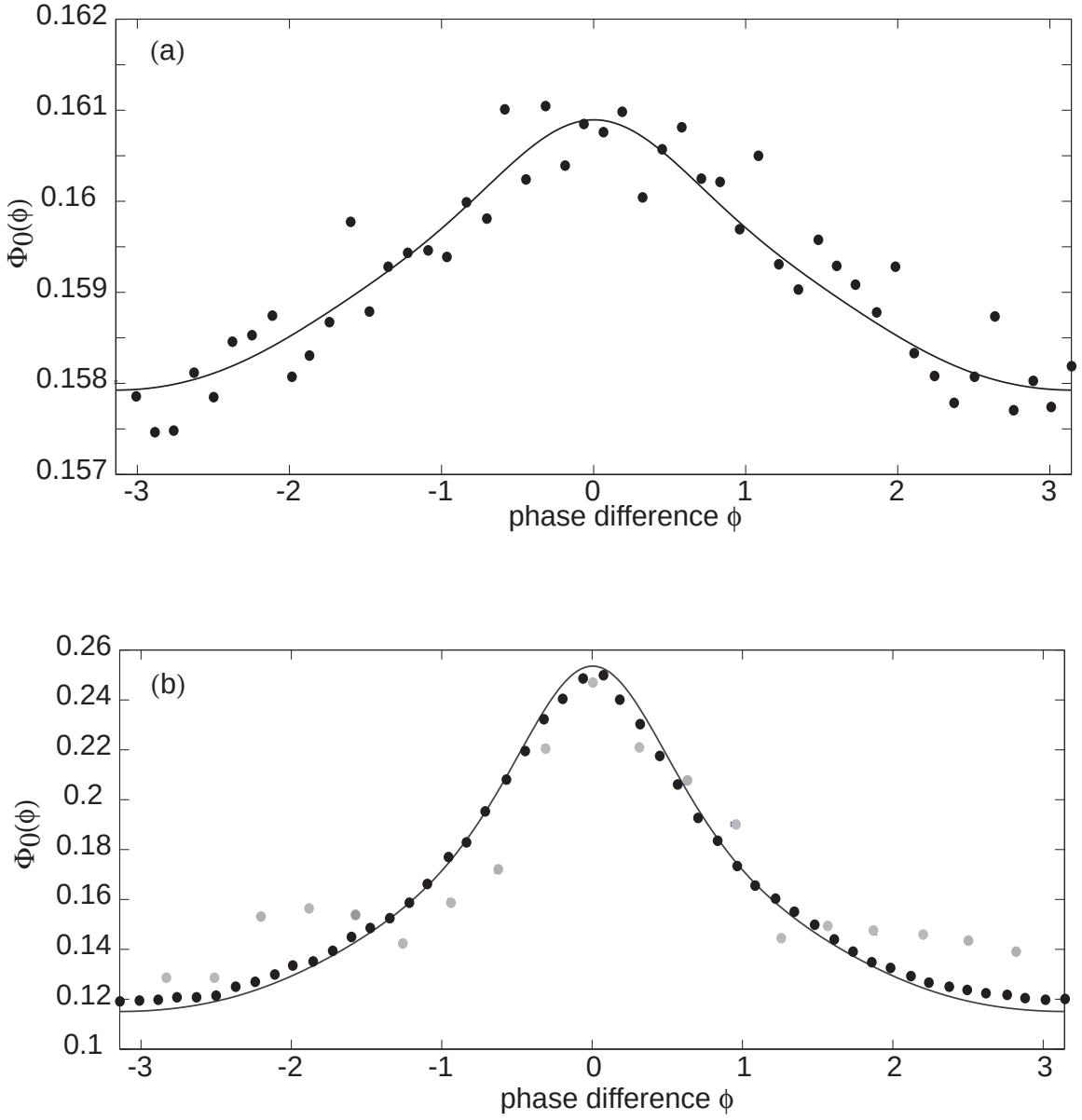

Figure 4.8: Probability distribution of the phase difference between a two E-I oscillators, parameters as before. Solid curves are based on analytical calculations, whereas black (gray) filled circles correspond to stochastic simulations of the phase-reduced (planar) Langevin equations. Top: Low ratio of extrinsic to intrinsic noise - $\sigma = 0.01$, $\epsilon = 10^{-2.5}$. The curve is very flat, showing little synchronization. Bottom: High ratio of extrinsic to intrinsic noise: $\sigma = 0.08$, $\epsilon = 10^{-2.5}$. Increasing σ causes the curve to have a much sharper peak and much more synchronization.

methods used to arrive at our analytical results; it also tells us that the PDF of the phase difference of a single pair of oscillators is representative of the PDF of the

pairwise phase differences in an ensemble of oscillators. That is to say, while the phases of the oscillators themselves are definitely not independent, their pairwise phase differences can be approximated as being identically distributed. As such, it shows that the methods presented here are just as useful for understanding the behaviour of large ensembles of neuronal columns as well as just a pair, which would have limited applications.

As compared to the ecological case, where the mean population levels are often the only easily observable quantity, neuroscientists have been able to obtain detailed spatio-temporal data from various techniques , both in vitro (such as recordings from slices of brain tissue) as well as in vivo (such as EEG recordings). As such the pattern of neuronal activity is often at least as important, if not more, than the mean levels. In the next section, we look at a different mode of noise-induced synchrony - clustering.

4.5.1 Clustering

Nakao *et al.* have previously shown that in the case of Stuart-Landau or Fitzhugh-Nagumo limit cycle oscillators with both correlated and uncorrelated noise, parameter regimes can be found where the periodic function g, and hence the PDF Φ_0, has multiple peaks [97]. This can occur when higher harmonics of the PRC become dominant or when the common noise source is multiplicative. The presence of these multiple peaks in Φ_0 results in an ensemble of oscillators forming clustered states, with intermittent transitions between these clusters induced by the uncorrelated noise.

For our E-I oscillators, we have been looking at the case where the external stochastic drive is appled symmetrically to the excitatory and inhibitory subpopulations ($\chi_E = \chi_I = 1/2$). In this instance we are unable to find a parameter regime where we obtain multiply peaked g and Φ_0. However, we can observe multiple peaks when we introduce an asymmetry between the excitatory and inhibitory stochastic drives, as shown by the plots of g in Figure 4.9.

Correspondingly, Φ_0 develops multiple peaks. When the common stochastic input is mainly presented to the inhibitory population, we find a peak at $\phi = 0$ and smaller peaks at $\phi = \pm 2\pi/3$. We verify this against simulations of our phase-reduced Langevin equations for the ensemble. The multiply peaked PDF causes the ensemble of oscillators to cluster in three regions around the limit cycle - we illustrate this in the inset of Fig. 4.10(top) with a snapshot of our simulated oscil-

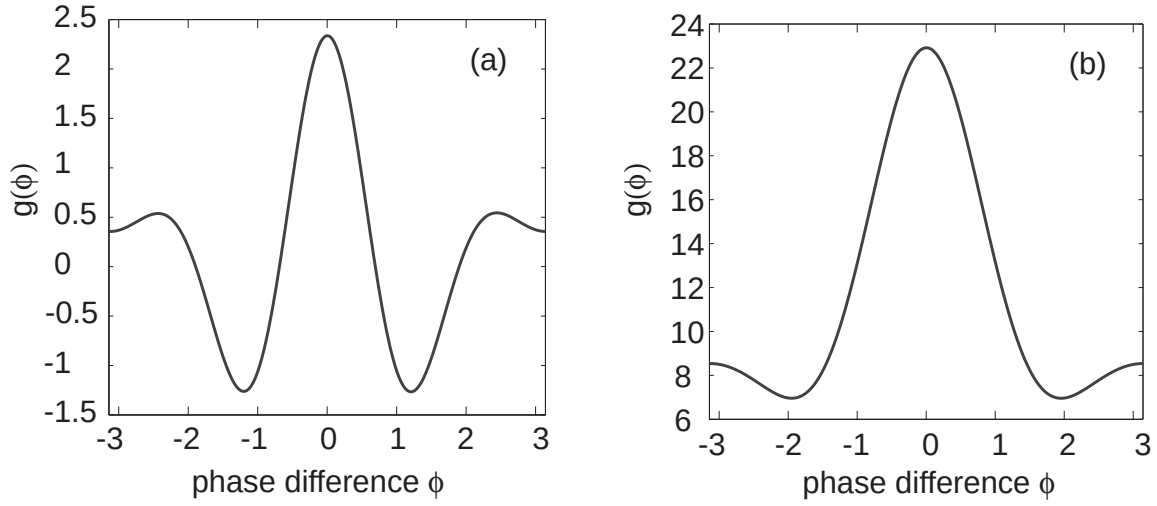

Figure 4.9: Periodic function g with multiple peaks when there is an asymmetry in the common extrinsic noise source to the excitatory and inhibitory populations. Other parameters are as before. Left: $\chi_E = 1/8, \chi_I = 7/8$ so that common stochastic drive is mainly to the inhibitory population. Right: $\chi_E = 7/8, \chi_I = 1/8$ so that common stochastic drive is mainly to the excitatory population.

lators at a point in time. On the other hand, when the stochastic drive is predominantly to the excitatory population (Figure 4.10(bottom)), we find a much sharper peak at $\phi = 0$ (compared to the symmetric case, for the same values of σ and ϵ) and a small peak at $\phi = \pi$. However, the latter does not contribute significantly to the dynamics, so that the oscillators are strongly synchronized. (If we had observed a larger peak at $\phi = \pi$ we would expect two clusters to form on the limit cycle.) Again, this is illustrated in the inset, which shows the oscillators strongly synchronized at one region of the limit cycle, with only a few individual oscillators out of phase.

Our results on clustering show that the techniques presented in this thesis have the potential to explain the appearance of more complicated patterns of neural behaviour than just synchrony. In addition, we see that a small change in the way neurons react to a noisy input can cause large qualitative differences in the modes of behaviour. This is a useful foundation in studying various neural phenomena, for example, as a starting point in examining the hypothesis that certain neuropathological disorders cause anomalous patterns of neural behaviour by altering the excitation of certain neurons. We look forward to extending the methods here to more specific neurobiological problems. In order to demonstrate that our techniques can be easily applied to other systems of neuronal oscillators, in the next

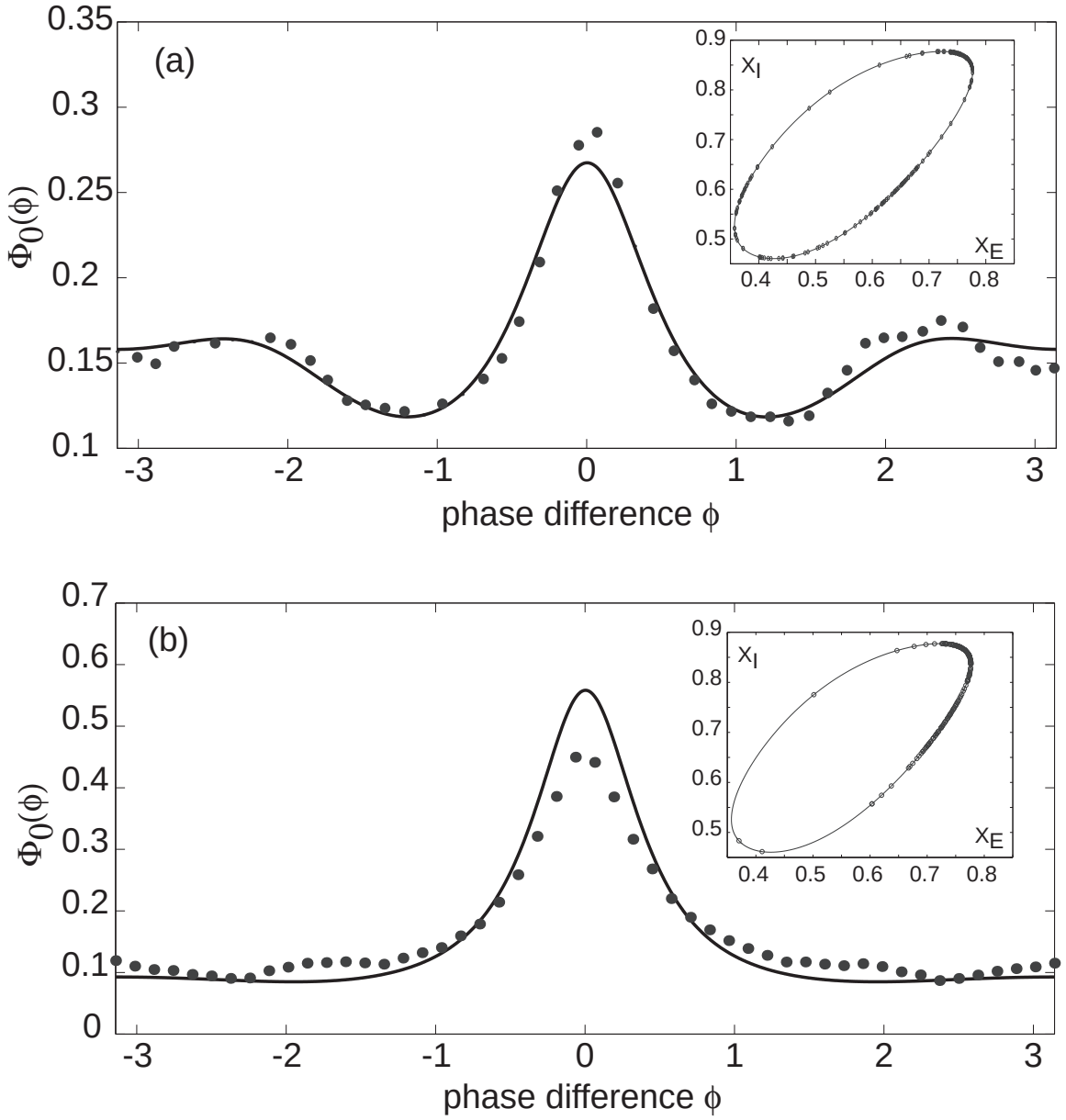

Figure 4.10: PDF $\Phi_0(\phi)$ when there is an asymmetry in the common extrinsic noise source to the excitatory and inhibitory populations. Here $\sigma = 0.01$, $\epsilon = 10^{-2.5}$ and other network parameters are as before. Solid curves are based on analytical calculations, whereas black filled circles correspond to stochastic simulations of the phase-reduced Langevin equations. Top: The common stochastic drive is mainly to the inhibitory population ($\chi_E = 1/8, \chi_I = 7/8$). Bottom: The common stochastic drive is mainly to the excitatory population ($\chi_E = 7/8, \chi_I = 1/8$). The insets show instantaneous distributions of the oscillators on the limit cycle.

section, we apply them to the ensemble of a recurrent excitatory populations with synaptic depression.

4.6 Noise-induced synchronization in a recurrent excitatory network

For a recurrent excitatory network, we recall from sections 4.3 and 4.4, that the neural master equation approach gives us a SDE of the form

$$dX = A(X)dt + \epsilon B(X)dW + \sigma\hat{B}(X) \circ d\hat{W}, \tag{4.30}$$

where we have chosen the transition rates of the master equation so that

$$\begin{aligned} A(x) &= -x + F(qx+h) \\ B(x) &= x + F(qx+h) \\ \hat{B}(x) &= \frac{1}{\sqrt{F_0}}F'(qx+h). \end{aligned}$$

However, this is non-autonomous because the synaptic depression q itself evolves according to:

$$\frac{dq}{dt} = k_+(1-q(t)) - k_-X(t)q(t), \tag{4.31}$$

i.e. q evolves deterministically in between jumps of X. However, since we have approximated the jumps in X to be infinitesimal and now describe X by a Langevin equation, we can write $\mathbf{X} = (X, Q)^T$ and write down the SDE for the population activity coupled with synaptic depression:

$$\begin{aligned} d\begin{pmatrix} X \\ Q \end{pmatrix} &= \begin{pmatrix} -X + F(QX+h) \\ k_+(1-Q) - k_-XQ \end{pmatrix}dt + \begin{pmatrix} X + F(QX+h) \\ 0 \end{pmatrix}dW \\ &\quad + \begin{pmatrix} \frac{1}{\sqrt{F_0}}F'(QX+h) \\ 0 \end{pmatrix} \circ d\hat{W}. \end{aligned} \tag{4.32}$$

In the absence of noise, we had previous analysed the bifurcation structure of the system - for the specific choice of parameters $k_+ = 0.02, \gamma = 20, F_0 = 1$ and $h = -0.15$, which is taken from previous studies of such populations, we found that it undergoes Hopf bifurcations, giving us the desired limit cycle behaviour for $0.07 < k_- < 0.18$ (approximately). For concreteness we set $k_- = 0.1$ in the rest

of this analysis. We can then numerically calculate the limit cycle exhibited by the population - plotted in Figure 4.11.

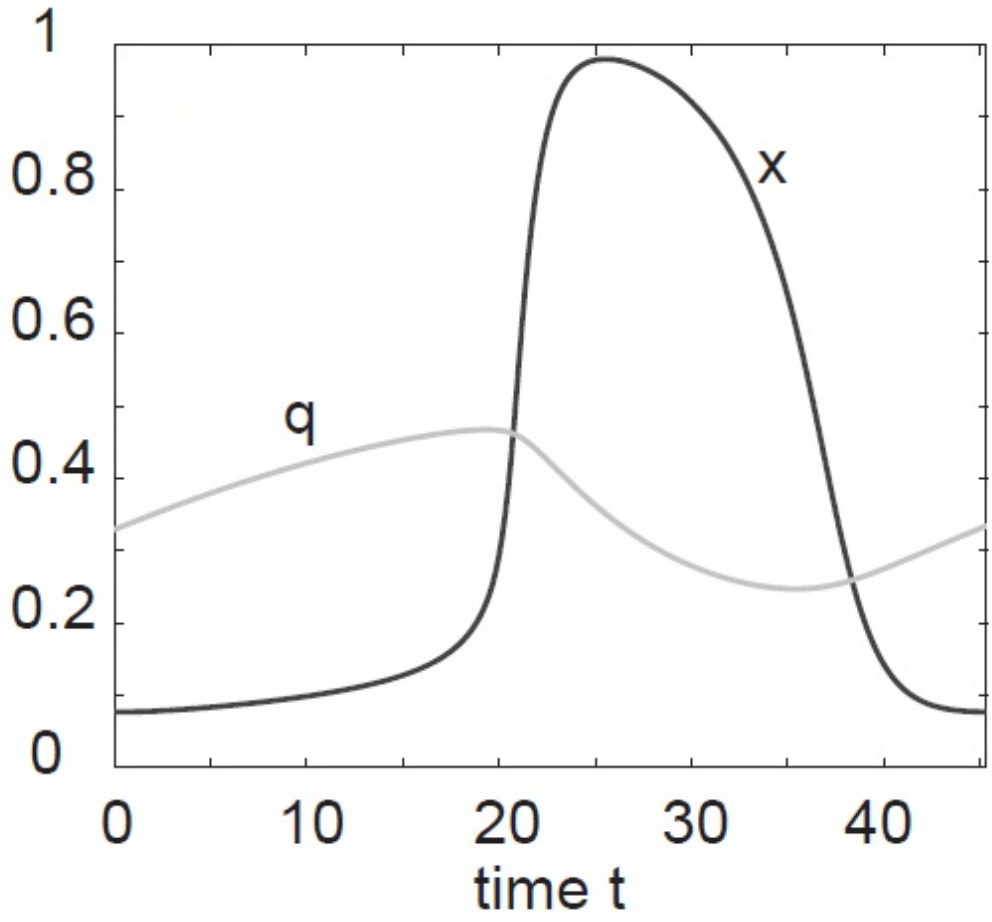

Figure 4.11: Limit cycle for an excitatory network with synaptic depression. The black line is the activity variable x and the gray line is the depression variable q. Parameter values are $F_0 = 1$ and $\gamma = 20$ for the sigmoid function, and $h = -0.15$, $k_+ = 0.02$, $k = 0.1$.

As in the previous cases, we would like to consider the phase of an oscillating population. In order to do so, we first calculate the phase response curve (Figure 4.12).

This allows us to carry out a phase reduction of equation 4.32. First, we note that the intrinsic noise term was being treated in the sense of Itō while the common noise term was being treated in the sense of Stratonovich. In order to perform the phase reduction, we first convert it into a Stratonovich SDE, which means the

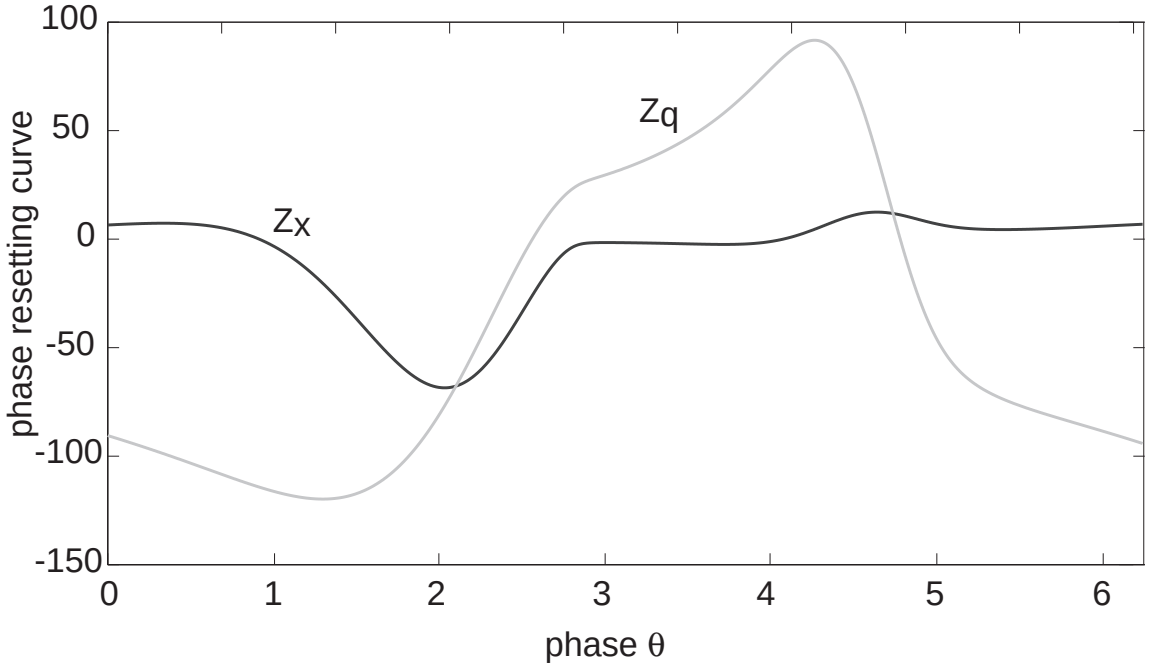

Figure 4.12: PRC $\mathbf{Z} = (Z_x, Z_q)^T$ for an excitatory network with synaptic depression. Parameter values as before.

normal rules of calculus will apply:

$$d\begin{pmatrix} X \\ Q \end{pmatrix} = \begin{pmatrix} A(\mathbf{X}) - \frac{\epsilon^2}{2} B(\mathbf{X}) \frac{\partial B(\mathbf{X})}{\partial x} \\ k_+(1-Q) - k_- XQ \end{pmatrix} dt + \begin{pmatrix} B(\mathbf{X}) \\ 0 \end{pmatrix} \circ dW + \begin{pmatrix} \hat{B}(\mathbf{X}) \\ 0 \end{pmatrix} \circ d\hat{W}. \tag{4.33}$$

After making the change of variables $\mathbf{X} \to \Theta$, we obtain:

$$\begin{aligned} d\Theta &= [\omega - \frac{\epsilon^2}{2} Z_x(\Theta) B(x(\Theta), q(\Theta)) \frac{\partial B(x(\Theta), q(\Theta))}{\partial x}] dt \\ &\quad + \epsilon Z_x(\Theta) B(x(\Theta), q(\Theta)) \circ dW + \sigma Z_x(\Theta) \hat{B}(x(\Theta), q(\Theta)) \circ d\hat{W}, \end{aligned} \tag{4.34}$$

where Z_x is the x-component of the PRC and all the functions are evaluated on the

limit cycle. We simplify notation by defining the following functions:

$$\begin{aligned}\alpha(\theta) &= Z_x(\theta)\hat{B}(x(\theta),q(\theta))\\ \beta(\theta) &= Z_x(\theta)B(x(\theta),q(\theta))\\ \Omega(\theta) &= \frac{\epsilon^2}{2}Z_x(\theta)B(x(\theta),q(\theta))\frac{\partial B(x(\theta),q(\theta))}{\partial x}-\frac{\epsilon^2}{2}\beta(\theta)\frac{\partial\beta(\theta)}{\partial\theta}-\frac{\sigma^2}{2}\alpha(\theta)\frac{\partial\alpha(\theta)}{\partial\theta}.\end{aligned}$$

This is particularly helpful as we would like to look for the Fokker-Planck equation for the PDF of the ensemble, and hence need to re-express the Langevin equation 4.34 in Itō form:

$$d\Theta = (\omega-\Omega(\Theta))dt+\beta(\Theta)dW+\alpha(\Theta)d\hat{W}. \tag{4.35}$$

Now, if we consider an ensemble of M uncoupled recurrent excitatory populations with synaptic depression, we are therefore able to follow the procedure of the previous sections and describe the phases by an Itō SDE:

$$d\Theta^{(\mu)} = \mathcal{A}(\Theta^{(\mu)})dt+d\zeta^{(\mu)}, \tag{4.36}$$

where we have labelled the populations $1,\dots,M$ by μ, $\mathcal{A}=\omega-\Omega$ and the Wiener processes $(\zeta^{(1)},\dots,\zeta^{(M)})$ are such that $\zeta^{(\mu)}=\beta(\Theta^{(\mu)})dW^{(\mu)}+\alpha(\Theta^{(\mu)})d\hat{W}$. This means that the ζs are non-trivially correlated by the fact that they have independent and common components, which are themselves phase-dependent - we get the following expressions for their mean and (co-)variance:

$$\begin{aligned}\langle d\zeta^{(\mu)}\rangle &= 0\\ \langle d\zeta^{(\mu)}d\zeta^{(\nu)}\rangle &= [\alpha(\Theta^{(\mu)})\alpha(\Theta^{(\nu)})+\beta(\Theta^{(\mu)})\beta(\Theta^{(\nu)})\delta_{\mu,\nu}]dt.\end{aligned}$$

We can therefore see from the Itō SDE describing the ensemble that the FPE describing the evolution of the PDF $\mathbb{P}(\mathbf{\Theta})$ of the ensemble is:

$$\frac{\partial\mathbb{P}(\mathbf{\Theta})}{\partial t} = -\sum_{\mu=1}^{M}\frac{\partial}{\partial\theta^{(\mu)}}\mathcal{A}(\mathbf{\Theta})\mathbb{P}(\mathbf{\Theta})+\frac{1}{2}\sum_{\mu=1}^{M}\sum_{\nu=1}^{M}\frac{\partial}{\partial\theta^{(\mu)}\theta^{(\nu)}}C(\mathbf{\Theta})\mathbb{P}(\mathbf{\Theta}), \tag{4.37}$$

where the matrix C is such that

$$C_{\mu,\nu}(\mathbf{\Theta})dt = \langle d\zeta^{(\mu)}d\zeta^{(\nu)}\rangle.$$

We note that this equation (4.37) is of exactly the same form as equation (4.26) that we obtained in the case of the ensemble of E-I oscillators. Hence, if we follow the same procedure and set the size of the ensemble to two populations ($M = 2$), we obtain the same expression for the steady-state PDF for the phase difference between them:

$$\Phi_0(\phi) = \frac{\Gamma_0}{\sigma^2[g(0) - g(\phi)] + \epsilon^2 h(0)} \tag{4.38}$$

with Γ_0 a normalization constant as before. The key difference between the two systems is through the functions g and h - in this case they are defined as:

$$\begin{aligned} g(\phi) &:= \frac{1}{2\pi}\int_{-\pi}^{\pi} \alpha(s)\alpha(\phi + s)ds \\ h(\phi) &:= \frac{1}{2\pi}\int_{-\pi}^{\pi} \beta(s)\beta(\phi + s)ds. \end{aligned}$$

We can evaluate these functions for the choice of parameters we have been working with, and plot them in Figure 4.13. The g-function has a peak at $\phi = 0$ indicating that we expect there to be a corresponding peak in the steady-state PDF $\Phi_0(\phi)$, indicating noise-induced synchronization. We see this in our analytically calculated PDF (Figure 4.14), and obtain good agreement with stochastic simulations of the phase-reduced Langevin equation for the system (equation 4.34).

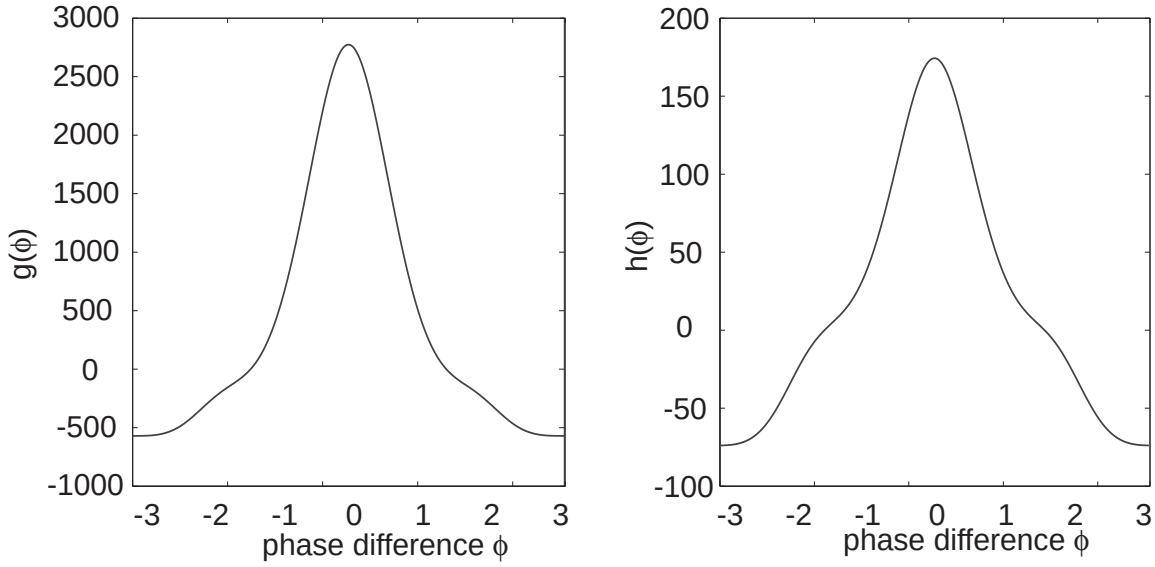

Figure 4.13: Plot of the functions g and h for an excitatory network with synaptic depression. Parameters as before.

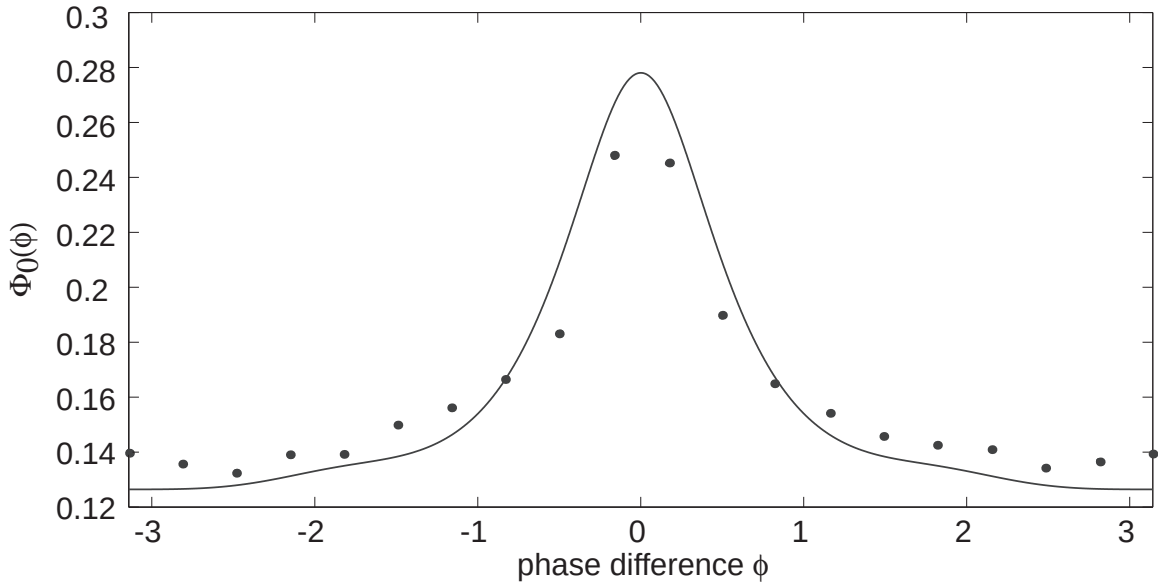

Figure 4.14: Probability distribution of the phase difference $\Phi_0(\phi)$ between a pair of excitatory networks with synaptic depression. Solid curves are based on analytical calculations, whereas black filled circles correspond to stochastic simulations of the phase-reduced Langevin equation. Parameters as before, with extrinsic noise strength $\sigma = 2.5 \times 10^{-3}$, $\epsilon = 10^{-2}$.

This application of our techniques to an ensemble of recurrent excitatory networks with synaptic depression is important as it shows that our results are independent of the particular choice of oscillating unit or biological model. Furthermore, we have showed how one can take into account the potentially large effects of synaptic depression into a master equation formulation of population activity - similar methods could be used for other forms of synaptic fatigue or plasticity. In general, these hybrid systems have also been used to model a variety of other processes, which we discuss in the concluding chapter of this thesis.

Before moving onto such future directions for work, we would like to present one further chapter of results in this thesis, that is, to study the behaviour of systems in which both coupling and noise-induced synchronization are present.

Chapter 5

Dispersively coupled ecological populations

So far, we have examined synchrony using the relatively new theory of noise-induced synchronization. However, there is a large volume of literature on synchronization induced by various forms of coupling between oscillators - for example, the Kuramoto model mentioned at the end of section 3 usually involves global sinusoidal coupling in an ensemble of oscillators. Hence, a natural step would be to examine the effects of both correlated noise and coupling on the synchrony of a system. This is an extremely broad question and not much work has been done on it. In ecology, Goldwyn and Hastings [52] considered the effect of both dispersive coupling and environmental fluctuations on ensembles of predator-prey oscillators - they did this by simulating ensmebles of Rosenzweig-Macarthur models with coupling and spatially correlated Poisson inputs. Most of the results in that paper were numerical; here, we use a complementary approach with Gaussian noise instead in order to obtain some analytical results.

Our approach gives us similar equations to that considered in the case of Ly and Ermentrout [84] within the context of a pair of coupled Morris-Lecar neurons. However, these authors were mainly concerned with devloping a computationally efficient method for calculating the steady-state PDF based on the use of Fourier methods and asymptotic reduction techniques. In contrast, by consider the PDF of the phase difference, rather than the full system of a pair of oscillators, we are able to simplify the study of this system considerably, as well as presenting novel results on the transient behaviour by solving the time-dependent Fokker-Planck equation.

To begin, we first introduce the Rosenzweig-Macarthur model.

5.1 Rosenzweig-Macarthur model

In the Holling-Tanner model we examined in chapter three, both predators and prey grow logistically. An alternative model, attributed to Rosenzweig and Macarthur [108], has the predators multiplying at a rate proportional to the rate of consumption of prey, and dying due to natural causes at a linear rate:

$$\begin{aligned} \frac{dx}{dt} &= rx(1-\frac{x}{K})-\frac{mxy}{A_0+x} \\ \frac{dy}{dt} &= \frac{h'mxy}{A_0+x}-dy, \end{aligned} \tag{5.1}$$

where d is the death rate of the predators and h' is a coefficient relating to how many prey are required to support a predator. As before we would like to rescale this system in order to reduce the number of parameters. We follow the approach of [50] and substitute $\bar{t} = mt$, $\bar{x} = x/A_0$, $\bar{y} = (mh'/rA_0)y$ to obtain (after dropping overbars):

$$\begin{aligned} \epsilon\frac{dx}{dt} &= x(1-\alpha x)-\frac{xy}{1+x} \\ \frac{dy}{dt} &= \frac{xy}{1+x}-\eta y, \end{aligned} \tag{5.2}$$

where $\alpha = A_0/K$, $\eta = d/m$, $\epsilon = m/r$. Also note that ϵ is assumed to be small, and the system becomes a relaxation oscillator in the limit $\epsilon \to 0$.

5.1.1 Critical points and stability analysis

In order to look for parameter regimes with stable limit cycles, we seek the critical points of the system. Setting $dy/dt = 0$ gives us $y = 0$ or $x = \eta/(1-\eta)$. If $y = 0$, setting $dx/dt = 0$ gives us $x = 0$ or $x = 1/\alpha$. On the other hand, if $x = \eta/(1-\eta)$, we must have $y = (1-(1+\alpha)\eta)(1-\eta)^{-2}$. As with the previous ODE models we start by calculating the Jacobian:

$$J = \begin{pmatrix} \frac{1}{\epsilon}(1-2\alpha x-\frac{y}{(1+x)^2} & -\frac{1}{\epsilon}\frac{x}{1+x} \\ \frac{y}{(1+x)^2} & \frac{x}{1+x}-\eta \end{pmatrix}. \tag{5.3}$$

Since $J|_{(0,0)} = \begin{pmatrix} \frac{1}{\epsilon} & 0 \\ 0 & -\eta \end{pmatrix}$, its eigenvalues are $1/\epsilon$ and $-\eta$, so the origin is a saddle. $J|_{(\frac{1}{\alpha},0)} = \begin{pmatrix} -\frac{1}{\epsilon} & -\frac{1}{\epsilon(1+\alpha)} \\ 0 & \frac{1}{1+\alpha} - \eta \end{pmatrix}$ which gives us eigenvalues of $-1/\epsilon$ and $1/(1+\alpha) - \eta$. This means that it is a saddle if $\eta(1+\alpha) < 1$, and a stable node otherwise. At the non-trivial equilibrium $(x^*, y^*) = (\eta/(1-\eta), (1-(1+\alpha)\eta)(1-\eta)^{-2})$, we obtain

$$J|_{(x^*,y^*)} = \begin{pmatrix} \frac{1}{\epsilon}\frac{\eta}{1-\eta}(1-\alpha-\eta-\alpha\eta) & -\frac{\eta}{\epsilon} \\ 1-(1+\alpha)\eta & 0 \end{pmatrix}.$$

Solving for the eigenvalues:

$$\lambda\left(\lambda - \frac{1}{\epsilon}\frac{\eta}{1-\eta}(1-\alpha-\eta-\alpha\eta)\right) + \frac{\eta}{\epsilon}(1-(1+\alpha)\eta) = 0$$

Denoting the determinant of the above quadratic equation as Δ, we see that $\lambda_1, \lambda_2 = \frac{1}{2\epsilon}\frac{\eta}{1-\eta}(1-\alpha-(1+\alpha)\eta) + \frac{\Delta}{2}$, with both eigenvalues negative for $\eta > \frac{1-\alpha}{1+\alpha}$, so our equilibrium is a stable node. As η is decreased, the system undergoes a Hopf bifurcation at $\frac{1-\alpha}{1+\alpha}$, meaning that our equilibrium becomes an unstable node and we obtain a stable limit cycle around it, in agreement with the results of [59]. In this chapter we focus on two sets of parameters: (a) $\epsilon = 0.1$, $\alpha = 0.4$, $\eta = 0.4$, and (b) $\epsilon = 0.1$, $\alpha = 0.3$, $\eta = 0.3$. If we consider two Rosenzweig-Macarthur systems coupled by dispersal, parameter set (a) leads to synchrony, while parameter set (b) leads to asynchronous phase-locking. We choose these parameter sets in particular in order to build on the work of, and compare our results to, those of [50, 51]. Figure 5.2 shows a bifurcation diagram for parameter set (a).

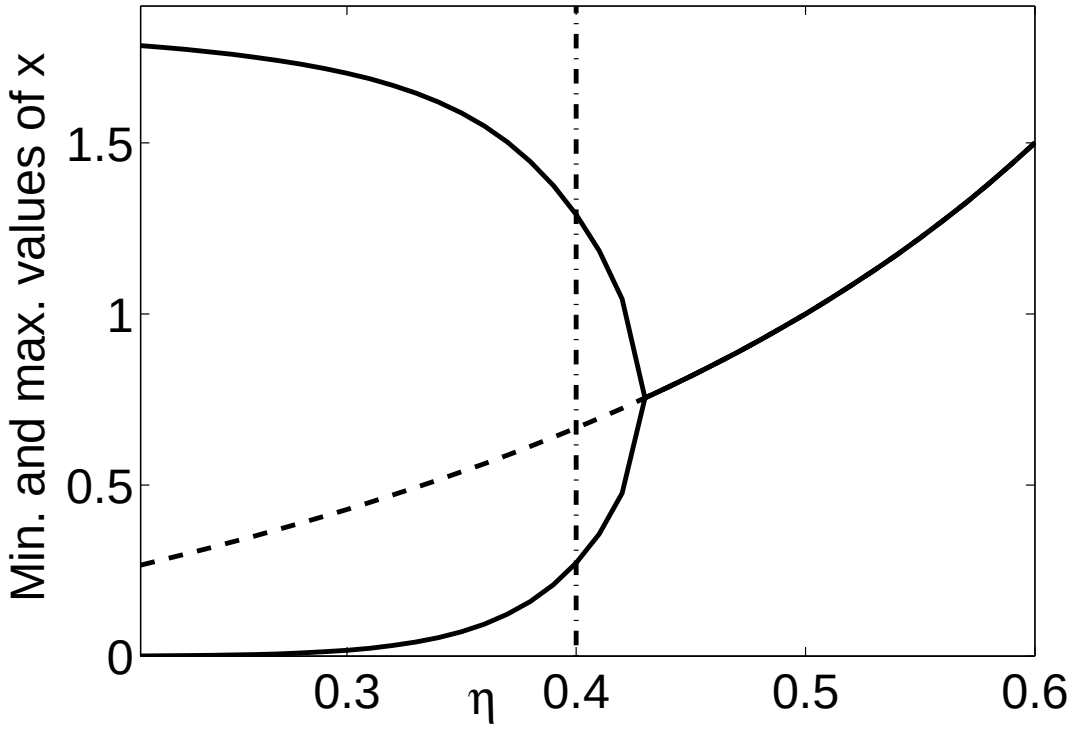

Figure 5.2: Bifurcation diagram for the Rosenzweig-Macarthur model, parameter set (a). Here we kept ϵ and α constant while varying η. The y-axis shows the maximum and minimum values of x in the limit cycles where they exist, or x^* when it is the stable equilibrium (it is represented as a dotted line when unstable). The vertical dotted line corresponds to the parameter value $\eta = 0.4$ which is used in later chapters.

5.2 Coupled oscillators

Before looking at the effects of noise on the system, we would like to examine the effects of dispersive coupling. In order to do that, we first show how the phase reduction method introduced in section 2.1 suggests a natural way to study coupled oscillators in general. This could arise, for example, from synaptic coupling between neurons or neuronal populations, or in our case, dispersive coupling between ecological populations. For simplicity we consider a pair of coupled oscillators in the most general sense:

$$\begin{aligned} \dot{\mathbf{x}_1} &= \mathbf{F}(\mathbf{x}_1) + D\,\mathbf{F}^*(\mathbf{x}_1, \mathbf{x}_2) \\ \dot{\mathbf{x}_2} &= \mathbf{F}(\mathbf{x}_2) + D\,\mathbf{F}^*(\mathbf{x}_2, \mathbf{x}_1), \end{aligned} \tag{5.4}$$

where $D \ll 1$ is the strength of the coupling, and $\mathbf{F}^*$ is a general function representing the coupling between the two oscillators. Applying the phase reduction method as previously described in this chapter will give us

$$\begin{aligned} \dot{\theta_1} &= \omega + D\,\mathbf{Z}(\theta_1) \cdot \mathbf{F}^*(\theta_1, \theta_2)) \\ \dot{\theta_2} &= \omega + D\,\mathbf{Z}(\theta_2) \cdot \mathbf{F}^*(\theta_2, \theta_1)). \end{aligned} \tag{5.5}$$

Since we have assumed that the coupling is weak, we can assume that the change in phase due to coupling is small compared to ω. We can therefore average the effect of coupling on the phase over one cycle [97], that is, we make the approximation

$$\dot{\theta_1} \approx \omega + \frac{D}{2\pi} \int_0^{2\pi} Z(\theta_1) \cdot \mathbf{F}^*(\theta_1, \theta_1 + [\theta_2 - \theta_1]) d\theta_1 \tag{5.6}$$

(and likewise for θ_2). Hence, defining a H-function:

$$H(\phi) = \frac{1}{2\pi} \int_{-\pi}^{\pi} \mathbf{Z}(\omega s) \cdot \mathbf{F}^*(\omega s, \omega s + \phi)) ds \tag{5.7}$$

allows us to write our system as:

$$\begin{aligned} \dot{\theta_1} &= \omega + DH(\theta_2 - \theta_1) \\ \dot{\theta_2} &= \omega + DH(\theta_1 - \theta_2) \end{aligned} \tag{5.8}$$

Now introducing a new variable ϕ to denote $\theta_2 - \theta_1$ and taking the difference of these equations gives us

$$\dot{\phi} = D[H(-\phi) - H(\phi)] := DG(\phi) \tag{5.9}$$

This means that we can extract useful information about the behaviour of the coupled oscillators merely by calculating this G-function. The steady states ϕ^* such that $G(\phi^*) = 0$ correspond to phase-locking, and are stable when the gradient $G'(\phi^*) < 0$ and unstable when $G'(\phi^*) > 0$. Furthermore, the magnitude of $G(\phi)$ tells us the rate of convergence to a stable steady state at the phase ϕ. From the derivation of the G-function, we know that it is odd and 2π periodic, which gives us steady states at 0 and π.

Now, we will illustrate the use of these techniques by applying them to our predator-prey systems.

5.2.1 Dispersively coupled Rosenzweig-Macarthur populations

In population ecology, dispersal or migration between populations is a very natural way to introduce coupling into a system. Here we employ the techniques of the previous section by considering a pair of Rosenzweig-Macarthur predator-prey populations coupled by dispersal, as in [50, 128]. Each of the populations is governed by the ODEs described in section 5.1 (equation 5.1, with the addition of the $D_x(x_j - x_i)$ and $D_y(y_j - y_i)$ terms, which represent the dispersal of strength D_x and D_y in the prey and predator populations respectively:

$$\begin{aligned} \frac{dx_i}{dt} &= rx_i(1 - \frac{x_i}{K}) - \frac{mx_iy_i}{A_0 + x_i} + D_x(x_j - x_i) \\ \frac{dy_i}{dt} &= \frac{h'mx_iy_i}{A_0 + x_i} - dy_i + D_y(y_j - y_i) \qquad i, j = 1, 2; i \neq j. \end{aligned} \tag{5.10}$$

Rescaling as before gives us

$$\begin{aligned} \frac{dx_i}{dt} &= \frac{1}{\epsilon}[x_i(1 - \alpha x_i) - \frac{x_iy_i}{1 + x_i}] + D(x_j - x_i) \\ \frac{dy_i}{dt} &= \frac{x_iy_i}{1 + x_i} - \eta y_i + D(y_j - y_i) \end{aligned} \tag{5.11}$$

where we have set the dispersal $D = D_x/a = D_y/a$ for simplicity. (Depending on the situation one may want to consider significantly more dispersal in one species than

another, for example in herbivore-plant systems.) Next, we would like to perform a phase reduction:

$$\begin{aligned}\frac{d\theta_1}{dt} &= \omega + \mathbf{Z}(\theta_1)\cdot D\begin{pmatrix} x^*(\theta_2)-x^*(\theta_1) \\ y^*(\theta_2)-y^*(\theta_1)\end{pmatrix} \\ \frac{d\theta_2}{dt} &= \omega + \mathbf{Z}(\theta_2)\cdot D\begin{pmatrix} x^*(\theta_1)-x^*(\theta_2) \\ y^*(\theta_1)-y^*(\theta_2)\end{pmatrix}\end{aligned}$$

where $x^*(\theta)$ and $y^*(\theta)$ refer to the x and y values on the limit cycle that correspond to a phase θ. [50] examines this system for four sets of parameter values - here we carry out the calculations for the two sets of parameters that show the most striking differences. For each of them, we numerically evaluate the limit cycles and PRCs. (Fig. 5.3).

One we have evaluated the limit cycle $\mathbf{x}^*$ we can then calculate the PRC $\mathbf{Z}$ by using the adjoint method described in the previous section, that is, solving the differential equation

$$\frac{d\mathbf{Z}}{dt} = -[D_{\mathbf{x}}\mathbf{F}(\mathbf{x})|\mathbf{x}^*(t)]^T\cdot\mathbf{Z} \tag{5.12}$$

backwards in time, and normalizing such that

$$\mathbf{Z}\cdot\frac{d\mathbf{x}^*}{dt} = \omega. \tag{5.13}$$

As the phase response curve is a measure of how the system responds to a perturbation at any given phase, we can see from the figures that noise and/or dispersal have different effects on the system depending on when they occur - in particular, for parameter set (b), we see that prey migration can have a very large impact on the dynamics of the system. The large spike in the PRC correponds to the section of the limit cycle where the prey population is low, which matches one's intuitive understanding of the system.

Next, we evaluate the G-functions with the expressions from earlier:

$$\begin{aligned}G(\phi) &= H(-\phi)-H(\phi) \\ &= \frac{1}{2\pi}\int_{-\pi}^{\pi}\mathbf{Z}(s)\cdot\mathbf{F}^*(s,s-\phi))ds - \frac{1}{2\pi}\int_{-\pi}^{\pi}\mathbf{Z}(s)\cdot\mathbf{F}^*(s,s+\phi))ds \\ &= \frac{1}{2\pi}\int_{-\pi}^{\pi}\mathbf{Z}(s)\cdot[\mathbf{F}^*(s,s-\phi))-\mathbf{F}^*(s,s+\phi))]ds\end{aligned} \tag{5.14}$$

In this case $\mathbf{F}^*(s_1,s_2) = (x^*(s_2)-x^*(s_1), y^*(s_2)-y^*(s_1))^T$.

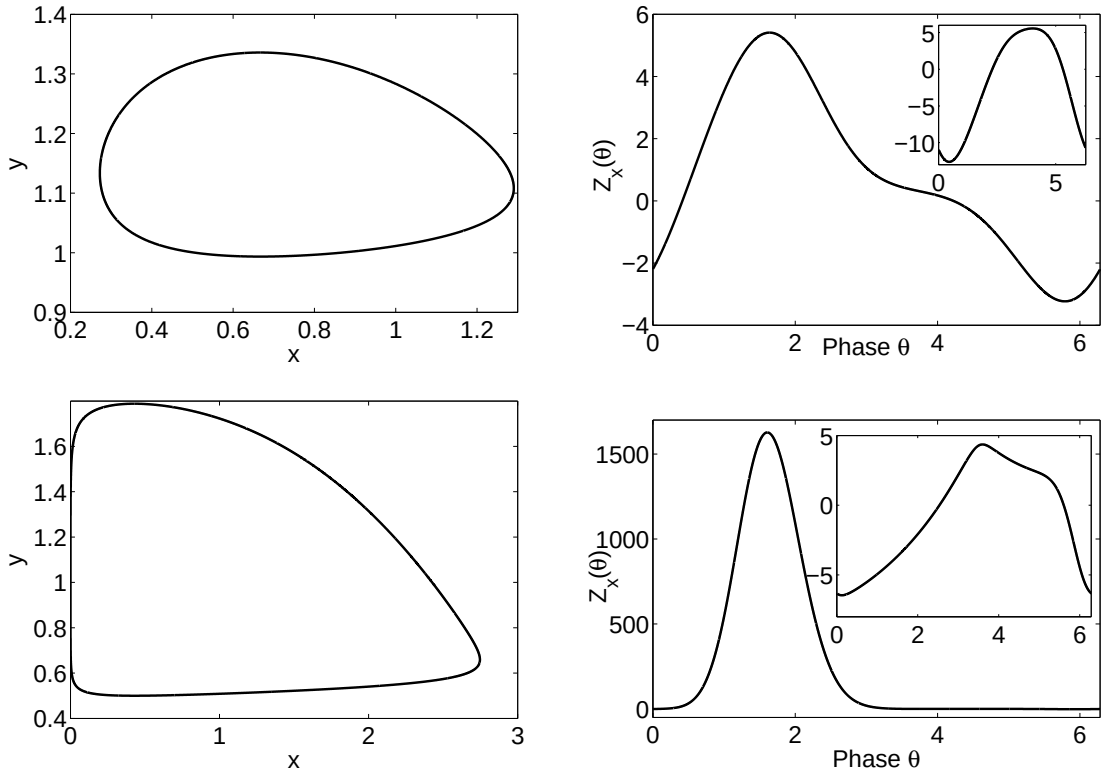

Figure 5.3: Limit cycles and PRCs for the Rosenzweig-Macarthur system. Left: Limit cycles. Right: x-component of the PRC. (y-component is inset). Top row: Parameter set (a): $\epsilon = .1$, $\alpha = .4$, $\eta = .4$. Bottom row: Parameter set (b): $\epsilon = .1$, $\alpha = .3$, $\eta = .3$.

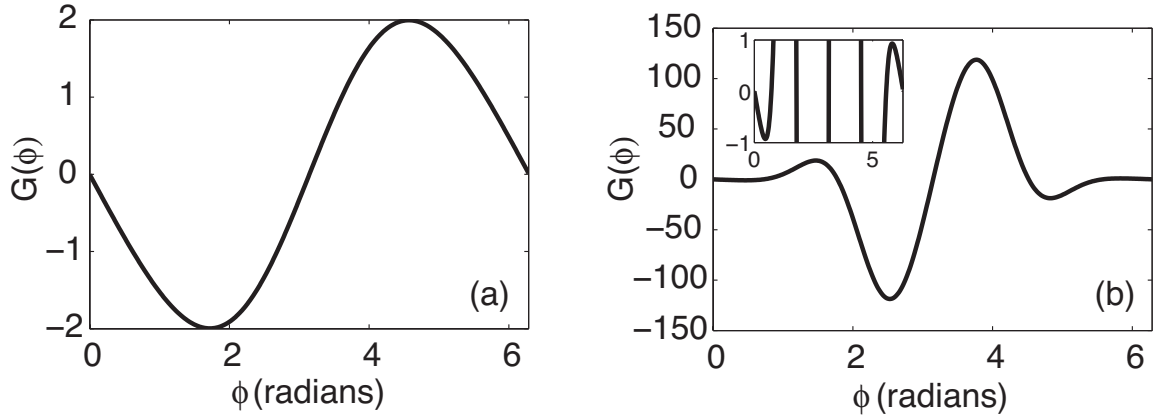

Figure 5.4: Numerically evaluated G-functions. (a) $\epsilon = 0.1$, $\alpha = 0.4$, $\eta = 0.4$. Only stable phase-locked state is the synchronous state $\phi = 0$. (b) $\epsilon = 0.1$, $\alpha = 0.3$, $\eta = 0.3$. There is now an additional pair of stable asynchronous states. Inset: Close-up of behaviour near $\phi = 0$.

In Fig. 5.4, we plot $G(\phi)$ for the same two sets of parameters used earlier. In Fig. 5.4(a) the synchronous state $\phi = 0$ is the only stable steady state, whereas in Fig. 5.4(b) there are additional stable asynchronous states at $\phi \approx 1.78$ (and by symmetry $\phi \approx 2\pi - 1.78$); the asynchronous states have a much larger basin of attraction compared to the synchronous state. This implies that dispersal always causes the system to go to synchrony for parameter set (a), while for (b), it causes asynchronous phase-locking for a large range of initial conditions. The fact that this relatively small change in parameters may mean large qualitative differences in the behaviour of the system could potentially be important in designing experiments. For example, the Rosenzweig-Macarthur model was used to compare against experimental data in [128]. As it is difficult to obtain exact parameters, the authors there obtain results by varying parameters and running simulations over multivariate parameter space - our analysis here shows that one could potentially study experimentally the effect of dispersal on such populations in order to determine which parameter regime the system is in.

Moreover, as we shall see later in this chapter, the relative sizes of the basins of attraction play a much larger role in the presence of noise. In the case of parameter set (b), if the system was subject to uncorrelated background noise, which is an assumption often made in biological systems, one would expect the system to spend the majority of its time in the asynchronous state, with only short excursions to the synchronous state before the noise causes it to jump back into the basin of attraction of the asynchronous state. (The exact dynamics of course would depend

on the rate of attraction to the different states and the magnitude of the noise.) Having calculated the response of a pair of Rosenzweig-Macarthur oscillators to dispersive coupling, we can then examine how the modes of synchrony caused by coupling are affected by noise, both correlated and uncorrelated.

5.3 Effects of correlated noise on dispersively coupled populations

We start by recalling that we described a pair of dispersively coupled RM oscillators with the following coupled ODEs (after rescaling):

$$\begin{aligned} \frac{dx_i}{dt} &= \frac{1}{\epsilon}[x_i(1-\alpha x_i) - \frac{x_i y_i}{1+x_i}] + D(x_j - x_i) \\ \frac{dy_i}{dt} &= \frac{x_i y_i}{1+x_i} - \eta y_i + D(y_j - y_i) \end{aligned} \tag{5.15}$$

where $i, j = 1, 2$. We assume in this case that we can model common extrinsic noise by assuming that all our predator populations and all the prey populations are driven by common (Stratonovich) white noise terms $\xi_y(t)$ and $\xi_x(t)$ respectively. We do this in order to simplify our analysis and look at the basic qualitative effects it has on our system. Hence, in this case, we can write our system with extrinsic noise of strength σ as

$$\begin{aligned} \frac{dX_i}{dt} &= F_x(X_i, Y_i) + D(X_j - X_i) + \sigma\xi_x(t) \\ \frac{dY_i}{dt} &= F_y(X_i, Y_i) + D(Y_j - Y_i) + \sigma\xi_y(t), \end{aligned} \tag{5.16}$$

where for simplicity we have defined

$$\mathbf{F}(\mathbf{x}) = \begin{pmatrix} F_x(x,y) \\ F_y(x,y) \end{pmatrix} = \begin{pmatrix} \frac{1}{\epsilon}[x(1-\alpha x) - \frac{xy}{1+x}] \\ \frac{xy}{1+x} - \eta y \end{pmatrix}, \tag{5.17}$$

so that in the absence of noise or dispersal each Rosenzweig-Macarthur oscillator behaves according to $d\mathbf{x}/dt = \mathbf{F}(\mathbf{x})$. ξ_x and ξ_y refer to white noise processes affecting the prey and predator populations respectively. In section 3 when we considered noise-induced synchronization of Holling-Tanner predator-prey populations we took $\xi_x = \xi_y$, meaning that extrinsic noise affected prey and predators similarly; here, we take them to be different in order to illustrate that our analysis works in

different cases. Ecologically, this corresponds to the case where prey and predators are affected by very different environmental conditions, such as when they operate on very different scales. For instance, one could envision that in host-pathogen systems, the hosts and pathogens would be affected by completely different factors.

(In the final section of this chapter, we use an alternative model with noise introduced in a different way. This is to demonstrate that the results obtained here are qualitatively unaffected by the specific way that noise is introduced into the system, whether such noise is Itō or Stratonovich, and other such factors.)

Returning to our analysis, as our extrinsic noise is treated in the sense of Stratonovich, as discussed in previous sections, we can carry out phase reduction. This is identical to the case discussed in section 2.4.1 except with an additional noise term:

$$\begin{aligned}
\frac{d\Theta_1}{dt} &= \omega + \mathbf{Z}(\Theta_1)\cdot D\begin{pmatrix} x^*(\Theta_2)-x^*(\Theta_1) \\ y^*(\Theta_2)-y^*(\Theta_1)\end{pmatrix} + \mathbf{Z}(\Theta_1)\cdot\sigma\begin{pmatrix}\xi_x(t)\\ \xi_y(t)\end{pmatrix} \\
\frac{d\Theta_2}{dt} &= \omega + \mathbf{Z}(\Theta_2)\cdot D\begin{pmatrix} x^*(\Theta_1)-x^*(\Theta_2) \\ y^*(\Theta_1)-y^*(\Theta_2)\end{pmatrix} + \mathbf{Z}(\Theta_2)\cdot\sigma\begin{pmatrix}\xi_x(t)\\ \xi_y(t)\end{pmatrix}.
\end{aligned}$$

The limit cycle and corresponding PRC, for both of the sets of parameters we would like to consider in this thesis, have been presented in section 2.4.1 as Figure 5.3. As in section 2.4.1, we simplify notation by writing the effect of dispersal as:

$$\mathbf{F}^*(s_1,s_2) = \begin{pmatrix} x^*(s_2)-x^*(s_1) \\ y^*(s_2)-y^*(s_1)\end{pmatrix}. \tag{5.18}$$

As before, in order to look PDF of the system, it is helpful to convert it into Itō form:

$$\begin{aligned}
\frac{d\Theta_1}{dt} &= \omega + \frac{\sigma^2}{2}\mathbf{Z}(\Theta_1)\cdot\frac{\partial}{\partial\Theta_1}\mathbf{Z}(\Theta_1) + \mathbf{Z}(\Theta_1)\cdot D\,\mathbf{F}^*(\Theta_1,\Theta_2) + \mathbf{Z}(\Theta_1)\cdot\sigma\begin{pmatrix}\xi_x(t)\\ \xi_y(t)\end{pmatrix} \\
\frac{d\Theta_2}{dt} &= \omega + \frac{\sigma^2}{2}\mathbf{Z}(\Theta_2)\cdot\frac{\partial}{\partial\Theta_2}\mathbf{Z}(\Theta_2) + \mathbf{Z}(\Theta_2)\cdot D\,\mathbf{F}^*(\Theta_2,\Theta_1) + \mathbf{Z}(\Theta_2)\cdot\sigma\begin{pmatrix}\xi_x(t)\\ \xi_y(t)\end{pmatrix}.
\end{aligned}$$

This means that if we would like to proceed as in the sections on noise-induced

synchronization by writing down a pair of Itō SDEs:

$$\begin{aligned} d\Theta_1 &= \mathcal{A}_1(\mathbf{\Theta})dt + d\zeta_1(\mathbf{\Theta}, t) \\ d\Theta_2 &= \mathcal{A}_2(\mathbf{\Theta})dt + d\zeta_2(\mathbf{\Theta}, t), \end{aligned} \tag{5.19}$$

where $\mathbf{\Theta} = (\Theta_1, \Theta_2)^T$, then we must define our drift terms $\mathcal{A}$ and correlated Wiener processes ζ_1, ζ_2 such that

$$\begin{aligned} \mathcal{A}_1(\mathbf{\Theta}) &= \omega + \frac{\sigma^2}{2}\mathbf{Z}(\Theta_1)\cdot\frac{\partial}{\partial\Theta_1}\mathbf{Z}(\Theta_1) + D\,\mathbf{Z}(\Theta_1)\cdot\mathbf{F}^*(\Theta_1,\Theta_2) \\ \mathcal{A}_2(\mathbf{\Theta}) &= \omega + \frac{\sigma^2}{2}\mathbf{Z}(\Theta_2)\cdot\frac{\partial}{\partial\Theta_2}\mathbf{Z}(\Theta_2) + D\,\mathbf{Z}(\Theta_2)\cdot\mathbf{F}^*(\Theta_2,\Theta_1), \end{aligned}$$

and

$$d\zeta_i(\mathbf{\Theta}, t) = \sigma\,\mathbf{Z}(\Theta_i)\cdot d\,\mathbf{W}(t). \tag{5.20}$$

where $d\,\mathbf{W}(t) = (dW_x(t), dW_y(t))$ is the extrinsic noise - $dW_x(t) = \xi_x(t)dt$, $dW_y(t) = \xi_y(t)dt$. This means that

$$\begin{aligned} \langle d\zeta_i(\mathbf{\Theta}, t)\rangle &= 0 \\ \langle d\zeta_i(\mathbf{\Theta}, t)d\zeta_j(\mathbf{\Theta}, t)\rangle &= C_{ij}(\mathbf{\Theta})dt, \end{aligned}$$

where $C_{ij}(\mathbf{\Theta})$ is the equal-time correlation matrix

$$C_{ij}(\mathbf{\Theta}) = \sigma^2\,\mathbf{Z}(\Theta_i)\cdot\mathbf{Z}(\Theta_j). \tag{5.21}$$

Hence, in the case of dispersive coupling, we have managed to use the mathematical framework described in the previous chapters to reach a pair of Itō SDEs describing our pair of coupled oscillators. As in the previous sections, the PDF $\mathbb{P}(\boldsymbol{\theta}, t)$ of the pair of oscillators can be described by a FPE:

$$\frac{\partial\,\mathbb{P}(\boldsymbol{\theta}, t)}{\partial t} = -\sum_{i=1}^{2}\frac{\partial}{\partial\theta_i}[\mathcal{A}_i(\boldsymbol{\theta})\,\mathbb{P}(\boldsymbol{\theta}, t)] + \frac{1}{2}\sum_{i,j=1}^{2}\frac{\partial^2}{\partial\theta_i\partial\theta_j}[C_{ij}(\boldsymbol{\theta})\,\mathbb{P}(\boldsymbol{\theta}, t)] \tag{5.22}$$

We have made the assumption that both dispersal and noise are sufficiently weak that their effects change the phase of the oscillators much slower than the intrinsic frequency of the oscillators, so we can define slow variables $\phi_1 = \theta_1 - \omega t$, $\phi_2 = \theta_2 - \omega t$ as in the previous sections. Next, we follow the averaging procedure we

have previously discussed to obtain a PDF $Q(\boldsymbol{\phi}, t)$ for these slow variables:

$$\frac{\partial Q(\boldsymbol{\phi}, t)}{\partial t} = -\sum_{i=1}^{2} \frac{\partial}{\partial \phi_i}[(\bar{\mathcal{A}}_i(\boldsymbol{\phi}) - \omega)Q(\boldsymbol{\phi}, t)] + \frac{1}{2}\sum_{i,j=1}^{2} \frac{\partial^2}{\partial \phi_i \partial \phi_j}[\bar{C}_{ij}(\boldsymbol{\phi})Q(\boldsymbol{\phi}, t)] \tag{5.23}$$

where the overbar indicates averaging over one limit cycle, so that

$$\begin{aligned} \bar{\mathcal{A}}_i(\boldsymbol{\phi}) &= \frac{1}{T}\int_0^T \mathcal{A}_i(\omega t + \phi_1, \omega t + \phi_2)dt \\ &= \omega + \frac{D}{T}\int_0^T \mathbf{Z}(\omega t + \phi_i) \cdot \mathbf{F}^*(\omega t + \phi_i, \omega t + \phi_j)dt + \frac{\sigma^2}{2T}\int_0^T \mathbf{Z}(\theta_i) \cdot \frac{\partial}{\partial \theta_i}\mathbf{Z}(\theta_i)dt \\ &= \omega + DH(\phi_j - \phi_i), \end{aligned} \tag{5.24}$$

since the periodicity of $\mathbf{Z}$ implies $[\mathbf{Z}(\theta_i)^2 \cdot \mathbf{Z}(\theta_i)^2]_0^T = 0$, and $H(\phi_j - \phi_i)$ is the H-function used in section 2, that is,

$$H(\phi) = \frac{1}{T}\int_0^T \mathbf{Z}(\omega s) \cdot \mathbf{F}^*(\omega s, \omega s + \phi)ds. \tag{5.25}$$

As such, in this chapter we manage to tie together several different techniques. We see that the work described on coupled Rosenzweig-Macarthur oscillators earlier comes into play here via the same H- and G-functions that determined the phase-locked states of the system in the absence of noise.

Meanwhile, to examine the effects of the correlated noise, we can define a function

$$\Delta(\phi) = \frac{1}{T}\int_0^T \mathbf{Z}(\omega t) \cdot \mathbf{Z}(\omega t + \phi)dt \tag{5.26}$$

in order to simplify the averaged correlation matrix $\bar{C}(\boldsymbol{\phi})$:

$$\begin{aligned} \bar{C}_{ij}(\boldsymbol{\phi}) &= \frac{1}{T}\int_0^T C_{ij}(\omega t + \phi_1, \omega t + \phi_2)dt \\ &= \frac{\sigma^2}{T}\int_0^T \mathbf{Z}(\omega t + \phi_i) \cdot \mathbf{Z}(\omega t + \phi_j)dt \\ &= \sigma^2 \Delta(\phi_j - \phi_i) \end{aligned} \tag{5.27}$$

The averaged FPE can then be written in the following simplified form:

$$\frac{\partial Q(\boldsymbol{\phi},t)}{\partial t} = -\sum_{i=1}^{2}\frac{\partial}{\partial \phi_i}[DH(\phi_j-\phi_i)Q(\boldsymbol{\phi},t)] + \frac{1}{2}\sum_{i,j=1}^{2}\frac{\partial^2}{\partial\phi_i\partial\phi_j}[\sigma^2\Delta(\phi_j-\phi_i)Q(\boldsymbol{\phi},t)] \tag{5.28}$$

In the case of uncoupled oscillators synchronized by noise, we were able to change variables and solve the averaged FPE for the steady-state PDF. However, in this case, it is instructive to consider the Itō SDEs corresponding to the above FPE. If we denote the stochastic (slow) phases by $\varphi = (\Phi_1,\Phi_2)^T$, then they must evolve according to:

$$\begin{aligned} d\Phi_1 &= DH(\Phi_2-\Phi_1)dt + d\bar{\zeta}_1(\varphi,t) \\ d\Phi_2 &= DH(\Phi_1-\Phi_2)dt + d\bar{\zeta}_2(\varphi,t) \end{aligned} \tag{5.29}$$

with

$$\begin{aligned} \langle d\bar{\zeta}_i(\varphi,t)\rangle &= 0 \\ \langle d\bar{\zeta}_i(\varphi,t)d\bar{\zeta}_j(\varphi,t)\rangle &= \Delta(\Phi_j-\Phi_i)dt. \end{aligned}$$

So far, the equations here are similar to the equations we previously obtained in section 2.1 on coupled oscillators, with the addition of the noisy terms. As in that section, we would like to now consider the phase difference $\Phi = \Phi_2 - \Phi_1$, by taking the difference of the equations (5.30), to obtain:

$$d\Phi = DG(\Phi)dt + \sigma K(\Phi)dW(t), \tag{5.30}$$

where $G(\Phi) = H(\Phi) - H(-\Phi)$ the G-function we defined in section 2, and $W(t)$ is a Wiener process. Using the result that the difference between two Gaussian random variables is also Gaussian tells us that the function $K(\Phi)$ is of the form

$$\begin{aligned} K(\Phi) &= \frac{1}{\sigma}\sqrt{\langle[d\bar{\zeta}_2(\varphi,t)-d\bar{\zeta}_1(\varphi,t)][d\bar{\zeta}_2(\varphi,t)-d\bar{\zeta}_1(\varphi,t)]\rangle} \\ &= \sqrt{2[\Delta(0)-\Delta(\Phi_j-\Phi_i)]} \\ &= \sqrt{2[\Delta(0)-\Delta(\Phi)]}. \end{aligned} \tag{5.31}$$

This means that in the absence of noise ($\sigma = 0$), the dynamics of the phase differ-

ence ϕ is given by the deterministic ODE

$$\frac{d\phi}{dt} = DG(\phi) \tag{5.32}$$

which we have seen in Section 5.2.1 (Equation 5.9). We have plotted the G-functions (Figure 5.4), and we plot the corresponding K-functions in Figure 5.5.

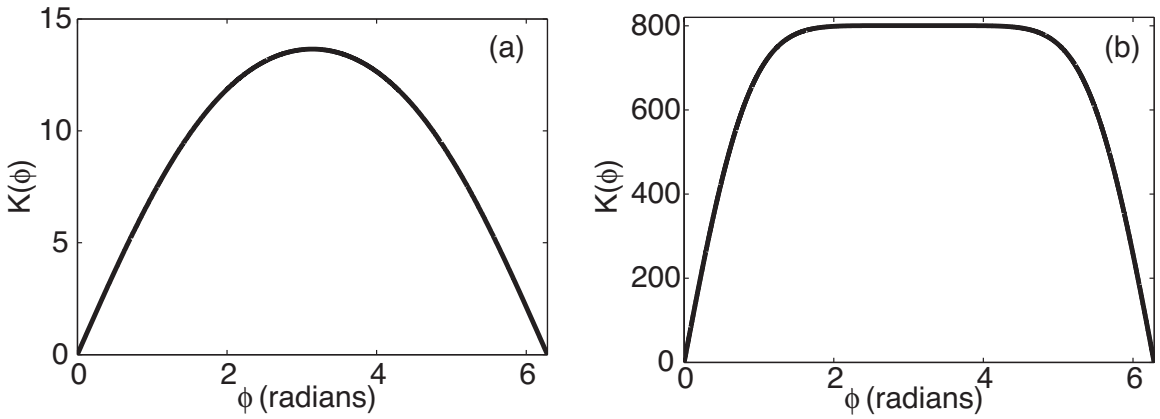

Figure 5.5: Numerically evaluated K-functions. Left: Parameter set (a) - $\epsilon = 0.1$, $\alpha = 0.4$, $\eta = 0.4$. Right: Parameter set (b): $\epsilon = 0.1$, $\alpha = 0.3$, $\eta = 0.3$. (These parameters are the same as in Section 2.4.1.)

Hence, we have succeeded in showing how environmental noisiness affecting a pair of dispersively coupled predator-prey populations translates to an additional noisy term in the equation governing the dynamics of the phase difference between them, modulated by our K-function. As mentioned earlier, we focus on two parameter regimes: in the absence of noise, one only has a stable state at synchrony ($\phi = 0$), while the other has an additional pair of stable asynchronous states. We would now like to see how the common noise source affects this.

When noise is included ($\sigma > 0$), the stochastic phase difference evolves according to the SDE (5.30) with a corresponding FPE for the PDF of Φ, $P(\phi, t)$:

$$\frac{\partial P(\phi,t)}{\partial t} = -D\frac{\partial}{\partial \phi}G(\phi)P(\phi,t) + \frac{\sigma}{2}\frac{\partial^2}{\partial \phi^2}K(\phi)^2 P(\phi,t) \tag{5.33}$$

The steady-state solution P_0 must therefore satisfy

$$G(\phi)P_0(\phi) = \frac{\sigma^2}{2D}\frac{d}{d\phi}[K(\phi)^2 P_0(\phi)] \tag{5.34}$$

which implies that

$$K(\phi)^2 P_0(\phi) = A \exp\left(\int_0^\phi \frac{2DG(s)}{\sigma^2 K(s)^2} ds \right) \tag{5.35}$$

where A is a constant of integration that we can find from the normalization condition $\int P_0(\phi) = 1$. From the plots of the K-functions, we can see that they have zeros at $\phi = 0 = 2\pi$. This suggests that the steady-state PDF $P_0(\phi)$ blows up at $\phi = 0$, that is, $P_0(\phi) = \delta(\phi)$. This means that the common extrinsic noise source causes total synchronization, at least in the limit $t \to \infty$. This agrees with our results for noise-induced synchronization - in both chapters 3 and 4, we obtained complete synchronization in the absence of any intrinsic noise. However, here it seems counter-intuitive that dispersal would not affect noise-induced synchronization. Hence, we examine the transient behaviour of the system. If the only steady-state is total synchrony, but the population takes an extremely long time to achieve it, it would be not readily translatable into real-world results, especially considering that real systems are often subject to uncorrelated noise and other factors.

5.4 Transient behaviour

In order to look at the transient behaviour of the system, we solve the FPE (equation 5.33) numerically, with the initial condition $P(\phi, 0) = \delta(\phi - \phi_0)$, meaning that we assume that the pair of oscillators start at some initial phase difference ϕ_0. We use a simple FTCS scheme here - if we write F_i^n to represent the approximation to a function F at a point ϕ_i at time t_n, then

$$\begin{aligned} \frac{P_i^{n+1} - P_i^n}{\delta t} &= -D \frac{G_{i+1}^n P_{i+1}^n - G_{i-1}^n P_{i-1}^n}{2\delta\phi} \\ &\quad + \frac{\sigma^2}{2} \frac{(K_{i+1}^n)^2 P_{i+1}^n - 2(K_i^n)^2 P_i^n + (K_{i-1}^n)^2 P_{i-1}^n}{(\delta\phi)^2} \end{aligned} \tag{5.36}$$

where δt is the time-step and $\delta\phi$ is the ϕ-step. (Hence we approximate our initial condition numerically by setting $P_j^0 = 1/\delta\phi$ where ϕ_j is the mesh point corresponding to the initial phase difference ϕ_0.) The results are shown in Figure 5.6 for the first parameter set (a), for which there are no asynchronous phase-locked states. Hence, we expect both dispersal and common noise to enhance the synchrony of the system.

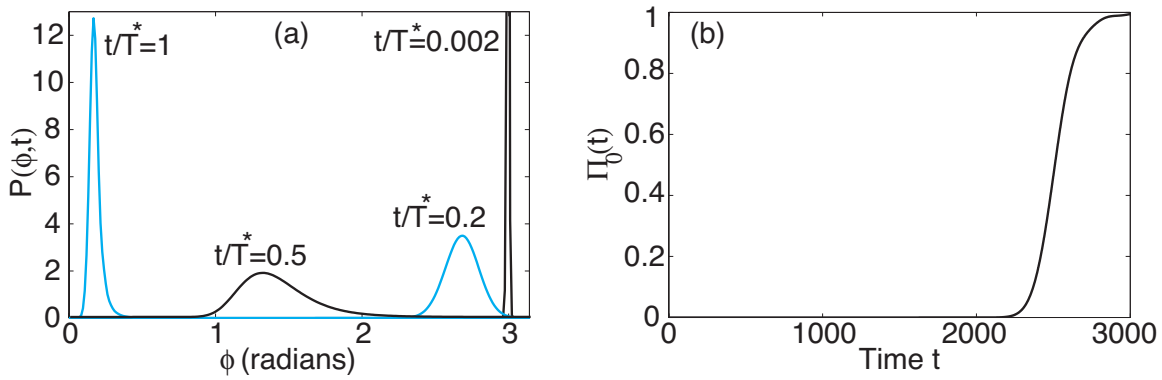

Figure 5.6: Parameters as in the case where the deterministic system is monostable: $\epsilon = 0.1$, $\alpha = 0.4$, $\eta = 0.4$ with dispersal coefficient $D = 0.001$ and $\sigma = 2 \times 10^{-4}$. The initial condition is a delta function $\delta(\phi - \phi_0)$ with $\phi_0 = 3$ radians. (a) The PDF $P(\phi, t)$ is plotted as a function of ϕ at several points in time t, normalised with respect to the time T^* taken to synchrony. (The peak at $t/T^* = 0.002$ is not shown here as it would distort the scale of the figure.) Synchrony here is defined as when $\Pi_0(t) = \int_{-0.2}^{0.2} P(\phi, t) d\phi > 0.75$, which yields $T^* = 2589$ or around 500 cycles. (b) Plot of $\Pi_0(t)$ against time.

On the left (Figure 5.6(a)) we see that the initial delta function at $\phi = \phi_0 \neq 0$ first broadens as it moves towards the steady state at $\phi = 0$, and then narrows again as it tends towards a delta function centered at $\phi = 0$, indicating complete phase synchronization. Furthermore, our PDF at each time-step is well-approximated by a localized Gaussian, as the phase-difference moves steadily towards the synchronous state. Besides looking at the PDF, we would also like some way of measuring the degree of synchrony. Hence, we define one measure $\Pi_0(t)$, where we have set

$$\Pi_0(t) = \int_{-\Delta}^{\Delta} P(\phi, t) d\phi \tag{5.37}$$

that is, $\Pi_0(t)$ is the probability that at time t the phase difference ϕ is within Δ radians of the synchronous state $\phi = 0$. For concreteness we take $\Delta = 0.2$, although the results do not depend on the precise choice for Δ provided $\Delta \ll \pi$. Further to that, we can also define a time to synchrony $T^* = \inf(t | \Pi_0(t) > 0.75)$, the first time at which our measure of synchrony Π_0 exceeds 3/4. (The specific value that Π_0 has to exceed is not particularly important.) We demonstrate our measure of synchrony by plotting it in Figure 5.6(b). The long latency before Π_0 increases corresponds to the time where our PDF is moving from being centred around $\phi = 3$ to $\phi = 0$.

However, for the second parameter set (b) of Section 2.2, the synchronous state coexists with a pair of stable asynchronous states in the absence of noise. In ad-

dition, these asynchronous states have much larger basins of attraction. Hence, for most starting values ϕ_0, we would obtained asynchronous phase-locking. As such, we expect this to be reflected in the transient behaviour of the system when noise is added. Indeed, as we see in Figure 5.7, the temporal evolution of the PDF is very different. For example, if the initial phase is within the basin of attraction of the asynchronous state $\phi = \phi_a \approx 1.78$ in the absence of noise, then the corresponding PDF develops a bimodal structure at intermediate times before moving towards $\phi = 0$ and eventually converging to the expected delta function, see Figure 5.7(a). This is indicative of the mutually contradictory effects of dispersal and noise-induced synchronization. In terms of the ecological implications, this could mean that even if there was a strongly synchronizing common noise source, one could still observe behaviour resembling asynchronous phase-locking from this sort of transient behaviour.

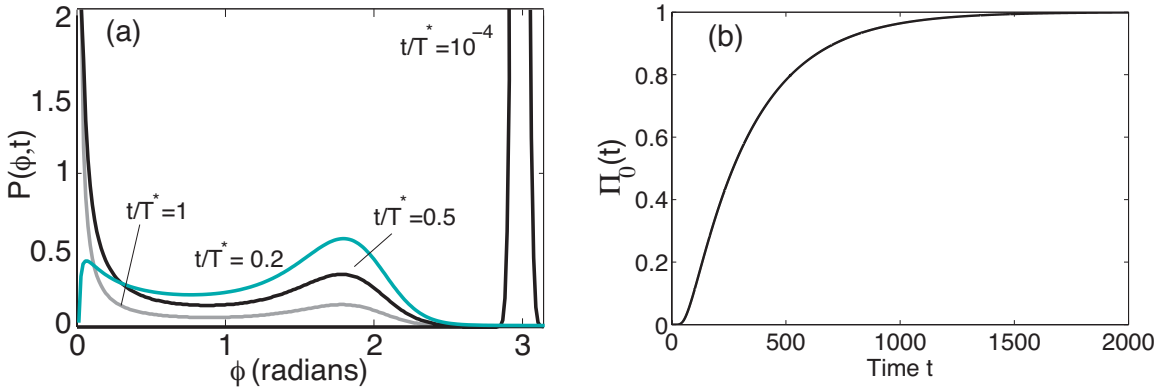

Figure 5.7: Parameters as in the case where the deterministic system is multistable: $\epsilon = 0.1$, $\alpha = 0.3$, $\eta = 0.3$ with dispersal $D = 0.001$ and $\sigma = 2 \times 10^{-4}$. The initial condition is a delta function $\delta(\phi - \phi_0)$ with $\phi_0 = 3$ radians. (a) The PDF $P(\phi, t)$ is plotted as a function of ϕ at several points in time t normalised with respect to the time T^* taken to synchrony. Synchrony is defined as in Fig. 5.6 but now $T^* = 461$. (b) Plot of $\Pi_0(t)$ against time.

However, we note that the approach to synchrony in this parameter regime is now much faster, see Figure 5.7(b). This is due to the fact that the synchronization rate depends on the scale of the phase interaction function $G(\phi)$, which is much larger for the second scenario. If we look at Fig. 5.4, we see that with parameter set (a), $\max(abs(G)) \approx 2$, while for parameter set (b), the maximum value of G is of the order of 100. This means that we need to look for a different way to directly compare the two cases. One way that we have found is to directly compare the two cases by determining how the time to synchrony T varies with the initial phase ϕ_0

(Figure 5.8(a)). In order to make the comparison, we normalize time with respect to the total time to synchrony T^*. In the absence of an asynchronous state, T varies approximately linearly with ϕ_0, which corresponds to our observations that the PDF resembles a localised Gaussian, with the centre moving approximately linearly towards $\phi = 0$. On the other hand, for the other parameter set, T is a step-like function of ϕ_0 in the presence of the asynchronous state ϕ_a. This corresponds with our observations of bistability at intermediate time-scales.

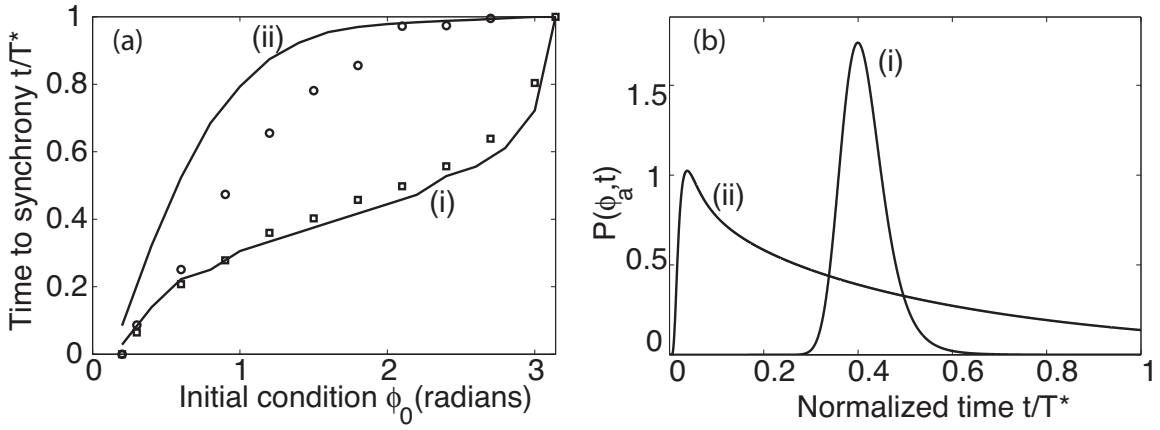

Figure 5.8: Comparison of (i) monostable and (ii) multistable cases. (a) Plots of time taken to synchrony T (normalized with respect to $T^* = T(\phi_0 = 3)$) as a function of the initial condition ϕ_0. Continuous curves are based on solutions to the FPE (5.33). Data points are based on numerical solutions of the full system of RM equations (5.16). (b) Plot of the PDF $P(\phi, t)$ at the asynchronous state $\phi_a \approx 1.78$. Initial conditions here are $\phi_0 = 3$ again.

We also show data points based on direct numerical simulations of the full system of RM equations (5.16). It can be seen that there is excellent agreement between the full model and the reduced phase model in the monostable case. The reduced model is less accurate in the multistable case but the basic trend is still captured.

One potential source of error is that the criterion for synchrony in the reduced model and the full model are different. In the former case, we define the time to synchrony to be when $\Pi_0(t) = \int_{-0.2}^{0.2} p(\phi, t) d\phi > 0.75$. On the other hand, in simulations of the full model equations we first calculated the deterministic limit cycle by solving the RM equations (5.1), and used this to generate an initial condition with phase difference ϕ_0. We then ran the full stochastic equations (5.16) forward in time until the root-mean-squared distance between the two oscillators (in the H-P plane) was less than 10^{-4}. This criterion for synchrony allowed us to avoid

having to determine the phase of each oscillator at each time-step in time, which would have been computationally intensive and potentially inaccurate due to the highly curved isochrons. As before, our stochastic simulations were carried out using an Euler-Maruyama scheme.

In agreement with what we observed from solving the FPE numerically, we observed that in parameter set (a), the trajectories were noisy but their mean tended to move towards synchrony. On the other hand, in parameter set (b), the trajectories often moved to and hovered around a phase-locked state, before eventually moving rapidly towards synchrony. Hence another source of error in this case may be that the time spent at the phase-locked state appeared to be drawn from a heavy-tailed distribution, thus increasing the variance in our observations. This is borne out by our plot of the probability density $P(\phi_a, t)$ as a function of time, as we see in Figure 5.8(b). In the monostable case, we see that the probability increases then decreases in a manner consistent with our approximation of the PDF as a localized Gaussian. On the other hand, in the multistable case, a peak at the asynchronous state ϕ_a forms rapidly before gradually disappearing as the probability density slowly flows to the synchronous state.

The analysis presented here may have implications on experimental design - for example, in [128], the authors modelled their ecosystem using a Rosenzweig-Macarthur model, as we do. However, as they were unsure of the precise parameters, their numerical results were obtained by running multiple simulations for different parameters and averaging over parameter space. By comparing the modes of behaviour here to those observed experimentally, one may be able to at least narrow down the range of parameters for a biological system, even if one cannot determine them exactly.

However, one important aspect of this system is that the systems stays at synchrony once it achieves it. This however may not be true if there is uncorrelated noise in the system, which would perturb it from synchrony. This is particularly important because of the ubiquity of uncorrelated noise in biological systems. In the case of parameter set (b), uncorrelated noise may even cause large changes to the behaviour of the system by moving it from synchrony to the asynchronous phase-locked state. In order to examine this, in the following section, we introduce uncorrelated noise into our system.

5.5 Effects of uncorrelated noise

We have already looked in detail at how uncorrelated intrinsic noise arises from individual-based models in the case of the Holling-Tanner system and the neural master equation. As we are merely concerned with the qualitative ways that uncorrelated noise modifies the behaviour of our system, and have previously established that the precise manner in which we introduce noise in to the system dpes not change its qualitative behaviour, we choose one of the simplest ways to add uncorrelated noise. Here we simply treat uncorrelated noise as an extra additive noise term in the Langevin equations (5.16)

$$\begin{aligned} \frac{dX_i}{dt} &= F_x(X_i, Y_i) + D(X_j - X_i) + \sigma\xi_x(t) + \rho\sigma\xi_{x,i}(t) \\ \frac{dY_i}{dt} &= F_y(X_i, Y_i) + D(Y_j - Y_i) + \sigma\xi_y(t) + \rho\sigma\xi_{y,i}(t) \end{aligned} \tag{5.38}$$

where each $\xi_{x,i}$ and $\xi_{y,i}$ are independent white noise processes. The above simplification is also motivated by the fact that the environment itself could be a source of uncorrelated noise. Another possible way to consider this is to consider the common noise source to be partially rather than entirely correlated, which we discuss at the end of this chapter.

Note that an analogous system of equations with a mixture of correlated and uncorrelated noise has been studied at some length in [84] within the context of a pair of coupled neuronal oscillators. (However, as mentioned earlier, that paper was mainly concerned with developing a computationally efficient method for calculating the steady-state PDF.) One of their main results was to show that the combination of weak coupling and partially correlated noise can lead to bistability (in the probabilistic sense) between a synchronous and an asynchronous state. An analogous result will hold in the case of our population model.

We conduct our analysis of this modified model by proceeding along identical lines to before. Here, applying the phase reduction method ultimately leads to the following Itō SDE for the stochastic phases:

$$\begin{aligned} d\Theta_1 &= \mathcal{A}_1^*(\mathbf{\Theta})dt + d\zeta_1(\mathbf{\Theta}, t) \\ d\Theta_2 &= \mathcal{A}_2^*(\mathbf{\Theta})dt + d\zeta_2(\mathbf{\Theta}, t), \end{aligned} \tag{5.39}$$

where in this case the drift terms $\mathcal{A}$ are given by

$$\begin{aligned}\mathcal{A}_1^*(\mathbf{\Theta}) &= \omega + \frac{(1+\rho^2)\sigma^2}{2}\mathbf{Z}(\Theta_1)\cdot\frac{\partial}{\partial\Theta_1}\mathbf{Z}(\Theta_1) + D\,\mathbf{Z}(\Theta_1)\cdot\mathbf{F}^*(\Theta_1,\Theta_2)\\ \mathcal{A}_2^*(\mathbf{\Theta}) &= \omega + \frac{(1+\rho^2)\sigma^2}{2}\mathbf{Z}(\Theta_2)\cdot\frac{\partial}{\partial\Theta_2}\mathbf{Z}(\Theta_2) + D\,\mathbf{Z}(\Theta_2)\cdot\mathbf{F}^*(\Theta_2,\Theta_1).\end{aligned}$$

In this case, the correlated Wiener processes ζ_1, ζ_2 are such that

$$d\zeta_i(\mathbf{\Theta},t) = \sigma\,\mathbf{Z}(\Theta_i)\cdot(d\,\mathbf{W}(t) + \rho d\,\mathbf{W}_i(t)); \tag{5.40}$$

this means that

$$\begin{aligned}\langle d\zeta_i(\mathbf{\Theta},t)\rangle &= 0\\ \langle d\zeta_i(\mathbf{\Theta},t)d\zeta_j(\mathbf{\Theta},t)\rangle &= C_{ij}^*(\mathbf{\Theta})dt,\end{aligned}$$

where the new correlation matrix $C_{ij}^*(\mathbf{\Theta})$ is

$$C_{ij}^*(\mathbf{\Theta}) = \sigma^2(1+\rho^2\delta_{i,j})\,\mathbf{Z}(\Theta_i)\cdot\mathbf{Z}(\Theta_j). \tag{5.41}$$

It follows that the ensemble is described by the FPE (5.33) with $\mathcal{A}_i(\mathbf{\Theta}) \to \mathcal{A}_i^*(\mathbf{\Theta})$ and $C_{ij}(\mathbf{\Theta}) \to C_{ij}^*(\mathbf{\Theta})$. Averaging over a single period as before generates the averaged FPE

$$\begin{aligned}\frac{\partial Q^*(\boldsymbol{\phi},t)}{\partial t} &= -\sum_{i=1}^{2}\frac{\partial}{\partial\phi_i}[(\bar{\mathcal{A}}_i^* - \omega)(\boldsymbol{\phi})Q^*(\boldsymbol{\phi},t)]\\ &\quad + \frac{1}{2}\sum_{i,j=1}^{2}\frac{\partial^2}{\partial\phi_i\partial\phi_j}[\bar{C}_{ij}^*(\boldsymbol{\phi})Q^*(\boldsymbol{\phi},t)],\end{aligned} \tag{5.42}$$

where

$$\bar{\mathcal{A}}_i^* = \bar{\mathcal{A}}_i \equiv \omega + DH(\phi_j - \phi_i), \tag{5.43}$$

and

$$\begin{aligned}\bar{C}_{ij}^* &= (1+\rho^2\delta_{i,j})\overline{C_{ij}}\\ &= (1+\rho^2\delta_{i,j})\sigma^2\Delta(\phi_j-\phi_i)\\ &= \sigma^2(\Delta(\phi_j-\phi_i) + \rho^2\Delta(0)),\end{aligned} \tag{5.44}$$

with H and Δ defined as before. As before, defining a phase difference $\Phi = \Phi_2 - \Phi_1$,

we obtain an SDE corresponding to our FPE (5.44):

$$\begin{aligned} d\Phi_1 &= DH(\Phi)dt + d\bar{\zeta_1}(\varphi,t) \\ d\Phi_2 &= DH(-\Phi)dt + d\bar{\zeta_2}(\varphi,t), \end{aligned} \tag{5.45}$$

with

$$\langle d\bar{\zeta}_1(\varphi,t)\rangle = \langle d\bar{\zeta}_1(\varphi,t)\rangle = 0$$

$$\begin{aligned} \langle d\bar{\zeta}_1(\varphi,t)d\bar{\zeta}_1(\varphi,t)\rangle &= \langle d\bar{\zeta}_2(\Phi,t)d\bar{\zeta}_2(\Phi,t)\rangle &= \sigma^2(1+\rho^2)\Delta(0)dt \\ \langle d\bar{\zeta}_1(\varphi,t)d\bar{\zeta}_2(\varphi,t)\rangle &= \langle d\bar{\zeta}_2(\Phi,t)d\bar{\zeta}_2(\Phi,t)\rangle &= \sigma^2\Delta(\Phi)dt. \end{aligned}$$

Taking the difference of the two equations yields the SDE

$$d\Phi = DG(\Phi)dt + \sigma K^*(\Phi)dW(t), \tag{5.46}$$

where $G(\Phi) = H(\Phi) - H(-\Phi)$ is the phase-interaction function seen in the previous sections, and

$$\begin{aligned} K^*(\Phi) &= \frac{1}{\sigma}\sqrt{\langle[d\bar{\zeta}_2(\Phi,t) - d\bar{\zeta}_1(\Phi,t)][d\bar{\zeta}_2(\Phi,t) - d\bar{\zeta}_1(\Phi,t)]\rangle} \\ &= \sqrt{2[(1+\rho^2)\Delta(0) - \Delta(\Phi)]}. \end{aligned} \tag{5.47}$$

From equation (5.46), Φ has an associated PDF $P(\phi,t)$ that evolves according to the FPE

$$\frac{\partial P}{\partial t} = -\frac{\partial}{\partial\phi}GP + \frac{\sigma^2}{2}\frac{\partial^2}{\partial\phi^2}[K^{*2}P]. \tag{5.48}$$

This is exactly the same as in the previous section, but with our function K replaced by K^*, which has an additional component $\rho^2\Delta(0)$ representing the effect of the uncorrelated noise. Solving for the steady state density P_0 gives

$$GP_0 = \frac{\sigma^2}{2}\frac{d}{d\phi}[K^{*2}P_0], \tag{5.49}$$

which implies that

$$K^{*2}(\phi)P_0(\phi) = A\exp\left(\int_0^\phi \frac{2DG(s)}{\sigma^2K^{*2}(s)}ds\right). \tag{5.50}$$

Thus, our steady-state PDF is:

$$P_0(\phi) = \frac{A}{2(1+\rho^2)\Delta(0) - \Delta(\phi)} \exp\left(\int_0^{\phi} \frac{DG(s)ds}{\sigma^2[(1+\rho^2)\Delta(0) - \Delta(s)]} \right). \tag{5.51}$$

Again, A is a constant of integration, which can be determined from the normalization condition

$$\int_0^{2\pi} P_0(\phi)d\phi = 1.$$

Note that as the level of uncorrelated noise goes to zero ($\rho \to 0$), $K^*(0) \to 0$ - hence P_0 tends to a delta function at zero, as in the case with only correlated noise.

We now explore the effects of uncorrelated noise on synchronisation by numerically solving the FPE (5.46). For the monostable case, we display our results in Figure 5.9. Here both dispersal and correlated noise cause the system to synchronize irrespective of initial conditions. In line with our intuition, adding uncorrelated noise simply broadens the steady-state PDF to give a unimodal function centred at $\phi = 0$ whose width increases with the level ρ of uncorrelated noise. In addition, we also plot our measure of synchrony, $\Pi_0(t) = \int_{-0.2}^{0.2} P(\phi, t)d\phi$ against time for various values of ρ. We find that when $\rho > 0$, partial synchrony occurs faster than the case of zero uncorrelated noise ($\rho = 0$), but it takes a longer time to reach higher levels of synchrony.

On the other hand, as seen in Figures 5.10 and 5.11, in the multistable case, we observe various modes of interesting behaviour. Firstly, as one might expect, introducing a small amount of uncorrelated noise ($\rho = 0.02$) does not change the behaviour significantly from the case without uncorrelated noise. We see that it leads to a PDF with multiple peaks at intermediate times before converging to a unimodal steady-state centred about $\phi = 0$, see Figure 5.10(a-c).

Ecologically, this shows that the results seen in the previous section are robust to small amounts of uncorrelated noise, which one expects in the vast majority of biological systems. This could also mean that if a pair of populations are phase-locked, increasing the amount of common noise to them could synchronize them - this would be useful knowledge, especially considering recent discussions of climate change; in addition, in the eradication of diseases, it is often crucial to time the distribution of curatives in order to prevent a new wave of infections.

Next, when we increase the level of uncorrelated noise ($\rho = 1$), the transient peaks are persistent so that the steady-state PDF develops multiple peaks, as shown in Figure 5.11(a),(b). This means that the level of noise causes the PDF to change

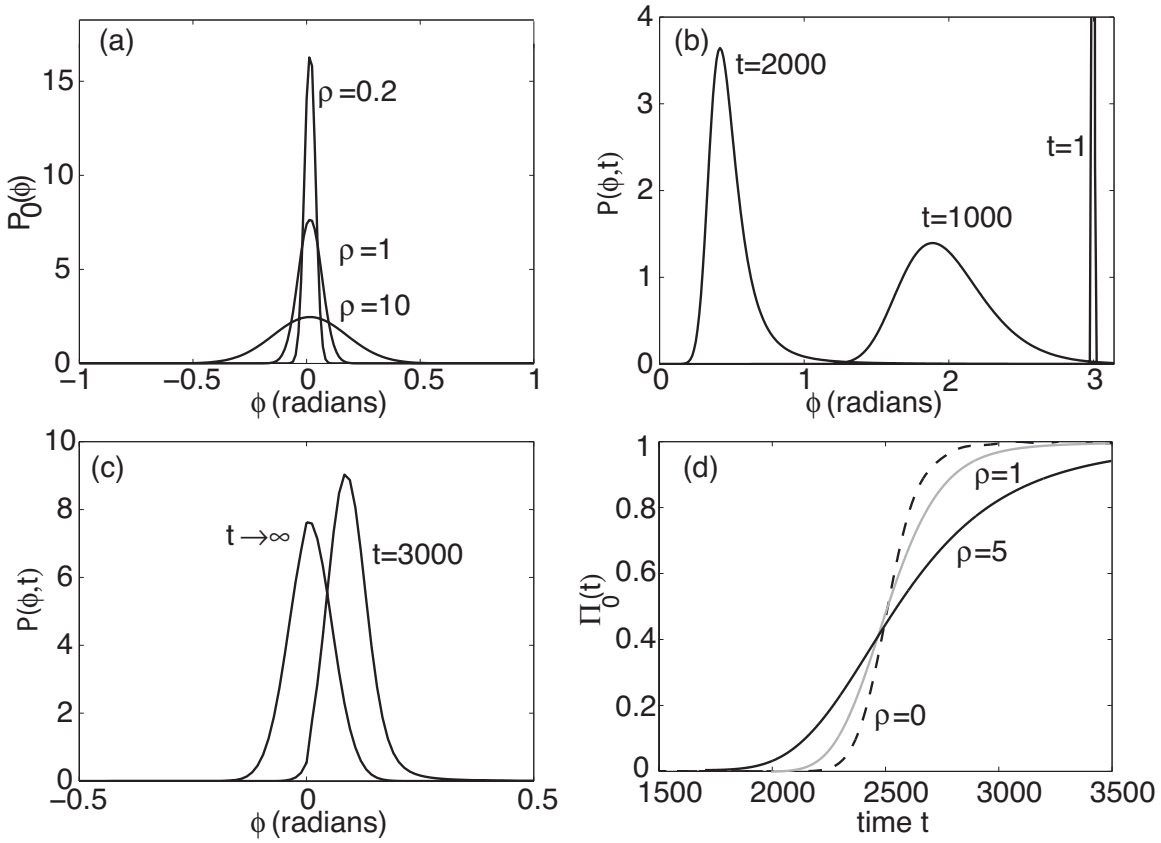

Figure 5.9: Monostable case with correlated and uncorrelated noise. All parameters except ρ are the same as in Figure 5.6. (a) Steady-state PDFs for various values of ρ. (b,c) For $\rho = 1$, the PDF is plotted at several points in time, starting from the initial condition $\phi_0 = 3$ radians. (d) Plot of $\Pi_0(t)$ against time for various values of ρ. ($\rho = 0$ is the case without uncorrelated noise.)

qualitatively from being singly-peaked to multiple peaks, indicating a stochastic bifurcation, where only noise is required to change the qualitative behaviour of the system. These multiple peaks are also reminiscent of the stochastic bistability seen in [84]. As in the neuronal case, this bistability would induce an intermittent switching of the system between a synchronous and asynchronous phase-locked state, which would be a clear qualitative marker to look for in experimental data.

Finally, adding a high amount of uncorrelated noise ($\rho = 10$) causes the steady-state PDF to approache a unform distribution as we see in Figure 5.11(c), though the multiply-peaked structure can still be discerned. This is due to the high amout of uncorrelated noise dominating the dynamics of the system.

Besides looking at the time-evolution of the PDF, we would also like to examine the relative probabilities of being in a synchronous or asynchronous phase-locked

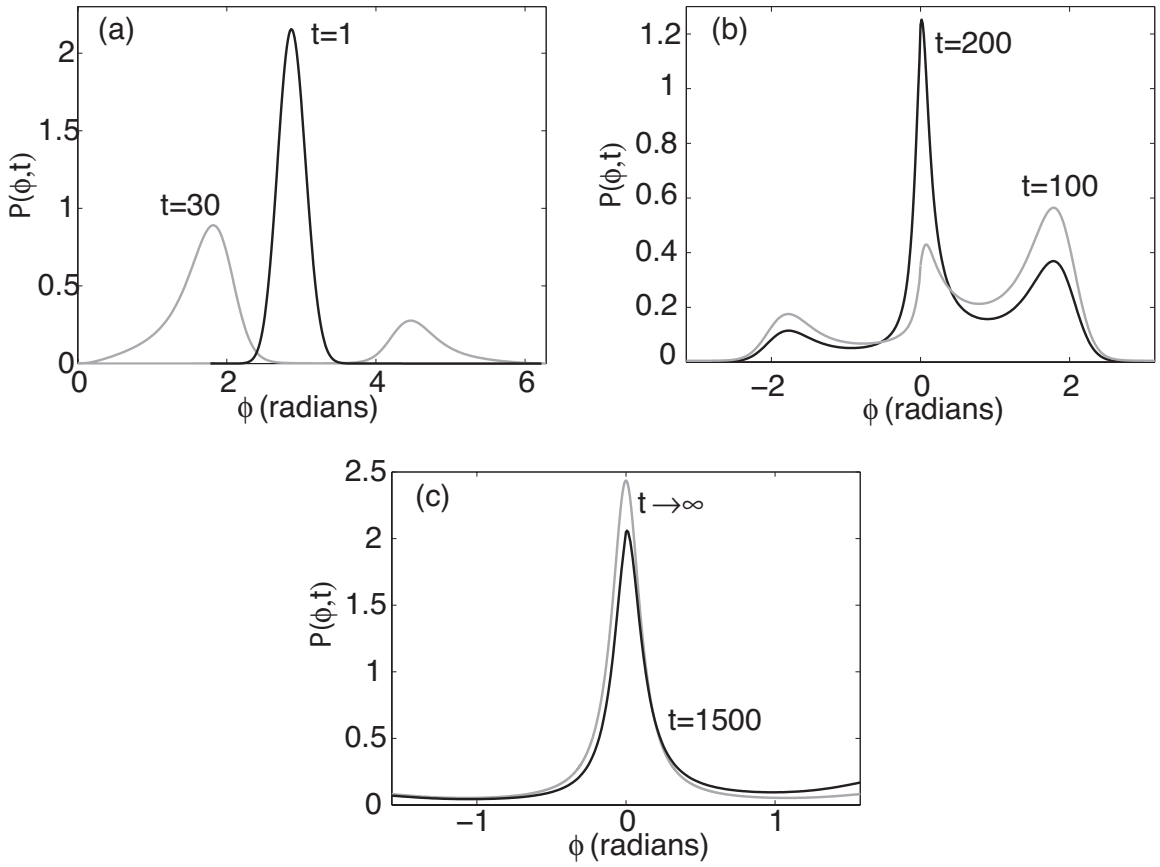

Figure 5.10: Multistable case with correlated noise and a low level of uncorrelated noise ($\rho = 0.02$). All other parameters are the same as Fig. 5.7. (a-c) Snapshots of the PDF $P(\phi, t)$ with $P(\phi, 0) = \delta(\phi - \phi_0)$ and $\phi_0 = 3$. (a) At relatively short times the PDF develops two peaks at the deterministic asynchronous states $\phi \approx 1.78$ and $2\pi - 1.78$. (b) At intermediate times the PDF develops a third peak at $\phi = 0$. (c) At longer times the PDF approaches the steady-state solution which is given by a single peak centered about the synchronous state.

state. It is instructive to see how the steady-state probability of being in a neighborhood of the synchronous state $\phi = 0$ or the asynchronous state $\phi = \phi_a = 1.78$ varies with ρ and σ. Thus we let $\Pi_\phi = \int_{\phi-\Delta}^{\phi+\Delta} P_0(\phi')d\phi'$ with $\Delta = 0.2$ be a measure of the degree of stochastic phase-locking around the phase ϕ (so Π_0 means the same as it did before).

In Figure 5.12 we plot Π_0 and Π_{ϕ_a} as a function of the noise level σ for various ρ. It can be seen that when the common noise source is dominant ($\sigma > 10^{-4}$, $\rho \ll 1$) there is a high probability that the oscillators are approximately synchronized with $\Pi_0 > 0.5$ and $\Pi_a \approx 0$. As the level of uncorrelated noise ρ is increased for fixed σ, the degree of synchronization decreases but there is still a low proba-

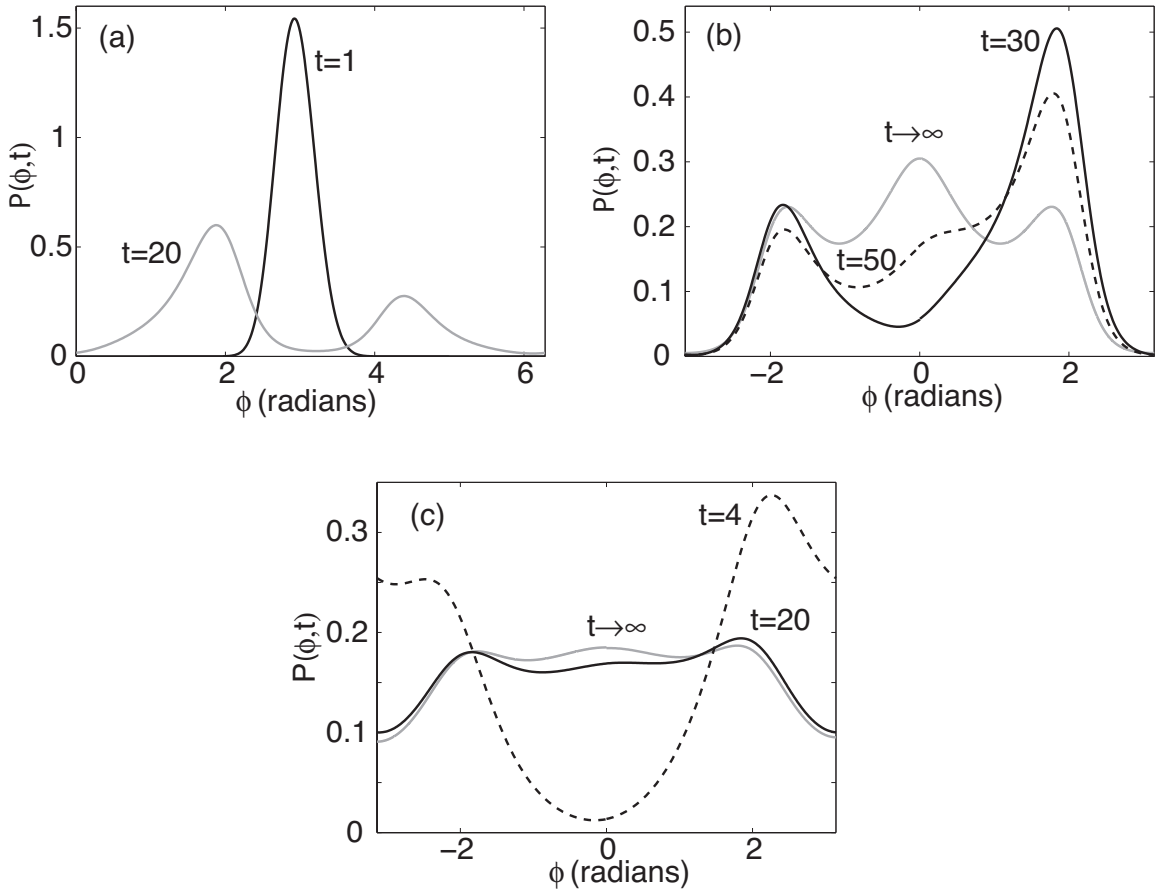

Figure 5.11: (a,b) Same as Figure 5.10 for an intermediate level of uncorrelated noise ($\rho = 1$). The PDF is plotted at various points in time to show the emergence of persistent peaks around the asynchronous states and convergence to a multistable steady state . (c) At high levels of uncorrelated noise ($\rho = 10$), the steady-state distribution becomes more uniform.

bility of being in the asynchronous states. On the other hand, for sufficiently low levels of the common noise source ($\sigma < 10^{-4}$), the oscillators occupy one of the two asynchronous states with a probability $\Pi_a \approx 0.5$, and this is insensitive to the level of uncorrelated noise. Interestingly, there is a sharp transition between synchrony and asynchrony as σ increases for fixed ρ.

This implies that in an ecological system, one should be able to see a marked difference as the amount of correlated noise in a system is increased, with a significant chance of synchrony above a certain threshold. In the wild, it may be able to conduct observations of different predator-prey systems, with different sensitivity to environmental variations, in order to see that those insensitive to climactic fluctuations remain asynchronously phase-locked, while those sensitive to such fluctuations display some degree of synchrony.

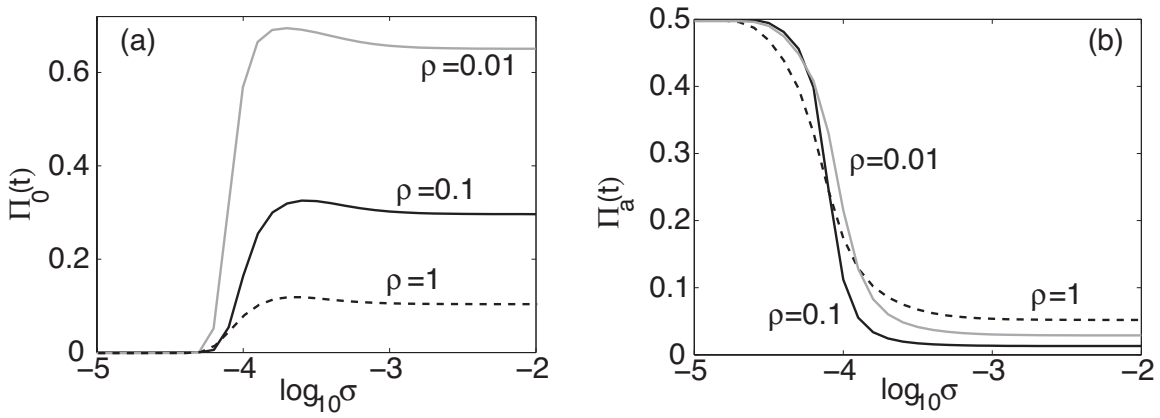

Figure 5.12: Plots of $\Pi_\phi = \int_{\phi-0.2}^{\phi+0.2} P_0(\phi)d\phi$ against $\log\sigma$ for different values of ρ. (a) Synchronous state $\phi = 0$; (b) Asynchronous state $\phi = \phi_a \approx 1.78$. Note that the maximum probability is 0.5 due to the symmetrical steady state at $\phi = 2\pi - 1.85$.

Mathematically, in the cases where the system displays bistability, one may be able to use the results here to simplify asynchronous phase-locking and synchronous phase-locking as two states in a simple discrete Markov model - this simplification would be extremely useful if one wanted to focus more on a spatial model with specific dispersion between different locations.

Hence, in this portion of the thesis, we have combined the theoretical techniques described in the sections on noise-induced synchronization and coupled oscillators in a novel way. We then applied this to a well-known ecological system - dispersively coupled Rosenzweig-Macarthur predator-prey oscillators, in order to develop new ecological insights complementary to those discussed in [52].

We first showed that in the case of common environmental noise, the oscillators ultimately synchronize. However, the approach to synchrony depends on whether or not there exist stable asynchronous states in the deterministic limit. We found that in the absence of asynchronous states, the time-dependent PDF was Gaussian-like with a width that first increased and then decreased as it moved towards the synchronous state. Moreover, the rate of stochastic synchronization varied approximately linearly with the initial phase difference between the two oscillators. On the other hand, if dispersal also supported asynchronous phase-locking, then the corresponding PDF exhibited a broad bimodal structure at intermediate times before ultimately converging to the synchronous state. This led to a sharp decrease in the rate of stochastic synchronisation as the initial phase difference increased from zero. We then investigated how these two distinct scenarios were affected by uncorrelated noise. In particular, we showed how uncorrelated noise can cause the

transient peaks in the PDF associated with asynchronous states to become persistent, resulting in a multimodal steady-state PDF.

Finally, in order to show that these results are independent of the specific choice of model, we use an alternative model and show that it behaves in the same manner.

5.6 Alternative model for the introduction of noise

As an alternative to the previous system, where all our predator populations and prey populations were driven by additive Stratonovich white noises, we instead consider that they are driven by a common Itō noise term, and that the noise strength is dependent on the population density. This is similar to the model considered recently in [38]. Hence, rather than 5.16, we now have that

$$\begin{aligned} \frac{dX_i}{dt} &= F_x(X_i, Y_i) + D(X_j - X_i) + \sigma X_i \xi_i(t) \\ \frac{dY_i}{dt} &= F_y(X_i, Y_i) + D(Y_j - Y_i) + \sigma Y_i \xi_i(t), \end{aligned} \tag{5.52}$$

with $\xi_i(t)$ now being Itō white noise, and all the other functions defined in the same way as before. To start off with we consider only common noise, that is, all the ξ_is are identical. Carrying out our phase reduction now yields the set of Stratonovich SDEs

$$\begin{aligned} d\Theta_i &= \left[\omega + D\,\mathbf{Z}(\Theta_i)\cdot\begin{pmatrix} X(\Theta_j) - X(\Theta_i) \\ Y(\Theta_j) - Y(\Theta_i) \end{pmatrix} - \frac{\sigma^2}{2}\mathbf{Z}(\Theta_i)\cdot\begin{pmatrix} X(\Theta_i) \\ Y(\Theta_i) \end{pmatrix}\right] dt \\ &\quad + \sigma\left[\mathbf{Z}(\Theta_i)\cdot\begin{pmatrix} X(\Theta_i) \\ Y(\Theta_i) \end{pmatrix}\right] \circ dW(t); \end{aligned} \tag{5.53}$$

as before, these can be written as the Itō SDEs

$$d\Theta_i = \mathcal{A}_i(\mathbf{\Theta})dt + d\zeta_i(\mathbf{\Theta}, t), \tag{5.54}$$

where $\{\zeta_i(\mathbf{\Theta}, t)\}$ are correlated Wiener processes and $\mathbf{\Theta} = (\Theta_1, \ldots, \Theta_N)$. If we define the shorthand

$$\alpha(s) = \mathbf{Z}(s)\cdot\begin{pmatrix} X(s) \\ Y(s) \end{pmatrix} \tag{5.55}$$

then we can write

$$d\zeta_i(\mathbf{\Theta}, t) \quad = \quad \sigma\alpha(\Theta_i)dW(t), \tag{5.56}$$

and the drift terms in this case take the slightly different form

$$\begin{aligned}\mathcal{A}_i(\mathbf{\Theta}) \quad &= \quad \omega + \frac{\sigma^2}{2}\alpha(\Theta_i)\partial_{\Theta_i}\alpha(\Theta_i) - \frac{\sigma^2}{2}\alpha(\Theta_i) \\ &\quad + D\,\mathbf{Z}(\Theta_i)\cdot\mathbf{F}^*(\Theta_i, \Theta_j).\end{aligned} \tag{5.57}$$

It follows that the ensemble is described by a multivariate Fokker-Planck equation of the form of equation (5.22):

$$\frac{\partial \mathbb{P}(\boldsymbol{\theta}, t)}{\partial t} = -\sum_{i=1}^{2}\frac{\partial}{\partial\theta_i}[\mathcal{A}_i(\boldsymbol{\theta})\,\mathbb{P}(\boldsymbol{\theta}, t)] + \frac{1}{2}\sum_{i,j=1}^{2}\frac{\partial^2}{\partial\theta_i\partial\theta_j}[C_{ij}(\boldsymbol{\theta})\,\mathbb{P}(\boldsymbol{\theta}, t)], \tag{5.58}$$

with a slightly different $\mathcal{A}$ and the correlation matrix C is now such that

$$C_{ij} = \sigma^2\alpha(\Theta_i)\alpha(\Theta_j). \tag{5.59}$$

Hence, we can carry out the same averaging procedure as before to obtain an FPE for the PDF Q of the slow variables:

$$\frac{\partial Q(\boldsymbol{\phi}, t)}{\partial t} = -\sum_{i=1}^{2}\frac{\partial}{\partial\phi_i}[DH(\phi_j - \phi_i) - \frac{\sigma^2}{2}\bar{\alpha}Q(\boldsymbol{\phi}, t)] + \frac{1}{2}\sum_{i,j=1}^{2}\frac{\partial^2}{\partial\phi_i\partial\phi_j}[\sigma^2\Delta(\phi_j - \phi_i)Q(\boldsymbol{\phi}, t)], \tag{5.60}$$

where

$$\Delta(\psi) = \frac{1}{T}\int_0^T \alpha(\omega t)\alpha(\omega t + \psi)dt. \tag{5.61}$$

As before, we continue our analysis by looking at a pair of oscillators, and define the phase difference $\Phi = \Psi_2 - \Psi_1$. This means we can explicitly write down the SDEs describing the evolution of the slow phases:

$$d\Psi_1 = (DH(\Phi) - \frac{\sigma^2}{2}\bar{\alpha})dt + d\overline{\zeta}_1(\Phi, t) \tag{5.62a}$$

$$d\Psi_2 = (DH(-\Phi) - \frac{\sigma^2}{2}\bar{\alpha})dt + d\overline{\zeta}_2(\Phi, t), \tag{5.62b}$$

with

$$\langle d\overline{\zeta}_1(\Phi,t)d\overline{\zeta}_1(\Phi,t)\rangle = \langle d\overline{\zeta}_2(\Phi,t)d\overline{\zeta}_2(\Phi,t)\rangle = \sigma^2\Delta(0)$$
$$\langle d\overline{\zeta}_1(\Phi,t)d\overline{\zeta}_2(\Phi,t)\rangle = \langle d\overline{\zeta}_2(\Phi,t)d\overline{\zeta}_1(\Phi,t)\rangle = \sigma^2\Delta(\Phi) \tag{5.63}$$

As before, taking the difference of the equations (5.62) leads to the scalar SDE

$$d\Phi = DG(\Phi)dt + \sigma K(\Phi)dW(t), \tag{5.64}$$

where $G(\phi)$ and $K(\Phi) = \sqrt{2[\Delta(0)-\Delta(\Phi)]}$ are defined as before except we have a new definition of Δ in this alternate model - the resulting K-functions for our two sets of parameters are plotted in Fig. 5.13.

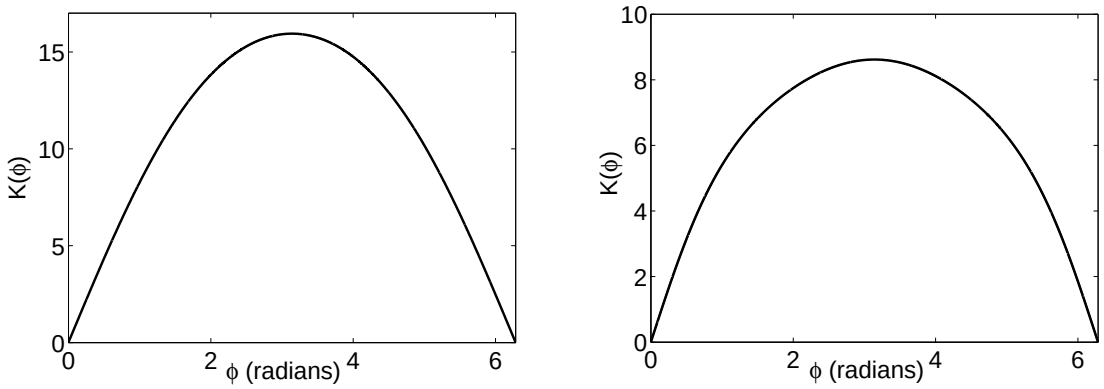

Figure 5.13: Numerically evaluated K-functions for the alternate model. Left: Parameter set (a) - $\epsilon = 0.1$, $\alpha = 0.4$, $\eta = 0.4$. Right: Parameter set (b): $\epsilon = 0.1$, $\alpha = 0.3$, $\eta = 0.3$. (These parameters are the same as before.)

Once again, the SDE (5.64) has a corresponding FPE for the PDF of the phase difference Φ, which is exactly the same as equation (5.33). As the zeros of the K-functions are still only at 0 and 2π, our steady-state PDF $P_0(\phi)$ still blows up at $\phi = 0$. In order to verify that the transient behaviour of our system is also the same in this model, we solve the FPE (5.33) numerically in this case and show that the behaviour is qualitatively the same.

By comparing the figures 5.6 and 5.7 with these new figures 5.14 and 5.15, we see that in both cases there is a clear difference between the behaviour of the systems in the monostable and multistable cases.

Previously, we had considered uncorrelated additive noise as a simplified phenomelogical representation of how intrinsic noise or other sources of noise affected the behaviour of the system. However, in this section, we take the opportunity to

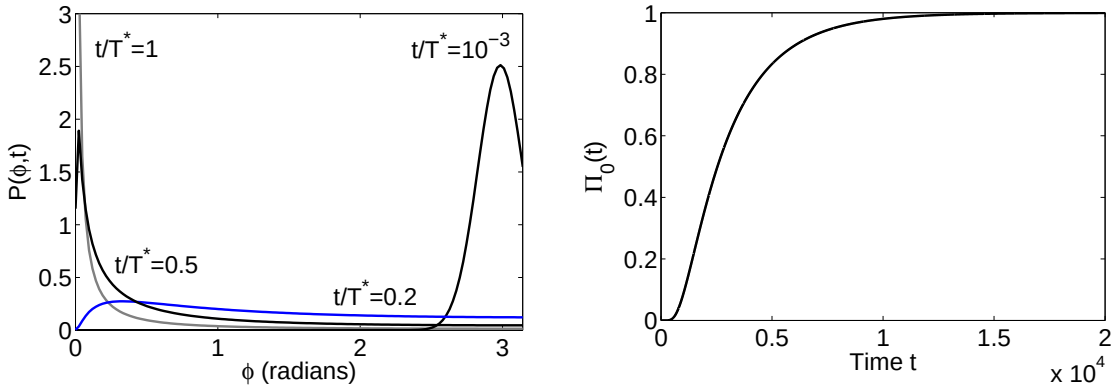

Figure 5.14: Parameters as in the case where the deterministic system is monostable: $\epsilon = 0.1$, $\alpha = 0.4$, $\eta = 0.4$ with dispersal coefficient $D = 10^{-4}$ and $\sigma = 5 \times 10^{-3}$. The initial condition is a delta function $\delta(\phi - \phi_0)$ with $\phi_0 = 3$ radians. (a) The PDF $P(\phi, t)$ is plotted as a function of ϕ at several points in time t, normalised with respect to the time T^* taken to synchrony. Synchrony here is defined as before, which yields $T^* = 4090$. (As before the tops of very sharp peaks are not shown as they would distort the scale of the figure.) (b) Plot of $\Pi_0(t)$ against time.

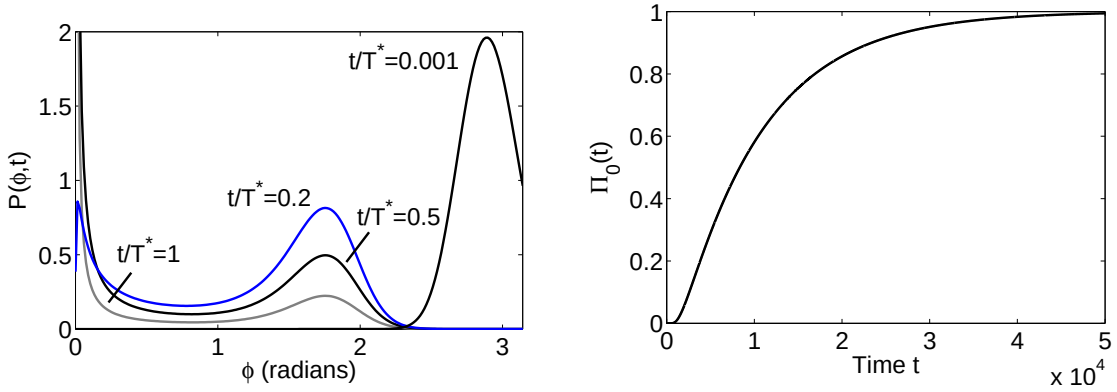

Figure 5.15: Parameters as in the case where the deterministic system is multistable: $\epsilon = 0.1$, $\alpha = 0.3$, $\eta = 0.3$ with dispersal $D = 10^{-4}$ and $\sigma = 5 \times 10^{-3}$. The initial condition is a delta function $\delta(\phi - \phi_0)$ with $\phi_0 = 3$ radians. (a) The PDF $P(\phi, t)$ is plotted as a function of ϕ at several points in time t normalised with respect to the time T^* taken to synchrony. Synchrony is defined as before, which gives $T^* = 14825$. (As before the tops of very sharp peaks are not shown as they would distort the scale of the figure.) (b) Plot of $\Pi_0(t)$ against time.

discuss another source of uncorrelated noise, arising from the assumption that environmental noise is only partially correlated between patches.

In [38], the authors introduced partially correlated environmental noise for a system of M populations by subjecting each of them to correlated Brownian motions $\boldsymbol{E}_t = \Gamma^T \boldsymbol{B}_t$, where $\boldsymbol{B}_t = (B_t^1, \ldots, B_t^M)$ is a vector of independent standard

Brownian motions, and the covariance matrix $\Sigma = \Gamma^T\Gamma$ represents the spatial dependence between the enviromental fluctuations on the populations. However, it is possible to show that one can obtain a vector of correlated Brownian motions with the same covariances by decomposing them into a common noise source and independent noise sources, and hence obtain SDEs similar to those we considered earlier in the chapter; we do it here for $M = 2$.

To follow the approach of [38], we imagine that our vector of noises $\zeta = \Gamma^T\eta$ where η is a vector of independent Brownian motions, and we have a correlation matrix $\Sigma = \Gamma^T\Gamma$. For symmetry consider $\Gamma_{ij} = \Gamma_{ji}$. Then we have $\langle\zeta_i\rangle = 0$ and

$$\langle\zeta_i\zeta_i\rangle = \sum_{j=1}^{N}\Gamma_{ji}^2, \tag{5.65}$$

$$\langle\zeta_i\zeta_j\rangle = \Gamma_{ii}\sum_{k\neq i}\Gamma_{ik} + \Gamma_{jj}\sum_{l\neq j}\Gamma_{lj} := \rho_{ij}^2, \tag{5.66}$$

as we want ρ to mean the correlation between patches. Since the patches are homogeneous, assume that $\Gamma_{ii} = \Gamma_{jj}\forall i, j$. Now we focus on two patches so that we have

$$\Gamma_{11}^2 + \Gamma_{12}^2 = \Gamma_{22}^2 + \Gamma_{21}^2 = 1. \tag{5.67}$$

Now our assumptions allow us to write

$$\Gamma_{11} = \Gamma_{22} =: \gamma, \tag{5.68}$$

$$\Gamma_{12} = \Gamma_{21} = \sqrt{1-\gamma^2}. \tag{5.69}$$

and we get that our correlation between patches ρ is such that

$$\rho^2 = 2\gamma\sqrt{1-\gamma^2}, \tag{5.70}$$

meaning that in order to get a desired correlation ρ we must decompose our noises:

$$\zeta_1 = \gamma\eta_1 + \sqrt{1-\gamma^2}\eta_2,$$

$$\zeta_2 = \sqrt{1-\gamma^2}\eta_1 + \gamma\eta_2.$$

where $\gamma = \sqrt{\frac{1\pm\sqrt{1-\rho^4}}{2}}$. (The $\pm$ sign is because Γ being $\begin{pmatrix} \gamma & \sqrt{1-\gamma^2} \\ \sqrt{1-\gamma^2} & \gamma \end{pmatrix}$ and

$\begin{pmatrix} \sqrt{1-\gamma^2} & \gamma \\ \gamma & \sqrt{1-\gamma^2} \end{pmatrix}$ is the same because the noises are independent and identically distributed.) When $\rho = 0$, $\gamma = 0$ or 1 as expected. In the case of fully correlated noise ($\rho = 1$), $\gamma = \frac{1}{\sqrt{2}}$, meaning that $\zeta_1 = \zeta_2 = \frac{1}{\sqrt{2}}(\eta_1 + \eta_2)$ which means that they are both the same Brownian motion as we expect.

Without loss of generality we select γ to be the larger root i.e. $\gamma^2 = (1 + \sqrt{1-\rho^4})/2$.

Thus if we now go back to our original Ito SDEs we replace the η_i term with $\zeta_i = \sum \gamma_{ij}\eta_j$ - in particular for the case of two populations we have

$$\begin{aligned} \zeta_1 &= \gamma\eta_1 + \sqrt{1-\gamma^2}\eta_2, \\ \zeta_2 &= \sqrt{1-\gamma^2}\eta_1 + \gamma\eta_2, \end{aligned}$$

where $1/\sqrt{2} < \gamma < 1$ and the correlation ρ is given by the relation earlier.

Therefore, performing the phase reduction as before gives an analogous Stratonovich SDE

$$d\Theta_i = \left(\omega + D\,\mathbf{Z}\cdot\mathbf{F}^* - \frac{\sigma^2\gamma^2}{2}\alpha - \frac{\sigma^2(1-\gamma^2)}{2}\alpha\right)dt + \sigma\alpha(\gamma \circ dW_i + (\sqrt{1-\gamma^2}) \circ dW_j). \quad (5.71)$$

We see here that changing the noise to be partially correlated does not affect the drift correction terms. Hence we can write our ensemble now as (in Ito formulation):

$$d\Theta_i = \mathcal{A}_i(\mathbf{\Theta}) + d\xi_i(\mathbf{\Theta}, t), \quad (5.72)$$

where $\mathcal{A}_i$ is the same as before but our noises are

$$d\xi_i = \sigma(\alpha(\Theta_i)\gamma dW_i + \alpha(\Theta_j)\sqrt{1-\gamma^2}dW_j). \quad (5.73)$$

Hence if we define a new correlation matrix C^* such that

$$\langle d\xi_i d\xi_j \rangle = C^*_{ij}dt, \quad (5.74)$$

we must have

$$\begin{aligned} C^*_{ii} &= \sigma^2\alpha(\Theta_i)^2, & (5.75) \\ C^*_{ij} &= 2\sigma^2\gamma\sqrt{1-\gamma^2}\alpha(\Theta_i)\alpha(\Theta_j) = \sigma^2\rho^2\alpha(\Theta_i)\alpha(\Theta_j), i \neq j, & (5.76) \end{aligned}$$

or more compactly:

$$C^*_{ij} = \sigma^2(\rho^2 + (1-\rho^2)\delta_{i,j})\alpha(\Theta_i)\alpha(\Theta_j). \tag{5.77}$$

This means that averaging as in the case with fully correlated noise will give us the same $\bar{\mathcal{A}}$ term, while now

$$\bar{C}^*_{ij} = \sigma^2(\rho^2\Delta(\psi_j - \psi_i) + (1-\rho^2)\Delta(0)), \tag{5.78}$$

with the function Δ defined the same way as before.

Now defining a phase difference Φ as before we obtain

$$d\Psi_1 = DH(\Phi)dt + d\overline{\zeta}_1(\Phi, t), \tag{5.79}$$
$$d\Psi_2 = DH(-\Phi)dt + d\overline{\zeta}_2(\Phi, t), \tag{5.80}$$

with

$$\begin{aligned}\langle d\overline{\zeta}_1(\Phi,t)d\overline{\zeta}_1(\Phi,t)\rangle &= \langle d\overline{\zeta}_2(\Phi,t)d\overline{\zeta}_2(\Phi,t)\rangle = \sigma^2\Delta(0),\\ \langle d\overline{\zeta}_1(\Phi,t)d\overline{\zeta}_2(\Phi,t)\rangle &= \langle d\overline{\zeta}_2(\Phi,t)d\overline{\zeta}_1(\Phi,t)\rangle = \sigma^2\rho^2\Delta(\Phi).\end{aligned} \tag{5.81}$$

Taking the difference of the equations leads to the scalar SDE

$$d\Phi = DG(\Phi)dt + \sigma K^*(\Phi)dW(t), \tag{5.82}$$

where $G(\phi) = H(\phi) - H(-\phi)$ is the same as before, $W(t)$ is a Wiener process and the new function

$$\begin{aligned}K^*(\Phi) &= \frac{1}{\sigma}\sqrt{\langle[d\overline{\zeta}_2(\Phi,t) - d\overline{\zeta}_1(\Phi,t)][d\overline{\zeta}_2(\Phi,t) - d\overline{\zeta}_1(\Phi,t)]\rangle}\\ &= \sqrt{2[\Delta(0) - \rho^2\Delta(\Phi)]}.\end{aligned} \tag{5.83}$$

Therefore we can derive an FPE and solve for a stationary distribution P_0 as before. Our expression is only slightly different:

$$P_0(\phi) = \frac{A}{\Delta(0) - \rho^2\Delta(\phi)}\exp\left(\int_0^\phi \frac{DG(s)ds}{\sigma^2(\Delta(0) - \rho^2\Delta(s))}\right). \tag{5.84}$$

Note that $\rho = 1$ gives us the case of fully correlated noise - whereas $\rho = 0$ (totally uncorrelated noise) means that our stationary distribution is only dependent on

the G-function, with peaks at the zeros as expected.

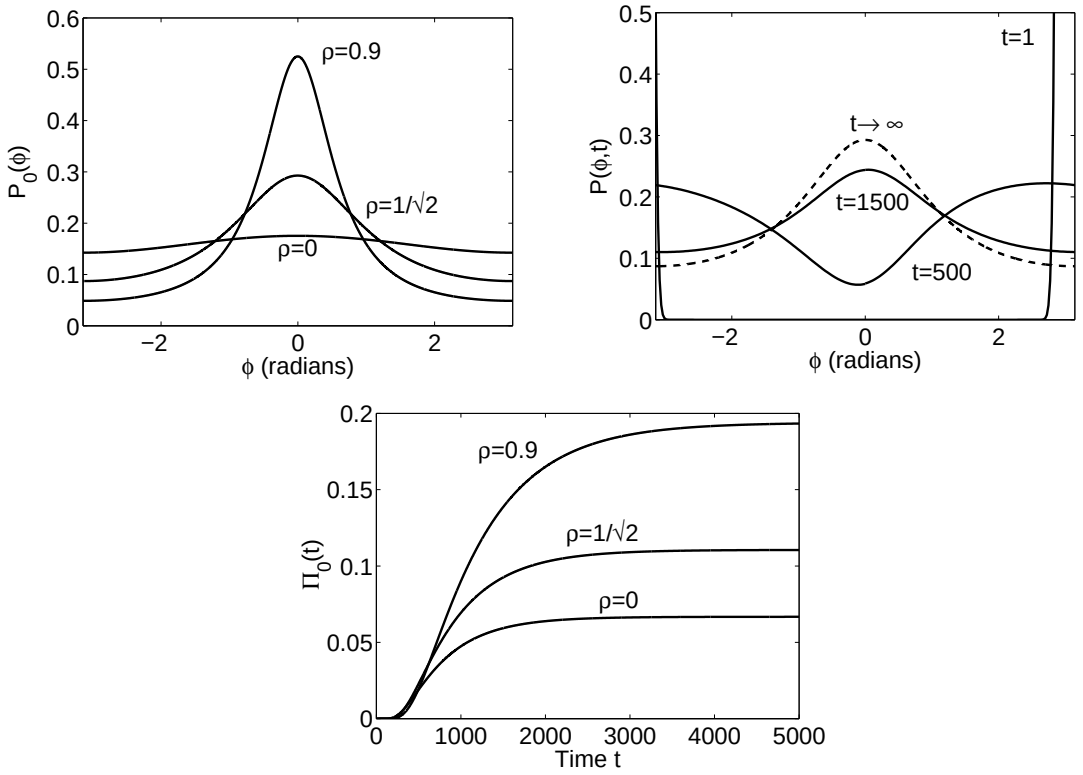

Figure 5.16: Monostable case with partially correlated noise. All parameters (except ρ) are the same as in Figure 5.14). Top left: Steady-state PDFs for various values of ρ. Top right: For an intermediate correlation ($\rho^2 = 1/2$), the PDF is plotted at several points in time, starting from the initial condition $\phi_0 = 3$ radians. Bottom: Plot of $\Pi_0(t)$ against time for various values of ρ.

Finally, we can compare the numerical results for the new model (Fig. 5.16 - 5.19) with our previous results (Fig. 5.9 - 5.12) and conclude that our main points are equally valid in both models.

Where there is purely correlated noise, both the monostable system and the multistable system eventually reach synchrony, although the transient behaviour differs significantly. On the other hand, for partially correlated noise, the monostable system always goes to the vicinity of the synchronous steady state, while in the multistable system, we observe a transition. At low levels of noise the asynchronous steady state dominates, while at high levels of noise the system tends towards synchrony, with bistable behaviour possible at intermediate levels of noise and/or correlation.

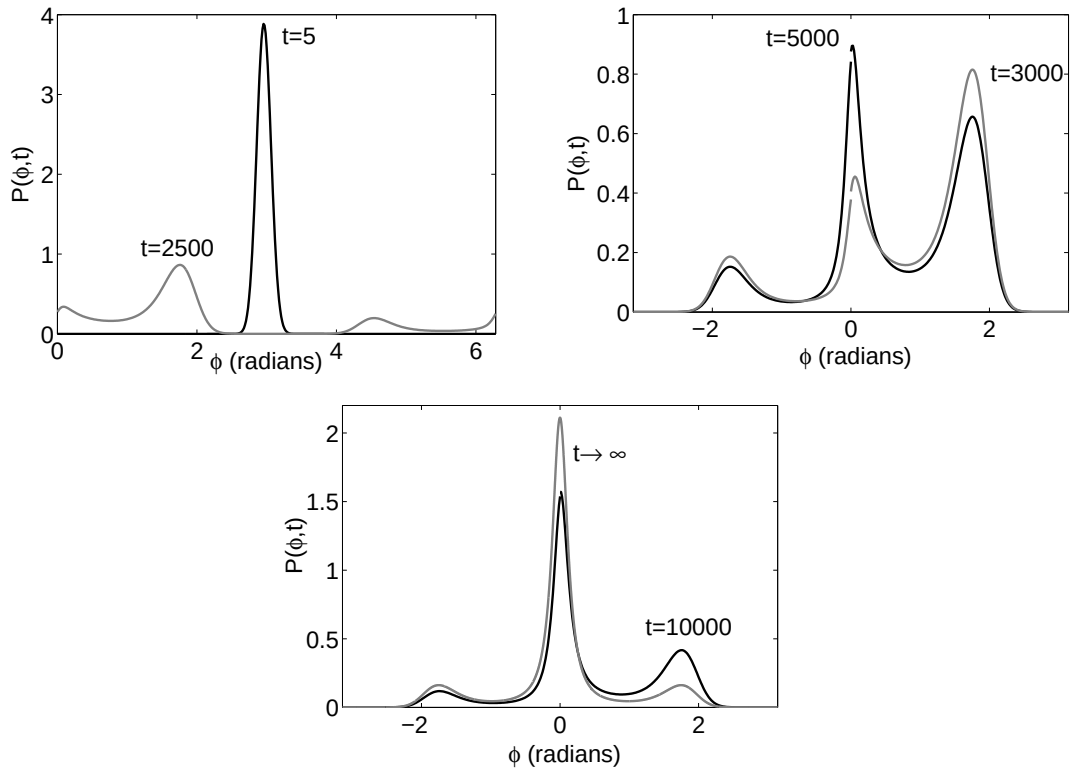

Figure 5.17: Multistable case with very high correlation: $\rho = 0.99$. All other parameters the same as in Fig. 5.15. Plots shown are snapshots of the PDF at various points in time starting from the initial condition $\phi_0 = 3$ radians.

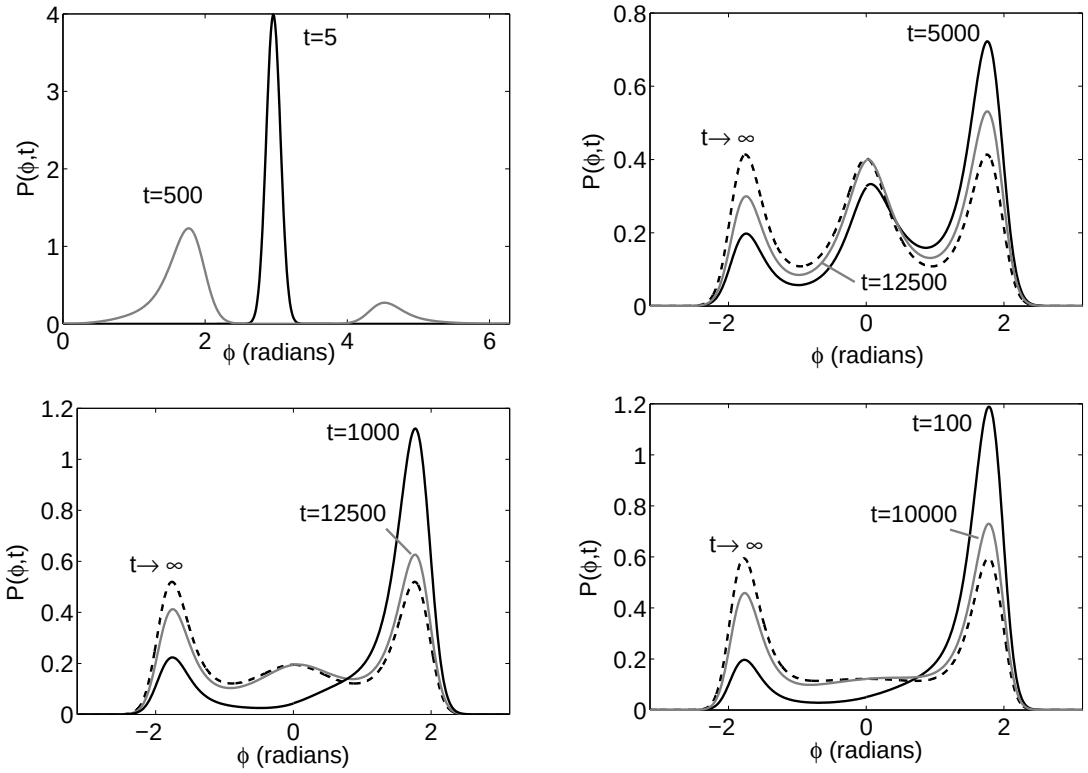

Figure 5.18: Multistable case, parameters the same as in Fig. 5.15. Top: High correlation ($\rho = 0.9$). We can clearly see stochastic bistability. Bottom left: Intermediate correlation ($\rho^2 = 0.5$). Bottom right: No correlation ($\rho = 0$).

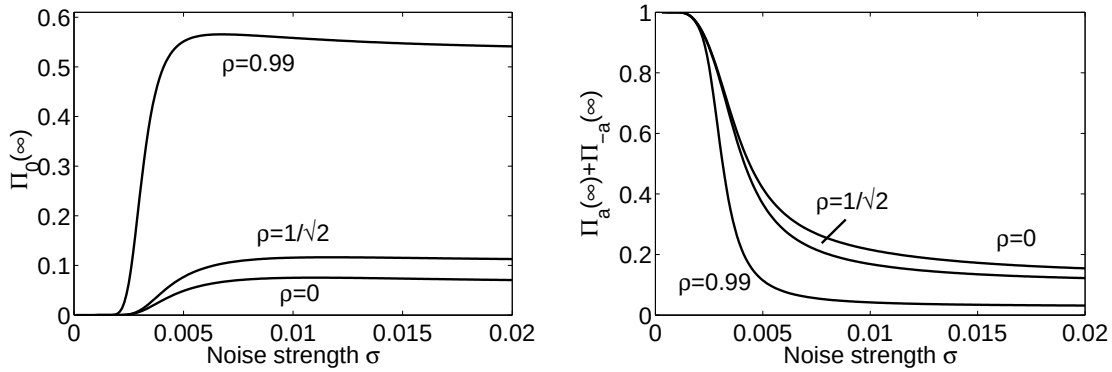

Figure 5.19: Multistable case, parameters the same as in Fig. 5.15. Plots are of the stochastic phase-locking about the synchronous and asynchronous steady-states. Left: Synchronous state $\phi = 0$; Right: Aysnchronous state $\phi \approx 1.78$. We see the same transition as before - this tells us that for very weak (but nonzero) noise, the dispersal causes the asynchronous state to dominate, as long as $\rho < 1$, while there is a transition to greater phase-locking about the synchronous steady state as the noise strength σ increases.

Chapter 6

Conclusions and future work

To conclude, in this thesis, we have explored the synchronization of neuronal and ecological oscillators through the relatively recent phenomenon of noise-induced synchronization. In the ecological case, we were able to extend our methods to study the combined effects of noise and dispersive coupling as well.

We were able to do this using a mathematical framework summarized as follows. First, we consider several examples of oscillating systems used in many previous studies, to make our results as generalisable as possible. In ecology, we use two canonical examples of predator-prey models that display limit cycle oscillations - the Rosenzweig-Macarthur and Holling-Tanner models. In the neuronal case, we use a pair of coupled E-I oscillators, which have been used as the basic oscillating units in various theoretical and experimental studies of synchrony in the brain. In order to show that our methods can also be extended to include the effects of synaptic plasticity, we also consider another basic oscillating unit - a recurrent excitatory population with synaptic depression.

Next, in order to simplify our multidimensional limit cycles, we perform a phase reduction, hence representing each oscillating population by a single phase variable; the effects of perturbations to this limit cycle, whether caused by noise or coupling, are captured by the phase response curve. Meanwhile, we use a master equation approach to study the individual-level behaviour of our populations. By performing appropriate Kramers-Moyal expansions and converting to Langevin equations, we show that the intrinsic stochasticity present in the systems due to the populations being composed of individuals, each behaving probabilistically, can be described with noisy terms added to the deterministic ODEs being used to model the systems in the absence of noise. Furthermore, the strength of said perturbations are proportional to the square root of the number of individuals in the

population. Finally, we introduce a common source of extrinsic noise and study the synchrony of the system.

By applying these mathematical tools to the chosen models, we are able to obtain a plethora of interesting results and corresponding biological implications. For example, by introducing common extrinsic noise into the birth rates of individuals in an ensemble of uncoupled Holling-Tanner predator-prey populations, we are able to observe synchronization. This provides a new and solid analytical framework for the Moran effect, which has been discussed in ecological journals for more than fifty years. The Moran effect refers to the correlation between fluctuations in population and fluctuations in the environment, and has previously been mainly studied using statistical tools. Here our phase-synchronization model explains the detailed mechanism behind it, as well as experimental observations such as why it only occurs when large-amplitude predator-prey cycles are already present. This may lead to future experimental work, for example, when selecting models and tuning parameters, the Moran effect indicates the presence of limit cycles. Furthermore, Moran's estimate of a linear relation between the environmental and population correlations can be refined here as we are able to calculate a steady-state PDF for the phases of populations - it would therefore be useful to re-look at population correlation data and compare it against the improved data from our modelling.

Moreover, in the converse case, we find that desynchronization of a metapopulation (due to uncorrelated noise or other effects) could explain the so-called "paradox of enrichment", where ecosystems fail to display large-amplitude cycles despite being enriched with nutrients that would (according to deterministic predictions) move the parameters into a regime with limit cycles. We suggest this be explored by experiments on stock tanks of different sizes, and/or detailed spatiotemporal data sampled from a large habitat.

We also obtained interesting results in the neuronal case. In the ensemble of E-I oscillators, we were able to observe various forms of synchronization, including coupling; this was achieved by introducing an asymmetry in the way our populations responded to noise. It would therefore be a starting point to examine how changes in membrane potentials could cause anomalous forms of synchrony, correlated to neuropathological ones observed in epilepsy and migraines. On the other hand, our observations of synchrony in the ensemble of recurrent excitatory populations with synaptic depression shows that our approach works for stochastic hybrid systems, as we had a stochastic population activity variable coupled to

a deterministic synaptic depression variable. This shows that our methods have potential applications to areas such as stochastic genetic switches and cell membranes, where the hybrid model provides a mathematical formulation of excitable membranes that incorporates the exact Markovian dynamics of single stochastic ion channels.

Another line of work that this thesis prompts is to consider more complicated network architectures that generate limit cycle oscillations at the population level. One particularly interesting example is a competitive network consisting of two excitatory populations with synaptic depression (or some other form of slow adaptation) that mutually inhibit each other. Such a network has recently been used to model noise-induced switching during binocular rivalry [79, 130, 95, 110, 111, 71], which concerns the phenomenon whereby perception switches back and forth between different images presented to either eye [6, 7]. Experimentally, it has been found that the eye dominance time statistics may be fit to a gamma distribution, suggesting that binocular rivalry is driven by a stochastic process. One possibility is that there is an extrinsic source of noise associated with the input stimuli.

Finally, our thesis also looks at the interplay of both noise-induced synchronization and dispersive coupling on the same system. In particular, we do this in the context of the Rosenzweig-Macarthur predator-prey model, where we find that the system can exhibit strikingly different modes of behaviour depending on the strength of the noise and dispersal, as well as the parameter regime. When there is a high ratio of common noise to uncorrelated noise, we find that the system reaches synchrony, although the approach to synchrony depends on the presence of asynchronous stable states in the deterministic limit. These asynchronous stable states then become persistent if one increases the ratio of uncorrelated to correlated noise, causing stochastic bistability. We perform our analysis firstly in the case where noise is introduced additively to make the system as simple as possible; next, by also considering a case where the noise is population-dependent, we show that our results apply to other models with different forms of noise.

Our results could provide an analytical background into various ecological experiments to determine the dominant factors behind the behaviour of ecosystems - for example, controlled experiments along the line of [128] could be done in phytoplankton-zooplankton systems, with different levels of environmental fluctuations and ease of dispersal between populations, that could be compared with our results to find out which parameter regime the system is in. In the field, population data could be processed in a similar manner - for instance, constant time-

lags between the peaks of populations of adjacent patches would be indicative of a constant phase difference, showing that the asynchronous dispersal-induced state was present; alternatively, switching between this constant delay and synchronization would demonstrate multistability.

Another obvious extension of our work would be to carry out similar analysis to Section 5 in the context of coupled neuronal populations. By modifying the coupling appropriately one could potentially model more complicated network architecture, with specific neurobiological applications in mind.

From a mathematical perspective, there is a large amount of work yet to be done in the area of noise-induced synchronization. For instance, while synchrony between a pair of oscillators is indicative of synchrony in general, it is unclear how a pairwise PDF would translate into the distribution of the ensemble. Solving a system of equations for a whole ensemble (without making the ansatz of considering just a pair of oscillators) would be a significantly more involved from an analytical perspective.

In addition, note that we observed multiple peaks in the PDF of the phase difference of the E-I oscillators, and correspondingly, multiple clusters in the stochastic simulations of the oscillators. However, it is unknown how these multiple peaks in a pairwise PDF would cause an ensemble to behave. Undoubtedly, it would depend on the form of coupling present in the ensemble, but there are many unanswered questions as to how one would deal with it precisely.

Bibliography

[1] Abbott, L.F. and van Vreeswijk, C. "Asynchronous states in networks of pulse-coupled oscillators." Phys. Rev. E, 48:1483-1490, 1993.

[2] Abbott, L.F., Varela, J.A., Sen, K. and Nelson, S.B. "Synaptic depression and cortical gain control". Science, 275:220-224, 1997.

[3] Amari, S. "Homogeneous nets of neuron-like elements." Biological Cybernetics, 17:211220, 1975.

[4] Amari, S. "Dynamics of pattern formation in lateral inhibition type neural fields." Biological Cybernetics, 27:7787, 1977.

[5] Arnold, L. Stochastic Differential Equations: Theory and Applications. Wiley-Interscience, NY, 1974.

[6] Blake, R. "A primer on binocular rivalry, including current controversies." Brain and Mind, 2:5-38, 2001.

[7] Blake, R. and Logothetis, N. "Visual competition." Nat. Rev. Neurosci., 3:13-23, 2002.

[8] Blasius, B. and Stone, L. "Ecology: nonlinearity and the Moran effect." Nature, 406:846-847, 2000.

[9] Borisyuk, R. and Kirillov, A.B. "Bifurcation analysis of a neural network model." Biol. Cybern., 66:319-325, 1992.

[10] Boustani, S.E. and Destexhe, A. "A master equation formalism for macroscopic modeling of asynchronour irregular activity states." Neural Comput. 21:46-100, 2009.

[11] Bressloff, P.C. "Stochastic neural field theory and the system-size expansion." SIAM J. Appl. Math., 70:1488-1521, 2009.

[12] Bressloff, P.C. "Metastable states and quasicycles in a stochastic Wilson-Cowan model of neuronal population dynamics." Phys. Rev. E, 85:051903, 2010.

[13] Bressloff, P.C. and Coombes, S. "Desynchronization, mode locking, and bursting in strongly coupled integrate-and-fire oscillators." Phys. Rev. Lett., 86(10):2168-2171, 1998.

[14] Bressloff, P.C. and Coombes, S. "Dynamics of strongly coupled spiking neurons." Neural Comput. 12(1):91-129, 2000.

[15] Bressloff, P.C. and Lai, Y.M. "Stochastic synchronization of neuronal populations with intrinsic and extrinsic noise." J. Math. Neurosci, 1:2, 2011.

[16] Bressloff, P.C. and Lai, Y.M. "Dispersal and noise: various modes of synchrony in ecological oscillators." J. Math. Biol., in print, 2012.

[17] Bressloff, P.C., Cowan, J.D., Golubitsky, M., Thomas, P.J., and Wiener, M. "Geometric visual hallucinations, Euclidean symmetry and the functional architecture of striate cortex." Phil. Trans. Roy. Soc. Lond. B, 356:299-330, 2001.

[18] Brunel, N. "Dynamics of sparsely connected networks of excitatory and inhibitory spiking neurons." J. Comput. Neurosci, 8:183-208, 2000.

[19] Brunel, N. and Hakim, V. "Fast global oscillations in networks of integrate-and-fire neurons with low firing rates." Neural Comput. 11:1621-1671, 1999.

[20] Buckwar E. and Riedler, M.G. "An exact stochastic hybrid model of excitable membranes including spatio-temporal evolution." J. Math. Biol., 63(6):1051-93, 2011.

[21] Buice, M. and Cowan, J.D. "Field-theoretic approach to fluctuation effects in neural networks." Phys. Rev. E 75:051919, 2007.

[22] Buice, M., Cowan, J.D., and Chow, C.C. "Systematic fluctuation expansion for neural network activity equations." Neural Comput., 22:377-426, 2010.

[23] Burrage, K. and Burrage, P.M. "High strong order explicit Runge-Kutta methods for stochastic ordinary differential equations." Appl. Numer. Math. 22:81-101, 1996.

[24] Buszaki, G. Rhythms of the Brain. Oxford University Press, Oxford. 2006.

[25] Canavier, C.C. Phase response curve. Scholarpedia, 1(12):1332, 2006.

[26] Colombo, A., Dercole, F. and Rinaldi, S. "Remarks on metacommunity synchronization with application to prey-predator systems." The American Naturalist, 171:430-442, 2008.

[27] Coombes, S. Neural Fields. Scholarpedia, 1(6):1373, 2006.

[28] Chow, C.C. "Phase-locking in weakly heterogeneous neuronal networks." Physica D 118: 343-370, 1998.

[29] de Roos, A.M., McCauley, E. and Wilson, W.G. "Mobility versus density-limited predator-prey dynamics on different spatial scales." Proc. R. Soc. London B, 246:117-122, 1991.

[30] De Witte, V. and Govaerts, W. "Convergence analysis of a numerical method to solve the adjoint linearized periodic orbit equations." Appl. Numer. Math., 60:1007-1023, 2010.

[31] Doiron, B. Lindner, B. Longtin, A., Maler, L. and Bastian, J. "Oscillatory activity in electrosensory neurons increases with the spatial correlation of the stochastic input stimulus." Phys. Rev. Lett. 93:048101, 2004.

[32] Earn, D.J.D., Rohani, P. and Grenfell, B.T. "Persistence, chaos and synchrony in ecology and epidemiology." Proc. Roy. Soc. B, 265:7-10, 1998.

[33] Ermentrout, G.B. "Noisy oscillators." In Stochastic methods in neuroscience. Edited by Laing, C.R. and Lord, G.J. Oxford University Press, Oxford, 2009.

[34] Ermentrout, G. B. and Cowan, J.D. "A mathematical theory of visual hallucination patterns." Bio. Cybern., 34:137-150, 1979.

[35] Ermentrout, G. B. and Cowan, J.D. "Large scale spatially organized activity in neural nets." SIAM J. Appl. Math., 38:1-21, 1980.

[36] Ermentrout, G.B. and Kopell, N. "Multiple pulse interactions and averaging in coupled neural oscillators." J. Math. Biol., 29:195-217, 1991.

[37] Estay, S.A., Albornoz, A.A., Lima, M., Boyce, M.S. and Stenset, N.C. "A simultaneous test of synchrony causal factors in muskrat and mink fur returns at different scales across Canada." PloS ONE 6(11):e27766, 2011.

[38] Evans, S.N., Ralph, P.L., Schreiber, S.J. and Sen, A. "Stochastic population growth in spatially heterogeneous environments." J. Math. Biol., 2012.

[39] Faugeras, O., Touboul, J. and Cessac, B. "A constructive mean-field analysis of multi-population neural networks with random synaptic weights and stochastic inputs." Frontiers in Comp. Neurosci., 3:1-28, 2009.

[40] Galan, R., Ermentrout, G.B. and Urban, N.N. "Correlation-induced synchronization of oscillations in olfactory bulb neurons." J. Neurosci., 26:3646-3655, 2006.

[41] Galan, R., Ermentrout, G.B. and Urban, N.N. "Optimal time scale for spike-time reliability: theory, simulations and experiments." J. Neurophysiol., 99:277-283, 2008.

[42] Gardiner, C.W. Stochastic Methods: a Handbook for the Natural and Social Sciences, 4th Ed. Springer, New York. 2009.

[43] Gasull, A., Kooij, R.E., and Torregrosa, J. "Limit cycles in the Holling-Tanner model." Publicacions Matematiques, 41:149-167, 1997.

[44] Gerstner, W. and Van Hemmen, J.L. "Coherence and incoherence in a globally coupled ensemble of pulse-emitting units." Phys. Rev. Lett., 99:312-315, 1993.

[45] Ghandi, A., Levin, S. and Orszag, S. "'Critical slowing down' in time-to-extinction: an example of critical phenomena in ecology." J. Theor. Biol. 192:363-76, 1998.

[46] Ghandi, A., Levin, S. and Orszag, S. "Moment expansions in spatial ecological models and moment closure through Gaussian approximation." Bull. Math. Biol., 62:595-632, 2000.

[47] Gillespie, D.T. "The chemical Langevin equation." J. Chem. Phys., 113:297-306, 2000.

[48] Goldobin, D.S. and Pikovsky, A. "Synchronization and desynchronization of self-sustained oscillators by common noise." Phys. Rev. E, 71:045201, 2005.

[49] Goldobin, D.S., Teramae, J.N., Nakao, H. and Ermentrout, G.B. "Dynamics of limit-cycle oscillators subject to general noise." Phys. Rev. Lett., 105:154101, 2010.

[50] Goldwyn, E.E. and Hastings, A. "When can dispersal synchronize populations?" Theor. Pop. Biol., 73:395-402, 2008.

[51] Goldwyn, E.E. and Hastings, A. "Small heterogeneity has large effects on synchronization of ecological oscillators." Bull. Math. Biol., 71:130-144, 2009.

[52] Goldwyn, E.E. and Hastings, A. "The roles of the Moran effect and dispersal in synchronizing oscillating populations." J. Theor. Biol. 289:237-246, 2011.

[53] Govaerts, W. and Sautois, B. "Computation of the phase response curve: a direct numerical approach." Neural. Comput.18: 817-947, 2006.

[54] Grannan, E.R., Kleinfeld D. and Sompolinsky H. "Stimulus-dependent synchronization of neuronal assemblies." Neural. Comput. 5:550-569, 1993.

[55] Gray, C.M. "The temporal correlation hypothesis of visual feature integration: still alive and well." Neuron, 24:31-47, 1999.

[56] Grenfell, B.T., Wilson, K., Finkenstädt, B.F., Coulson, T.N., Murray, S., Albon S.D., Pemberton, J.M., Clutton-Brock, T.H. and Crawley, M.J. "Noise and determinism in synchronized sheep dynamics." Nature, 394:674-677, 1998.

[57] Guillamon, A. and Huguet, G. "A computational and geometric approach to phase resetting curves and surfaces." SIAM J. Appl. Dyn. Sys., 8(3):1005-1042, 2009.

[58] Hanski, I. "Metapopulation dynamics." Nature, 396:41-49, 1998.

[59] Hastings, A. Population Biology: Concepts and Models. Springer, New York. 1997.

[60] Hodgkin, A. and Huxley, A. "A quantitative description of membrane current and its application to conduction and excitiation in nerve." J. Physiol. 117:500544, 1952.

[61] Holcman D. and Tsodyks M. "The emergence of Up and Down states in cortical networks." PLoS Comput. Biol., 2:174-181, 2006.

[62] Huang, X., Troy, W.C., Yang, Q., Ma, H., Laing, C.R., Schiff, S.J. and Wu, J.Y. "Spiral waves in disinhibited mammalian neocortex." J. Neurosci., 24(44):98979-99902, 2004.

[63] Hudson, P.J. and Cattadori, I.M., "The Moran effect: a cause of synchrony." Trends Ecol. Evol., 14:1, 1999.

[64] Hutt, A., Longtin, A. and Schimansky-Geier, L. "Additive noise-induced Turing transitions in spatial systems with application to neural fields and the Swift-Hohenberg equation." Physica D, 237:755-773, 2008.

[65] Igarashi, Y., Oizumi, M. and Okada, M. "Mean field analysis of stochastic neural network models with synaptic depression." J. Phys. Soc. Jap. 79:064001, 2010.

[66] Izhikevich, E.M. Dynamical Systems in Neuroscience: The Geometry of Excitability and Bursting. MIT Press, Cambridge, MA. 2007.

[67] Jansen, V.A.A. and Lloyd, A.L. "Local stability analysis of spatially homogeneous solutions of multi-patch systems." J. Math. Biol. 41:232-252, 2000.

[68] Jirsa, V.K. and Haken, H. "A derivation of a macroscopic field theory from the quasi-microscopic neural dynamics." Physica D, 99:503-526, 1997.

[69] Kilpatrick, Z.P. and Bressloff, P.C. "Spatially structured oscillations in a two-dimensional neuronal network with synaptic depression." J. Comp. Neurosci., 28:193-202, 2010.

[70] Kilpatrick, Z.P. and Bressloff, P.C. "Effects of synaptic depression and adaptation on spatiotemporal dynamics of an excitatory neuronal network." Physica D, 239:547-560, 2010.

[71] Kilpatrick, Z.P. and Bressloff, P.C. "Binocular rivalry in a competitive network with synaptic depression." SIAM J. Appl. Dyn. Syst., 9:1303-1347, 2010.

[72] Klausmeier, C.A. "Successional state dynamics: a novel approach to modeling nonequilibrium foodweb dynamics." J. Theor. Biol., 262:585-595, 2010.

[73] Kupferman, R., Pavliotis, G.A. and Stuart, A.M. "Itō vs Stratonovich white-noise limits for systems with inertia and colored multiplicative noise." Phys. Rev. E, 70:036120, 2004.

[74] Kuramoto, Y. Chemical Oscillations, Waves, and Turbulence. Springer-Verlag, Berlin. 1984.

[75] Kurebayashi, W., Fujiwara, K. and Ikeguchi, T. "Colored noise induces synchronization of limit cycle oscillators." Europhys. Lett., 97:50009, 2012.

[76] Kurtz, T.G. "Limit theorems and diffusion approximations for density dependent Markov chains." Math. Prog. Stud. 5:67, 1976.

[77] Lai, Y.M., Newby, J. and Bressloff, P.C. "Effects of demographic noise on the synchronization of a metapopulation in a fluctuating environment." Phys. Rev. Lett., 107(11):118102, 2011.

[78] Laing, C.R. "Spiral waves in nonlocal equations." SIAM J. Appl. Dyn. Syst., 4(3):588-606, 2005.

[79] Laing, C.R. and Chow, C.C. "Stationary bumps in networks of spiking neurons." Neural Comput., 19:2032-2092, 2007.

[80] Laing, C.R., Troy, W.C., Gutkin, B, and Ermentrout, G.B. "Multiple bumps in a neuronal model of working memory." SIAM J. Appl. Math., 63:62-97, 2002.

[81] Lei, J. "Stochasticity in single gene expression with both intrinsic noise and fluctuations in kinetic parameters." J. Theor. Biol, 256:485-492, 2009.

[82] Leibhold, A., Koenig, W.D. and Bjornstad, O.N. "Spatial synchrony in population dynamics." Ann. Rev. Ecol. Evol. Syst., 35:467-490, 2004.

[83] Logothetis, N., Leopold, D.A. and Sheinberg, D.L. "What is rivalling during binocular rivalry?" Nature, 380:621-624, 1996.

[84] Ly, C. and Ermentrout, G.B. "Synchronization of two coupled neural oscillators receiving shared and unshared noisy stimuli." J. Comput. Neurosci., 26:425-443, 2009.

[85] Mainen, Z.F. and Sejnowski, T.J. "Reliability of spike timing in neocortical neurons." Science, 268:1503-1506, 1995.

[86] Marella, S. and Ermentrout, G.B. "Class-II neurons display a higher degree of stochastic synchronization than class-I neurons." Phys. Rev. E 77:41918, 2008.

[87] Mattia, M. and Del Guidice, P. "Population dynamics of interacting spiking neurons." Phys. Rev. E, 66:051917, 2002.

[88] Meyer, C. and van Vreeswijk C. "Temporal correlations in stochastic networks of spiking neurons." Nerual Comput., 14:369-404, 2002.

[89] McCauley, E., Wilson, W.G. and de Roos, A.M. "Dynamics of age-structured predator-prey interactions: individual based models and population level formulations." Am. Nat. 142: 412-442, 1993.

[90] McCauley, E., Nisbet, R.M., Murdoch, W.W, de Roos, A.M. and Gurney, W.S.C. "Large-amplitude cycles of Daphnia and its algal prey in enriched environments." Nature, 402:653-656, 1999.

[91] McKane, A.J. and Newman, T.J. "Stochastic models in population biology and their deterministic analogs." Phys. Rev. E, 70:041902, 2004.

[92] McKane, A.J. and Newman, T.J. "Predator-prey cycles from resonant amplification of demographic stochasticity." Phys. Rev. Lett., 94: 218102, 2005.

[93] Milstein, G.N. and Tretyako, M.V. Stochastic numerics for mathematical physics. Springer, 2004.

[94] Moran, P.A.P. "The statistical analysis of the Canadian Lynx cycle." Austral. J. Zoology, 1:291-298, 1953.

[95] Moreno-Bote, R., Rinzel, J. and Rubin, N. "Noise-induced alternations in an attractor network mdoel of perceptual bistability." J. Neurophysiol. 98:1125-1139, 2007.

[96] Murdoch, W.W, Nisbet, R.M., McCauley, E., de Roos, A.M., and Gurney, W.S.C. "Plankton abundance and dynamics across nutrient levels: test of hypotheses." Ecology, 79(4): 1339-1356, 1998.

[97] Nakao, H., Arai, K. and Kawamura Y. "Noise-induced synchronization and clustering in ensembles of uncoupled limit cycle oscillators." Phys. Rev. Lett., 98:184101, 2007.

[98] Nesse, W.H., Borisyuk, A. and Bressloff, P.C. "Fluctuation-driven rhythmogenesis in an excitatory neuronal network with slow adaptation." J. Comput. Neurosci., 25:317-333, 2009.

[99] Nunez, P.I. Neocortical dynamics and human EEG rhythms. Oxford University Press, NY, 1995.

[100] Ohira T. and Cowan, J.D. "Stochastic neurodynamics and the system size expansion." In Proceedings of the first international conference on Mathematics of neural networks. Edited by Ellacott, S. and Anderson, I.J. Academic Press, NY, 1997.

[101] Pakdaman K., Thieullen M. and Wainrib G. "Fluid limit theorems for stochastic hybrid systems with application to neuron models." Adv. Appl. Probab., 42:761-794, 2010.

[102] Pecora, L.M. and Carroll, T.L. "Synchronization in chaotic systems." Phys. Rev. Lett. 64:821-824, 1990.

[103] Pikovsky, A.S. "Synchronization and stochastization of an ensemble of autogenerators by external noise." Radiophys. 27:576-581, 1984.

[104] Renart, A., Brunel, N. and Wang, X.J. "Mean-field theory of irregularly spiking neuronal populations and working memory in recurrent cortical networks." In Computational Neuroscience: a comprehensive approach. Edited by Feng, J. CRC Press, Boca Raton, Fl, 2004.

[105] Renshaw, E. Modelling Biological Populations in Space and Time. Cambridge University Press, 1993.

[106] Robinson, P.A., Rennie, C.J., Wright, J.J., Bahramali, H., Gordon, E. and Rowe, D.I. "Prediction of EEG spectra from neurophysiology." Phys. Rev. E, 63:021903, 2001.

[107] Rohani, P., Earn, D.J.D. and Grenfell, B.T. "Opposite patterns of synchrony in sympatric disease metapopulations." Science, 286:968-971, 1999.

[108] Rosenzweig, M. and MacArthur, R. "Graphical representation and stability conditions of predator-prey interaction." American Naturalist, 97:209-223, 1963.

[109] Salinas, E. and Sejnowski T.J. "Correlated neuronal activity and the flow of neural information." Nat. Rev. Neurosci., 4:539-550, 2001.

[110] Shpiro, A., Curtu, R., Rinzel, J. and Rubin, N. "Dynamical characteristics common to neuronal competition models." J. Neurophysiol. 97:462-473, 2007.

[111] Shpiro, A., Moreno-Bote, R., Rubin, N. and Rinzel, J. "Balance between noise and adaptation in competition models of perceptual bistability." J. Comp. Neurosci., 27:37-54, 2009.

[112] Shuster, H.G. and Wagner, P. "A model for neuronal oscillations in the visual cortex." Biol. Cybern., 64:77-82, 1990.

[113] Singer, W. and Gray, C.M. "Visual feature integration and the temporal correlation hypothesis." Annu. Rev. Neurosci, 18:555-586, 1995.

[114] Smith, G.D. "Modeling the stochastic gating of ion channels." In Computational cell biology. Edited by Fall, C.P., Marland, E.S., Wagner, J.M. and Tyson, J.J. Springer, NY, 2002.

[115] Softky, W.R. and Koch, C. "The highly irregular firing of cortical cells is inconsistent with temporal integration of random EPSPS." J. Neurosci., 13:334-350, 1993.

[116] Soula, H. and Chow, C.C. "Stochastic dynamics of a finite-size spiking neural network." Neural Comput. 19:3262-3292, 2007.

[117] Strogatz, S.H. "From Kuramoto to Crawford: exploring the onset of synchronization in populations of coupled oscillators." Physica D 143:1-20, 2000.

[118] Tabak, J., O'Donovan, M.J. and Rinzel, J. "Differential control of active and silent phases in relaxation models of neuronal rhythms." J. Comp. Neurosci., 21:307-328, 2006.

[119] Tabak, J., Senn, W., O'Donovan, M.J. and Rinzel, J. "Modeling of spontaneous activity in developing spinal cord using activity dependent depression in an excitatory network." J. Neurosci., 20:3041-3056, 2000.

[120] Tanner, J.T. "The stability and the intrinsic growth rates of prey and predator populations." Ecology, 56:855-867, 1975.

[121] Tass, P. "Cortical pattern formation during visual hallucination. J. Biol. Phys., 21:177-210, 1995.

[122] Teramae, J.N. and Tanaka D. "Robustness of the noise-induced phase synchronization in a general class of limit cycle oscillators." Phys. Rev. Lett. 93:204103, 2004.

[123] Teramae, J.N., Nakao, H. and Ermentrout G.B. "Stochastic phase reduction for a general class of noisy limit cycle oscillators." Phys. Rev. Lett., 102:194102, 2009.

[124] Tome, T. and de Oliviera, M.J. "Role of noise in population dynamics cycles." Phys. Rev. E, 79:061128, 2009.

[125] Troy, W.C. and Shusterman, V. "Patterns amd features of families of traveling waves in large-scale neuronal networks." SIAM J. Appl. Dyn. Syst., 6(1):263-292, 2007.

[126] Tsodyks, M.S., Pawelzik K. and Markram H. "Neural networks with dynamic synapses." Neural Comput. 10:821-835, 1998.

[127] Van Kampen, N.G. Stochastic processes in physics and chemistry. North-Holland, Amsterdam, 1992.

[128] Vasseur, D.A. and Fox, J.W. "Phase-locking and environmental fluctuations generate synchrony in a predator-prey community." Nature, 460: 1007-1010, 2009.

[129] Vladimirski, B., Tabak, J., O'Donovan, M.J. and Rinzel, J. "Neural networks with dynamic synapses." J. Comput. Neurosci., 25:39-63, 2008.

[130] Wilson, H.R. "Computational evidence for a rivalry hierarchy in vision." Proc. Natl. Acad. Sci. USA, 100:14499-14503, 2003.

[131] Wilson, H.R. and Cowan, J.D. "Excitatory and inhibitory interactions in localized populations of model neurons." Biophys. J., 12:1-23, 1972.

[132] Wilson, H.R. and Cowan, J.D. "A mathematical theory of the functional dynamics of cortical and thalamic nervous tissue." Kybernetik, 13:55-80, 1973.

[133] Wong, E. and Zakai, M. "On the convergence of ordinary integrals to stochastic integrals." Ann. Math. Statist., 36(5):1560-1564, 1965.

[134] Yoshimura,K. "Phase reduction of stochastic limit-cycle oscillators." In Reviews in nonlinear dynamics and complexity vol. 3. Edited by Schuster, H.G. Wiley, 2010.

[135] Yoshimura, K. and Arai, K. "Phase reduction of stochastic limit cycle oscillators." Phys. Rev. Lett., 101:154101, 2008.

[136] Yoshimura, K., Davis, P. and Uchida, A. "Invariance of frequency difference in nonresonant entrainment of detuned oscillators induced by common white noise." Prog. Theor. Phys., 120(4):621-633, 2008.

[137] Zeisler, S., Franz, U., Wittich, O. and Liebscher, V. "Simulation of genetic networks modelled by piecewise deterministic Markov processes." IET Syst. Bio. 2:113-135, 2008.